

STUDY OF OXIDATION AND MECHANICAL BEHAVIOUR OF MODIFIED 9Cr-1Mo FERRITIC STEEL

A Thesis Submitted

In Partial Fulfilment of the Requirements
for the Degree of
MASTER OF TECHNOLOGY

by

P. SOMANATHAN

to the

DEPARTMENT OF METALLURGICAL ENGINEERING
INDIAN INSTITUTE OF TECHNOLOGY KANPUR

JULY, 1986

23 SEP 1987
CENTRAL LIBRARY
Karpur.
Acc. No. A 98023

ME-1986-M-SOM-STU

Dedicated

To

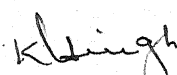
My

Parents and Brothers

CERTIFICATE

This is to certify that this work entitled 'Study of Oxidation and Mechanical Behaviour of Modified 9Cr-1Mo Ferritic Steel' by P. Somanathan has been carried out under my supervision and the same has not been submitted elsewhere for a degree.

July, 1986
IIT Kanpur.


K.P. SINGH
Professor
Department of Metallurgical Engineering
Indian Institute of Technology
Kanpur.

ACKNOWLEDGEMENTS

I feel great pleasure in expressing a profound sense of gratitude and indebtedness to Prof. K.P. Singh for his constant cooperation, inspiration, encouragement and able guidance during the course of the work.

I wish to express my deep-felt gratitude to Mr. M.N. Mungole for his unfailing help extended at every stage of this work, without which the present venture would not have been successful.

My thanks are due to M/s B.K. Jain of Materials Testing Lab., B.P. Sharma of Scanning Electron Microscopy Lab., Uma Shanker of X-ray Lab., K.P. Mukherjee of Physical Met. Lab., Pal of Material Sciences Lab., D.P. Tripathi and A. Sharma of Extractive Met. Lab., Sairam of Glass Blowing Lab., K.S. Bhamra, R.C. Sharma, K.K. Malhotra of Met. Workshop and Hari Shanker Singh of Thermodynamics Lab.

I wish to express my sincere thanks to all my friends M/s Deepak Goyal, Babu Viswanathan, Rajiv Mishra, D. Ramakrishna, Ashok Kumar, Asim Bag, Dinesh Shukla, H.S. Ranganath, Sanjiv Khosla, Avinash Bhaskare and other colleagues for their kind cooperation and assistance in time.

I would like to thank Dr. Keshav Kant for his constant encouragement and inspiration.

Thanks are due to Mr. B.K. Jain for careful tracing out the figures, Mr. V.P. Sharma for photography printing work and Mr. Dubey for cyclostyling.

I wish to thank the Department of Atomic Energy for the partial financial support.

Finally, I deeply acknowledge the effort put by Mr. C.M. Abraham in the patient and neat typing of the thesis with amazing efficiency.

P. SOMANATHAN

CONTENTS

	Page
Chapter 1 INTRODUCTION	1
1.1 Scope of the present work	3
Chapter 2 LITERATURE REVIEW	6
2.1 Constitution of the alloy	6
2.2 Oxidation of Iron	7
2.3 Oxidation of the alloys of Iron	12
2.4 Oxidation of Iron-Chromium alloys	15
2.5 Study of Chrome-Moly Ferritic Steels	19
2.6 Mechanical properties of modified 9Cr-1Mo Ferritic Steel	24
Chapter 3 EXPERIMENTAL	39
3.1 Material	39
3.2 Processing of the material	39
3.3 High pressure oxidation system	40
3.4 Oxidation studies	45
3.5 Mechanical properties	47
3.6 X-ray analysis	54
3.7 Metallography	54
3.8 Fractography	54

Chapter 4	OXIDATION STUDIES	55
	4.1 Thermogravimetry	55
	4.2 Oxidation behaviour of modified 9Cr-1Mo ferritic steel	56
	4.3 Examination of oxidation products	86
	4.4 Discussion	95
Chapter 5	RESULTS AND DISCUSSION ON MECHANICAL PROPERTIES	99
	5.1 Tensile test	99
	5.2 Fatigue and Creep Fatigue test	121
	5.3 Creep Test	121
	5.4 X-ray analysis	126
	5.5 Discussion	126
Chapter 6	CONCLUSION	142
Chapter 7	SUGGESTIONS FOR FUTURE WORK	144

List of Tables

Table No.	Description	Page
4.1	Values of n and k for the oxidation reactions at 202.65 KPa	77
4.2	Values of n and k for the oxidation reactions at 303.97 KPa	78
4.3	Values of n and k for the oxidation reactions at 506.62 KPa	79
4.4	Values of n and k for the oxidation reactions at 709.26 KPa	80
4.5	Values of n and k for the oxidation reactions at 911.91 KPa	81
4.6	Rate equations for modified 9Cr-1Mo in the temperature ranges 600-750 and 750-900°C for the various pressures	85
5.1	Results of tensile tests at room temperature	117
5.2	Results of tensile tests at 265°C	118
5.3	Results of tensile tests at 375°C	119
5.4	Results of tensile tests at 545°C	120
5.5	Results of low cycle fatigue tests at room temperature	122
5.6	Results of creep-fatigue tests at 545°C	123
5.7	Results of creep tests at 550°C	127

List of Figures

Fig.No.	Description	Page
2.1	Iron-Oxygen equilibrium diagram	8
2.2	Relation between rate constant and temperature on the oxidation of high purity iron	11
2.3	Oxidation mechanism of iron above 600°C	11
2.4	Effect of alloying elements on the oxidation of iron	14
2.5	Parabolic oxidation rate constants for Iron-Chromium alloys at various temperatures	14
2.6	Variation of the parabolic rate constant with Chromium content for Fe-Cr alloys oxidized at 1000°C in 1 atm. of oxygen	18
2.7	Iron content of scales in Iron-Chromium alloys oxidized for 6-18 hours	18
2.8	Shaded areas indicate regions of rapid oxidation in Fe-Mo-Cr alloys	20
2.9	Strength of high temperature alloys	20
2.10	Effect of increasing Si content in a 5Cr-0.5Mo steel on resistance to air oxidation	23
2.11	Comparison of scale growth rate in high temperature steam	23
2.12	Comparison of yield strength and ultimate tensile strength values of several materials as a function of temperature	26
2.13	Comparison of creep fatigue properties of normalized and tempered 9% Cr Mo variants	26
2.14	Comparison of estimated stress-rupture isothermals for several materials	29
2.15	Variation of estimated design allowable stress intensity, s_o and estimated allowable stress intensity, S_{mt} with temperature of several materials	30

3.1	Block diagram of high pressure oxidation system	44
3.2	High accuracy pressure measurement and control system	41
3.3	Heat-treatment set up	42
3.4	Calibration curves for the high pressure system	46
3.5	Sample design	49
3.6	Waveform of load applied in low cycle fatigue test	49
3.7	Temperature profile of furnace	51
4.1- 4.9	Weight gain plots at various pressures and temperatures	58-66
4.10	Comparison of weight gains at various pressures at 600°C and 900°C	67
4.11- 4.19	Double log plots	68-76
4.20	Arrhenius plot in the temperature range 600-750°C	83
4.21	Arrhenius plot in the temperature range 750-900°C	84
4.22- 4.40	Metallographs	89-94
5.1- 5.6	Variation of mechanical strength parameters with oxygen concentrations	101- 106
5.7a- 5.7f	Strengths of untreated and oxidised samples	107- 109
5.8a- 5.8f	Ductilities of untreated and oxidised samples	110- 112
5.9- 5.12	Flow curves of the untreated and treated samples at room temperature, 265°C, 375°C and 545°C	113- 116
5.13	Results of low cycle fatigue test at room temperature	124
5.14	Results of low cycle fatigue test at room temperature 545°C	125
5.15	Creep test at 550°C	128
5.16	Metallograph	133

5.17-5.33	Fractographs	133-135
5.34-5.44	Fractographs	138-139
5.45	Metallograph	

Nomenclature

k_p	parabolic rate constant
F	arbitrary oxidation rate parameter
σ_u	ultimate tensile strength
σ_y	0.2% offset yield strength
C_h^u, C_h^y	constants, which reflect to lot to lot variability in ultimate tensile strength and yield strength
T	temperature
t_r	rupture life in hours
C_h	lot constant
W	weight gain per unit surface area
t	time
k	rate constant
n	power index which implies the rate law
E_a	activation energy
A	constant
R	universal gas constant
O/M	oxide metal interface

ABSTRACT

Oxidation behaviour of modified 9Cr-1Mo ferritic steel was studied in pure dry oxygen. Isothermal runs were carried out at various temperatures and pressures, ranging from 600°C to 900°C and 202.65 KPa (2 atmospheres) to 911.91 KPa (9 atmospheres) respectively. Rate laws and activation energies were calculated for each temperature and pressure. Effect of time, temperature and pressure on oxidation rate has been described. Beyond 750°C, the oxidation rate tends to be linear for all the different pressures. Oxidation products have been examined systematically, using optical microscopy and X-rays. Thus the various oxide layers have been identified.

The effect of dissolved oxygen in the concentration range 0.06 - 0.14 wt % on mechanical properties (tensile, low cycle fatigue and creep strengths) in the temperature range 23°C to 550°C has been studied. Pure oxygen was dissolved in the samples at 607.92 KPa pressure (6 atmospheres) at 800°C. Tensile tests were done at 23°C, 265°C, 375°C and 545°C; low cycle fatigue tests were done at 23°C and 545°C and creep tests were carried out at 550°C. It is found that with increase in oxygen concentrations and temperature, tensile and fatigue strengths of the alloy are

adversely affected, but creep strength tends to increase. The dissolved oxygen tends to delay the creep failure. The observed variation in strength is attributed to the microstructural changes of the various carbide precipitation sequences taking place during the treatment at different temperatures. The samples tested for mechanical behaviour were examined using SEM, optical microscopy and X-rays.

CHAPTER 1

INTRODUCTION

Ferritic steels are among the most popular construction materials for high temperature power generating industries. Here, one of the most important requirements, other than the good mechanical properties, is the resistance to oxidation and corrosion. If the material is to be used in any gaseous environment like air, O_2 , SO_2 , inert gas or a mixture of several gases, then, the oxidation resistance is very important.

Oxidation leads to the degradation of the alloy and its surface because of the reaction with the gaseous atmosphere. This is a consequence of the innate tendency of the alloy to lower its energy state by forming oxides, sulphides etc. The resistance of the alloy to such interaction determines its ability to function and to be used adequately at high temperatures. Thus for evaluating the oxidation resistance of the alloys, one must determine the extent to which they interact with a particular environment of interest, that is one must know the kinetics from which long term behaviour can be predicted.

There are a number of ferritic steels which are being used for several applications. A great importance has been given to the Chrome-Moly steels, especially in the use of 9-12% Cr ferritic steels for elevated temperature service for both nuclear and

fossil application⁽¹⁻³⁾. A strong recommendation⁽⁴⁾ was made for the development of this modified 9Cr-1Mo ferritic steel to offset the difficulties encountered with commercially available steels of the 8-12% Cr group because of its good corrosion/oxidation resistance, mechanical properties, weldability, fabricability, high thermal conductivity etc. Substitution of 9Cr-1Mo steel for 18Cr-8Ni steels in certain applications will constitute significant conservation of both Chromium and Nickel⁽⁵⁾. Due to these good properties it is being considered for continued extended use as the structural material in nuclear power generation industry like Liquid Metal Fast Breeder Reactor (LMFBR) and Gas Cooled Fast Breeder Reactor (GCFBR). Also this alloy finds use in solar central receivers, fossil system, oil and petrochemical industries, petroleum refining and chemical industries.

A power plant utilized high pressure superheated steam; Advanced Gas Cooled Reactor (AGR) uses carbon dioxide gas as the coolant and a chemical industry requires vessels with high strength for high temperature and pressure. A number of papers have been published about the compatibility of Chrome-Moly steels in steam and carbon dioxide. A number of papers discuss the mechanical property of these in detail^(6,7). However, a very few publications which appeared in literature could highlight the oxidation characteristics of this modified 9 Cr-1 Mo

ferritic steel in pure oxygen at high temperatures and pressures. Also literatures regarding the effect of high pressure oxidation on mechanical properties of this steel are scanty. Present work has been carried out keeping this in view.

1.1 SCOPE OF THE PRESENT WORK

Oxidation behaviour of modified 9Cr-1Mo ferritic stainless steel has been studied in pure dry oxygen at high pressures from 202.65 KPa (2 atmospheres) to 709.26 KPa (7 atmospheres) in the temperature range of 600 °C to 900 °C. Activation energies were calculated from the rate laws determined at each temperature and pressure. Effect of temperature and pressure on the oxidation rate has been described.

Various mechanical properties, viz., tensile, fatigue, creep-fatigue and creep of modified 9Cr-1Mo steel (after oxidation at 607.92 KPa and 800 °C) have been studied at temperatures ranging from 23 °C (room temperature) to 550 °C.

REFERENCES

1. M.G. Robin and J. Birault, 'Design philosophy and functional requirements of a sodium heated steam generator made of ferritic steel,' pp 50-54 in Int. Conf. Ferritic Steels for Fast Reactor Steam Generators, 30 May - 2 June 1977, British Nuclear Energy Society, London.
2. J.K. van Westenbrugge et al., 'Material Selection and Optimization for Post-SNR 300 Steam Generators,' Nuclear Technology 55 (2), 250-258 (November 1981).
3. C. Willby and J. Walser, 'Material choices for the commercial fast reactor steam generators,' pp 40-49 in Int. Conf. Ferritic Steels for Fast Reactor Steam Generators, 30 May-2 June 1977, British Nuclear Energy Society, London.
4. G.W. Cunningham, P. Patriarca, and E.E. Hoffman, 'Ferritic Steels as Alternate Structural Materials for High-Temperature Applications,' pp 3-6, at the ASM International Conference on Production, Fabrication, Properties and Application of Ferritic Steels for High Temperature Applications, Warren, Pennsylvania, Oct. 6-8, 1981.
5. V.K. Sikka, 'Substitution of Modified 9Cr-1Mo Steel for Austenitic Stainless Steel,' ORNL-5841, April 1982.

6. S.J. Sanderson, 'Mechanical Properties and Metallurgy of 9% Cr 1% Mo Steel,' pp 85-99, at the ASM International Conference on Production, Fabrication, Properties and Applications of Ferritic Steels for High Temperature Applications, Warren, Pennsylvania, Oct. 6-8, 1981.
7. Wendell B. Jones, 'Effects of Mechanical Cycling on the Substructure of Modified 9Cr-1Mo Ferritic Steel,' pp 221-235, at the ASM International Conference on Production, Fabrication, Properties and Applications of Ferritic Steels for High Temperature Applications, Warren, Pennsylvania, Oct. 6-8, 1981

CHAPTER 2

LITERATURE REVIEW

The extensive literature review on the modified 9Cr-1Mo steel and the related alloy steels are given in this chapter.

2.1 CONSTITUTION OF THE ALLOY

A stringent composition of the alloy is very much necessary for the betterment of the performance of the ferritic steel in nuclear power generating industries. A minimum of 8-16% Cr in iron is found to form a protective scale in the temperature range of 647-947°C⁽¹⁾. In the early stages when the chromium content is low, the oxidation rate is very rapid. As soon as the scale of iron-chrome spinels⁽¹⁾ [(Cr,Fe)₂O₃ and/or FeCr₂O₄] are formed the protective effect is accomplished⁽²⁻⁴⁾. For high temperature oxidation resistance, carbon should be kept as low as possible⁽⁵⁾. Molybdenum enriched in iron helps in forming a passive film⁽⁶⁾. Small quantities of this element is tolerated, but large quantities lead to catastrophic destruction of the oxide⁽⁷⁾. Molybdenum a good carbide former, added in small quantities (0.5-1.0% sufficient to combine with carbon) gives good oxidation resistance and improves the creep and tensile strength of steel⁽⁸⁾. Ralph⁽⁹⁾ recently suggested various alloys formed by combination of Chromium and Molybdenum which have excellent corrosion resistance.

Vanadium and niobium are also good carbide formers, even small amounts less than 1% can be important. They improve the high temperature mechanical properties⁽⁸⁾. Silicon additions to steels are beneficial^(10,11) in high temperature oxidation. Its use is restricted because of the marked embrittlement of the alloy when its amount exceeds 2-3%. Also the higher percentage of silicon leads to high ductile to brittle transition temperature, low impact energy and an early onset of tertiary creep⁽⁸⁾.

The oxidation/sulphidation resistance of ferritic stainless steels is better than austenitic stainless steels. The Chromium depletion is less in ferritics than in austenitics. So ferritic stainless steels are more resistant to corrosion⁽¹²⁾. So all these have led to the development of modified 9Cr-1Mo ferritic stainless steel.

2.2 OXIDATION OF IRON

Iron is one of the most important metals which has been studied very elaborately. The equilibrium diagram of the iron-oxygen system is given in Fig. 2.1 taken from Hansen's monograph⁽¹³⁾ superimposed with the results of Engell⁽¹⁴⁾ and Marion⁽¹⁵⁾. Iron forms three stable oxides: Wustite, FeO, magnetite, Fe₃O₄, and hematite, Fe₂O₃. Wustite, FeO is a p-type conductor. The defects consists of vacant cation sites and an equivalent number of electron defects represented chemically by trivalent Fe³⁺ ions. Consequently, diffusion is essentially cationic via vacant cation sites. Magnetite, Fe₃O₄ also exists

with an excess of oxygen, but the excess is much smaller than with Wustite, and the defect concentration is correspondingly less. Results of Himmel et al.⁽¹⁶⁾ and Davies et al.⁽¹⁷⁾ shows that both cations and anions diffuse in Fe_3O_4 . Hematite, Fe_2O_3 is an n-type conductor⁽¹⁸⁾ in which anions largely diffuse⁽¹⁷⁾.

Above 250°C and at normal pressures of air or oxygen, the oxidation rate of iron has been found to be parabolic^(10,19-21). Fig. 2.2 shows the dependence of parabolic rate constant on temperature taken from the results of Davies et al.⁽¹⁷⁾ and Schmahl et al.⁽²²⁾. There is a distinct break in the curve at about 600°C which has also been observed at slightly lower temperatures⁽²²⁻²⁴⁾. The break at $560-600^\circ\text{C}$ is due to the fact that FeO is not stable in bulk below 570°C , according to the equilibrium diagram (Fig. 2.1), although it may continue to be present in the form of a thin film adjacent to the iron surface down to 400°C (25,26).

Paidassi⁽²⁷⁾ could describe from micrographical work the growth rates of the three oxides individually in terms of thicknesses as follows :

$$\text{Growth of FeO} : k'_p = 5.75 e^{-40500/RT} \text{ cm}^2 \text{ sec}^{-1}$$

$$\text{Growth of Fe}_3\text{O}_4 : k'_p = 1.05 \times 10^{-2} e^{-40500/RT} \text{ cm}^2 \text{ sec}^{-1}$$

$$\text{Growth of Fe}_2\text{O}_3 : k'_p = 5.4 \times 10^{-4} e^{-40500/RT} \text{ cm}^2 \text{ sec}^{-1}$$

The total growth rate,

$$k_p' = 6.1 e^{-40500/RT} \text{ cm}^2 \text{ sec}^{-1}$$

agrees well with Davies, Simuad and Birchenall⁽¹⁷⁾. As we see, the growth rate of Wustite is here much greater than that of the other two oxides.

Effect of oxygen pressure on the oxidation of iron was studied by Caplan et al.⁽²⁸⁾ at 500°C. They found that the oxidation was lower at 10 torr than at 760 torr owing to greater separation between the oxide and metal. Cold worked iron oxidizes faster than annealed iron since, Fe₃O₄ formed on cold worked iron either has leakage paths for easy diffusion or a steep cation vacancy or both⁽²⁹⁾. Impurities change the oxidation of annealed iron since the contact at Fe₃O₄-Fe interface is affected and increase the oxidation of cold worked iron by increasing the amount and persistence of the cold work effect.

Fig. 2.3 shows a simplified picture of the oxidation of iron above 600°C⁽³⁰⁾. The diffusion of oxygen in FeO and in Fe₃O₄ cannot be ruled out⁽³¹⁾. Dunnington et al.⁽³²⁾ found that vacancies formed in Wustite may diffuse across, so that one of the two interfaces may act as a sink for vacancies produced on both the sides. Tylecote et al.⁽³³⁾ produced additional evidence for this mechanism and proved that the main transport in Wustite is doubtless by cations.

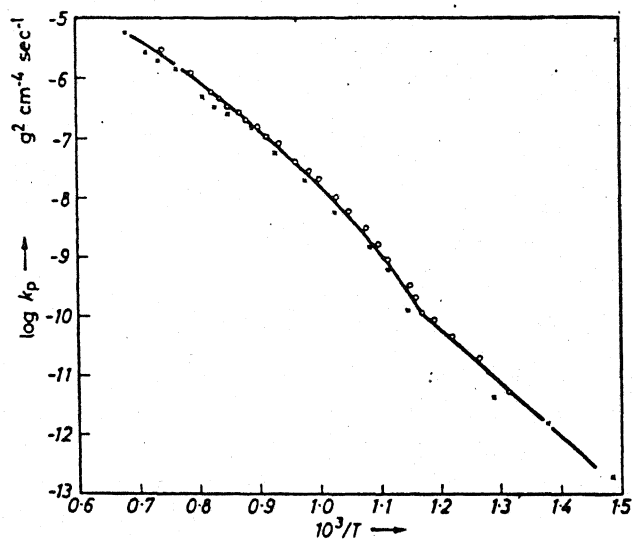
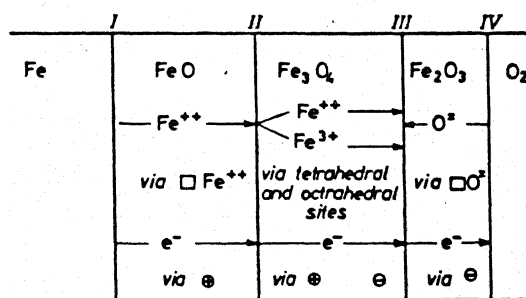


Fig. 2.2 Relation between rate constant and temperature on the oxidation of high purity Iron⁽¹⁷⁾



Phase boundary reactions:

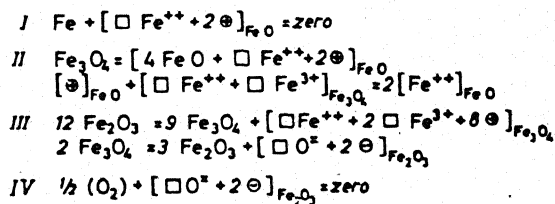


Fig. 2.3 Oxidation mechanisms of Iron above 600°C (30)

Below 700°C , the relative proportions of FeO and Fe_3O_4 in the scale does not appear to remain constant with time, but Fe_3O_4 is present in decreasing proportions⁽²⁴⁾. Below 570°C , FeO disappears almost completely. The results of Vernon et al.⁽³⁴⁾ who worked at low temperatures show that there is a pronounced change in the mechanism of oxidation of iron at about 200°C . Above this temperature, oxidation is essentially parabolic^(35,36); below it becomes logarithmic^(34,37,38).

2.3 OXIDATION OF THE ALLOYS OF IRON

There are extensive literatures on the oxidation resistance of steels, including stainless steels, chrome-moly steels, which are among many of the alloys at present in use as corrosion and oxidation resistant materials.

As regards the Fe-C alloys, the effect of carbon on the reactions of iron with oxygen containing gases is largely determined by the effect of decarburization above 700°C ^(10,39). Carbon containing iron in contact with even small concentrations of oxygen in the gas develops an appreciable carbon monoxide pressure depending on temperature, carbon concentration in the steel, and oxygen concentration in the gas. The irregular oxidation curves obtained in normal air with steels containing 0.15-0.9% carbon between 950°C and 1100°C by Siebert⁽⁴⁰⁾ are due to decarburization effect only. No such irregularities occur with high-purity iron low in carbon^(10,40). So for high-

temperature oxidation-resistant steels the carbon content should be a bare minimum.

Silicon addition (3-10%) is beneficial on the oxidation resistance of iron at 890-1000°C^(10,11,41). Fig. 2.4 also depicts the same trend. In that figure, the curve is for α Fe-Si from Schmahl et al.⁽⁴²⁾ after 4 hours of oxidation at 890°C. Silicon is oxidized preferentially in steel^(43,44) and it appears to have a low diffusion rate in the oxide layers. Thus the layer closest to the metal surface contains an excess of silicon compared with the metal phase, while very little is present in the outer layers⁽¹¹⁾. The effect of sulphur upto 0.016% on the oxidation resistance of iron was investigated between 900°C and 1200°C^(11,45), but no notable changes were observed. With sulphur contents higher than are usual in commercial steels, considerable attack by air occurred. This is due to the formation of sulphur dioxide. The addition of Nickel (2-6%) on the oxidation resistance of iron in air has very little effect⁽¹¹⁾. There is slight improvement with alloys of higher nickel content⁽²⁰⁾, and alloys with 30-42% Ni oxidize 30-40 times less than pure iron.

Small concentrations of molybdenum, upto a few percent improve the oxidation resistance of iron at 600-1000°C^(11,46) (refer Fig. 2.4). This is due to the formation of FeMoO_4 near the interface below 620°C, or $\text{Fe}_4\text{Mo}_6\text{O}_{16}$ ⁽⁴⁶⁾, compounds in which

the diffusion rates may be less than in Fe_3O_4 . More detailed studies of Fe-Mo alloys have been carried out by Brenner⁽⁴⁷⁾ at 800-1000°C. Molybdenum upto 20% decreases the oxidation rate of iron in oxygen at atmospheric pressure, the most marked decrease occurring with the addition of the first 2% Mo. The effect of molybdenum in decreasing the oxidation rate of iron can be attributed to the disappearance of the cation deficient Wustite normally found in iron at temperatures above 570°C. In the Fe-V alloys, vanadium is enriched in the oxide layers adjacent to the metal, and little is found in the upper layers^(11,45,48), owing to the relatively high free energy of formation of vanadium oxides and low diffusion rates of vanadium ions. Vanadium does not contribute to improvement of the oxidation resistance of steels^(11,49). Because of the very good oxidation resistance of Fe-Cr alloys, it has been dealt separately as given below.

2.4 OXIDATION OF IRON-CHROMIUM ALLOYS

Steels containing chromium are among the best oxidation resistant commercial alloys. In the first stages of oxidation of iron-chromium alloys, the rate of reaction is fairly rapid. Until a film thickness of 1000 Å is built up, the resistance to oxidation is less even than that of plain carbon steels⁽⁴⁾. As soon as a layer of $(\text{Cr,Fe})_2\text{O}_3$ and/or FeCr_2O_4 is formed, a protective effect is accomplished⁽²⁻⁴⁾. While low-chromium steels

show an oxidation resistance little better than iron, amounts of more than 12% Cr below 1000°C , and more than 17% above 1000°C , increase the oxidation resistance almost a hundred fold (10,11,50) (Refer Fig. 2.4).

When iron is alloyed with small amounts of chromium (4.7 at %) the oxidation kinetics transformed from parabolic to logarithmic and on further increase of chromium (from 4.7 to 17.2 at %) the oxidation rate reduced at 300°C . Driscoll et al ⁽⁵¹⁾ interpreted that chromium addition may alter the electronic properties of the metal-oxide interface in such a way, as to increase the energy difference between the metal Fermi level and conduction band in the oxide. As the Cr content increases, the rate limiting step of electron tunneling is reduced and so the oxidation rate reduces.⁽⁵²⁾ This interpretation is different from the accepted mechanism where the rate limiting step in the oxidation of Fe at 300°C is by the diffusion of Fe ions through previously formed oxide layer⁽⁵³⁾ and by adsorption, dissociation and incorporation of oxygen in the oxide surfaces⁽⁵⁴⁾.

Footner et al ⁽⁵⁵⁾ examined the kinetics of oxidation of Fe-Cr alloys in the range of 0-50 % Cr. Seeing his results from Fig. 2.5, it is found that the initial addition of chromium to iron results in a large decrease in the rate of the reaction. This is due to the elimination of Wustite as a scale-component

and the progressive appearance of chromium rich oxides. At about 20 and 30 wt % Cr, a minimum and maximum in the oxidation rate is reached respectively. Any further addition in chromium beyond 30 wt % brings down the rate and it becomes a constant after the chromium concentration is increased beyond 50 wt %. For Mortimer et al (56,57), the parabolic rate constant showed a minimum at 16-22% Cr for all temperatures between 923 and 1223 K. Results of Wood et al (58) (refer Fig. 2.6) also confirms the same. Electrical conductivity measurements of this oxide showed a minimum which is due to minimum in concentration of defects associated with p to n type transition of the oxide (59) as it is much evident from Fig. 2.7.

The mechanism of oxidation is essentially the same in oxygen, air, water vapour and carbon dioxide, namely the break-through of an initially protective Cr_2O_3 rich layer followed by growth. However, the actual rate may show considerable variation. It is reported that the oxidation is slower in air. Studies have been conducted in dry air and dry oxygen (59). Somewhat similar behaviour is observed in the two environments but the growth rate in the initial stages and the eventual break-through is appreciably faster as the partial pressure of oxygen is increased.

Gertsricken et al (60) have investigated the effects of various third metals (1% each) on the diffusion rate of chromium

in iron at 950-1050°C. Tin increases the rate, tungsten and nickel have little effect and Ti, Si, Nb and Be decrease it by a half to one power of ten. Molybdenum, silicon and carbon should be in small amounts to increase the oxidation resistance of the iron-chromium alloys.

2.5 STUDY OF CHROME-MOLY FERRITIC STAINLESS STEELS

It has been shown by Leslie et al ⁽⁷⁾ that a high molybdenum content in iron-chrome alloys are 'catastrophic' and are subject to very rapid oxidation. Brenner⁽⁶¹⁾ has shown that the addition of chromium to binary iron-molybdenum alloys induces catastrophic oxidation in certain concentration ranges indicated by the shaded areas of Fig. 2.8. The situation appears to depend on the Molybdenum and Chromium contents in the steel and on the temperature. Ralph⁽⁹⁾ has recently suggested various alloys formed by the combination of chromium and molybdenum which have excellent corrosion resistance. For example, 18 Cr-2 Mo steel has got superior corrosion resistance than that of AISI type 304, 26 Cr-1 Mo is a very good corrosion resistant alloy in caustic environment, other 9 Cr-1 Mo steel (both British commercial and modified form) ferritic steel, 2.25 Cr-1 Mo, 9 Cr-2 Mo (EM 12) etc. are very good high temperature oxidation resistant materials.

From Fig. 2.9 ⁽⁶²⁾, it is evident that the ferritic steels, have good strength over a wide range of temperature. There are

a number of ferritic steels which are being used for several applications. Of late, a high-level interest has come in the use of 9-12% Cr ferritic steels for elevated temperature service for both nuclear and fossil energy applications^(63,64). A great importance has been given to the development of this modified 9 Cr-1 Mo ferritic steel to offset the difficulties encountered with the steels of 8-12% Cr⁽⁶⁵⁾ because of good oxidation/corrosion resistance, mechanical properties etc.

Regarding the other important chrome-moly ferritic steels, Rolls et al⁽⁶⁶⁾ while studying the mechanism of scale detachment from the Fe-Cr-Mo alloy at elevated temperatures, reported that the scale formed on 1 Cr-0.5 Mo alloy is dependent on the silicon content of the alloy. Pritchard et al⁽⁶⁷⁾ reported that 1 Cr-0.5 Mo alloy undergoes breakaway oxidation in 20 atmosphere CO₂ at 500°C in about 2200 hours, compared to the plain mild steels which undergo breakaway oxidation in the same atmosphere in about 200-400 hours. Pinder⁽⁶⁸⁾ reported the variations in the oxides formed during air oxidation of 5 Cr-1 Mo steel as a function of temperature. These results showed that spinel formation is favourable at high temperatures. Beneficial effect of Si is again confirmed⁽⁶⁹⁾ on 5 Cr-0.5 Mo steel in one day air exposure at 750°C as shown in Fig. 2.10.

Modified 9 Cr-1 Mo ferritic steel is considered to be the best construction material in nuclear electric power generating industry. Fig. 2.11⁽⁷⁰⁾ shows the steam oxidation property of this alloy at 600°C. The anti-oxidation property of this modified steel is comparable with that of stainless steels. Here the exfoliation of scale formed was not detected upto 2000 hours.

As regards the mechanical properties, the modified 9 Cr-1 Mo ferritic steel is stronger than standard 9 Cr-1 Mo steel and has better ductility behaviour than reported⁽⁷¹⁾ for EM12 (9 Cr-2 Mo French steel). The thermal expansion coefficient of modified 9 Cr-1 Mo steel is the same as that reported for standard 9 Cr-1 Mo steel⁽⁷²⁾. However, the thermal conductivity of the modified 9 Cr-1 Mo steel is approximately 12% higher than observed for standard 9 Cr-1 Mo steel in the temperature range of room temperature to 700°C⁽⁷³⁾. The oxidation/sulphidation resistance⁽¹²⁾ of the ferritic stainless steels is slightly better than, that of austenitic stainless steels with similar chromium contents. Consideration of chromium diffusion rates in ferritic and austenitic steels indicates that chromium depletion at the corroding metal surface is greater in austenitics than in ferritics. Thus the metallic substrate of ferritics should be more resistant to corrosion following oxide spalling than that of austenitics.

2.6 MECHANICAL PROPERTIES OF MODIFIED 9Cr-1Mo FERRITIC STEEL

2.6.1 Tensile Strength

The study of tensile strength on this alloy by M.K. Booker et al⁽⁷⁴⁾ reveals (Fig. 2.12 a and b) that the yield and ultimate tensile strengths of the modified 9Cr-1Mo steel is consistently stronger than the British commercial 9Cr-1Mo steel⁽⁷⁵⁾ from room temp. to 700°C; above 600°C, the ultimate tensile strengths of the two materials appear to be quite close. The American annealed 9Cr-1Mo is weaker than any of the above materials. The modified and British materials exceed 304 stainless steel in ultimate tensile strength upto about 600°C.

According to V.K. Sikka⁽⁷³⁾, the tensile properties of modified 9Cr-1Mo steel are sensitive to strain rate at room temperature and three higher temperatures: 427, 538 and 649°C. The yield and ultimate tensile strengths decreases slightly with decreasing strain rate at room temperature. This occurs without any change in ductility. At 427°C and 538°C strength decreases and ductility increases with decreasing strain rate. At 649°C, strength decreases with some decrease in ductility.

Based on a number of tests on different lots of material, Booker et al⁽⁷⁴⁾ describes the ultimate tensile strength and yield strength (as they were analysed by a lot-centred regression procedure for British 9Cr-1Mo and austenitic stainless steels^(76,77)) as

$$\log \sigma_u = C_h^u - 1.010 \times 10^{-3} T + 4.152 \times 10^{-6} T^2 - 5.644 \times 10^{-9} T^3$$

and

$$\log \sigma_y = C_h^y - 1.508 \times 10^{-3} T + 6.150 \times 10^{-6} T^2 - 7.481 \times 10^{-9} T^3$$

where

σ_u - ultimate tensile strength (MPa)

σ_y - 0.2% offset yield strength (MPa)

T - temperature ($^{\circ}\text{C}$)

C_h^u and C_h^y - constants, which reflect to lot to lot variability in ultimate tensile strength and yield strength.

2.6.2 Fatigue and Creep-fatigue

According to Sikka et al.⁽⁷³⁾, the data available has shown that the modified alloy has about the same fatigue strength as 316 stainless steel in the range of 525 to 593 $^{\circ}\text{C}$. The alloy has superior fatigue life beyond 10^5 cycles to 2.25 Cr-1Mo, standard 9Cr-1Mo and type 304 stainless steel. Also, the fatigue crack growth rate of the modified 9Cr-1Mo steel is approximately the same as that observed for 2.25 Cr-1Mo and HT9 (contains 11 to 12% Cr and 0.17 to 0.25% C and it is strengthened by vanadium and tungsten) in the range of room temperature to 538 $^{\circ}\text{C}$ ⁽⁷⁸⁾.

Jones⁽⁷⁹⁾ who has studied the microstructural changes of this

steel during cycling says that very little microstructural evolution occurs in 1000 hr at 538°C without cycling while extensive changes occur with cycling. The synergism between temperature and mechanical cycling accelerates the development of equiaxed subgrains with low dislocation density and much coarsened MC and $M_{23}C_6$ carbides. The evolution in substructure changes the dominant strengthening mechanism from dislocation substructure and precipitation hardening to interaction solid solution strengthening from Mo and V. An increase in amount of Mo in $M_{23}C_6$ carbides indicate that longer duration creep-fatigue tests would yield even more softening. Wood et al (80) analysed the creep fatigue behaviour of normalized and tempered 9Cr-1Mo steel where it has been shown that imposed creep relaxation dwells have an insignificant effect on the continuous cycling fatigue endurance. Fig. 2.13 (81) shows the superior creep-fatigue strength of 9Cr-1Mo steel over the other 9Cr- Mo variant steels.

2.6.3 Creep Strength

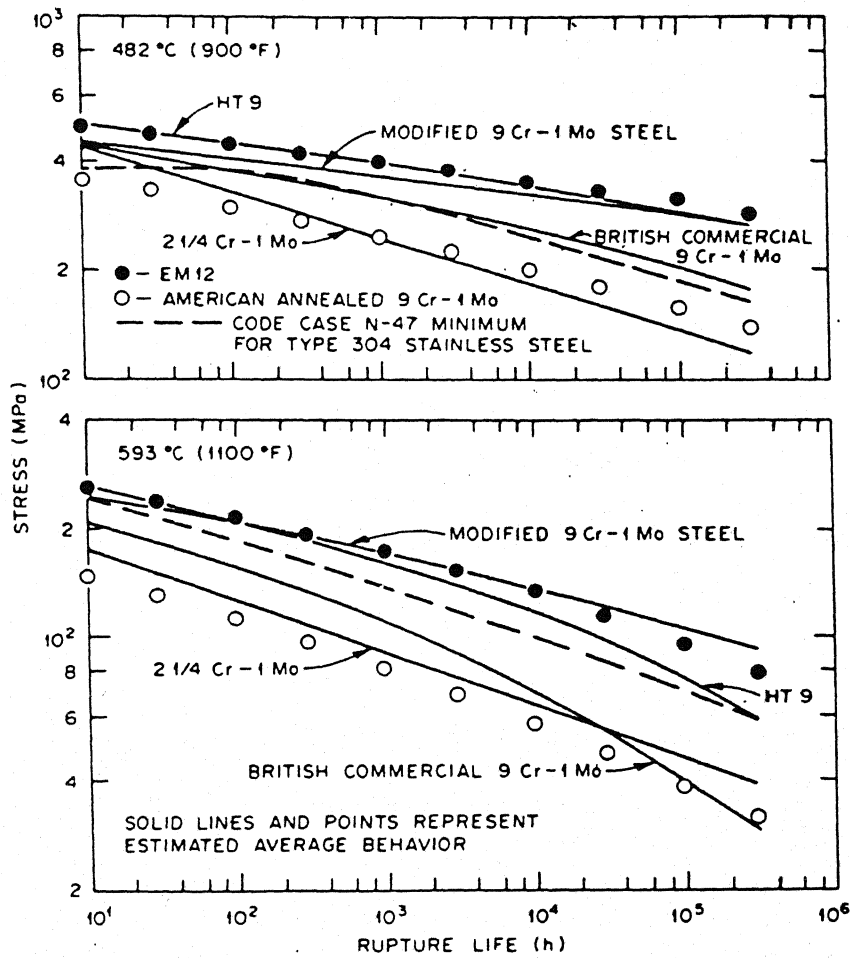
Orr et al. (82) have recently reviewed the physical metallurgy of chromium-molybdenum ferritic steels focussing on the microstructural influence on creep. They concluded that tempered bainite is the optimum structure and that a fine carbide distribution is the best precipitate morphology. The best carbides are those of molybdenum, vanadium or niobium because

they are fine and are very stable. The modified 9Cr-1Mo steel has this type of microstructure and hence its good creep behaviour.

Sikka⁽⁷³⁾ reports that the modified 9Cr-1Mo steel is much stronger than both Standard 9Cr-1Mo and EM12 for the entire creep temperature range. Also modified 9Cr-1Mo steel has better ductility behaviour than reported⁽⁷¹⁾ for EM12. Higher creep strength is also accompanied by total elongation and reduction of area values higher than 15% and 70% respectively. The creep strength of the alloy also matches the minimum strength for type 304 stainless steel upto 649°C. High creep strength of this alloy provides design allowable stresses that exceed those of 2.25Cr-1Mo to 12Cr-1Mo steels for the entire temperature range and those of type 304 stainless steel through 625°C. Fig. 2.14⁽⁷⁴⁾ shows the estimated overall average stress-rupture isothermals for various materials examined at temperatures of 482°C and 593°C. It is found that the modified 9Cr-1Mo has a higher estimated strengths than the annealed 9Cr-1Mo and 2.25Cr-1Mo steels.

Booker et al.⁽⁷⁴⁾ has analysed the creep rupture data using lot-centred regression^(76,77) with a generalized model selection procedure. Using this procedure the creep rupture data for modified 9Cr-1Mo can be written as,

$$\log t_r = C_h + a_1 \sigma + a_2 \log \sigma + a_3/T$$



where

T - temperature (K)

t_r - rupture life (h)

σ - stress (MPa)

a_1, a_2, a_3 - regression constants

C_h - lot constant .

Fig. 2.15 shows the comparison of the maximum allowable stress (S_o) and allowable stress intensity (S_{mt}) of the modified 9Cr-1Mo steel with the other Chrome-moly steels. The modified 9Cr-1Mo steel surpasses all the other ferritic materials in terms of allowable stress, yielding S_o values greater than or equal to those for 304 stainless steels upto 600°C and S_{mt} values greater than or equal to those for the stainless steel upto 625°C .

The overall conclusion is that the modified 9Cr-1Mo steel displays tensile and creep strengths comparable or superior to other ferritic materials and it is comparable to type 304 stainless steel from room temperature to about 625°C . These strength properties combined with other excellent characteristics like oxidation resistance, should make this material a prime candidate for use in future elevated temperature systems.

REFERENCES

1. A.U. Seybolt, J. Electrochemical Society, vol. 107 (1960) p. 147.
2. Yearian H.J., Randell E.C. and Longo T.A., Corrosion 12 (1956) 515t
3. Yearin H.J., Derbyshire W.D. and Radavich J.F., Corrosion 13 (1957) 597t
4. McAdam D.J. and Geil G.W., J.Res.Nat.Bur. Stand 23 (1939) 63.
5. O. Kubaschewski and B.E. Hopkins, 'Oxidation of Metals and Alloys', Butterworths, 1962.
6. T.N. Rhodin, Corrosion, 12 (1956), 123t, 465t.
7. Leslie W.C. and Fontana M.G., Trans. Amer.Soc.Metals 41 (1949) 1213.
8. Finne et al., Creep of Engineering Materials.
9. J.C. Ralph et al., Proc. 6th Int.Conf.on Heat Transfer, (Utah 14-17 Aug. 1977), 4(1978) 379.
10. Portevin A., Pretet E. and Jolivet H., Rev. Metall. 31(1934) 101, 186, 219.
11. Scheil E. and Kiwit K., Arch. Eisenhüttenw. 9(1936) 405.
12. S.K. Verma, 'Oxidation/Sulfidation Behaviour of Some Ferritic Stainless Steels in High Temperature Coal Gasification Atmospheres', pp 236-254 at the ASM Conf.on Production, Fabrication, Properties and Application of Ferritic Steels for High Temperature Applications, Warren, Pennsylvania, Oct. 6-8, 1981.

13. Hansen M. and Anderko K., Constitution of Binary Alloys, McGraw-Hill, New York, 1958.
14. Engell H.J., Arch. Eisenhüttenw. 28(1957) 109.
15. Marion F., Docum. metall. 24 No.24 (1955) 87.
16. Himmel L., Mehil R.F. and Birchenall C.E., J. Metals, N.Y. 5 (1953) 827.
17. Davies M.H., Simnad M.T. and Birchenall C.E., J. Metals, N.Y. 3 (1951) 889, 5.
18. Anderson J.S., Faraday Soc. Disc. 4 (1948) 163.
19. Pilling N.B. and Bedworth R.E., J.Inst. Met. 29(1923) 529.
20. Heindlhofer K. and Larsen B.M., Trans. Amer. Soc. Steel Treat. 21(1933) 865.
21. Winterbottom A.B., J. Iron St. Inst. 165 (1950) 9.
22. Schmahl N.G., Baumann H. and Schenck H., Arch. Eisenhüttenw. 29(1958) 147.
23. Moreau J. and Bardolle J., C.R. Acad. Sci., Paris 240 (1955) 524.
24. Paidassi J., Bol. Soc. Chil. Quim. 5 (1953) 46.
25. Gulbransen E.A. and Ruka R., J. Metals N.Y. 188 (1950) 1500.
26. Gulbransen E.A. and Hickman J.W., Trans. Amer. Inst. min. (metall.) Engrs. 171 (1947) 307.
27. Paidassi J., Acta Metallurg. 6 (1958) 184.
28. D. Caplan et al., Corrosion Science, vol. 10 (1970) pp 1-8.

29. D. Caplan, G.I. Srouls, and R.J. Hussey, Corrosion Science, vol. 10 (1970) pp 9-17.
30. Hauffe K., Metalloberfläche (A) 8 (1954) 97.
31. Engell H.J. and Wever F., Acta Metallurg. 5 (1957) 695.
32. Dunnington B.W., Beck F.H. and Fantana M.G., Corrosion 8(1952) 2t.
33. Tylecote R.F. and Mitchell T.E., J.Iron St.Inst. 196(1960) 445.
34. Vernon W.H.J., Calnan E.A., Clews C.J.B. and Nurse T.J., Proc. Roy.Soc. (A) 216 (1953) 375.
35. J. Bernard and J. Talbot, Comptes Rendus, vol. 229(1948), pp 912-954.
36. O.A. Tasche, Transactions, American Society for Metals, vol. 42 (1950), p. 641.
37. Kubaschewski O. and Brasher D.M., Trans. Faraday Soc. 55 (1959) 1200.
38. Moreau J. and Cagnet M., Rev. Metall. 55 (1958) 1091.
39. Upthegrove C. and Murphy D.W., Trans. Amer. Soc. Steel Treat. 21 (1933) 73.
40. Siebert C.A., Trans. Amer. Soc. Metals 27 (1939) 752.
41. Evans J.W. and Chatterji S.K., J. electrochem. Soc. 106(1959) 860.
42. Schmahl N.G., Baumann H. and Schenck H., Arch. Eisenhüttenw 30 (1959) 267, 415.

43. Bandel G., Arch. Eisenhuttenw. 15(1941) 271.
44. Baeyertz M., Trans. Amer. Soc. Metals 24(1936) 420.
45. Pfeil L.B., J. Iron St. Inst. 119(1929) 501 123(1931) 237.
46. Rahmel A., Jager W. and Becker K., Arch. Eisenhuttenw. 30 (1959) 351.
47. Brenner S.S., J. electrochem. Soc. 102 (1955) 7.
48. Hickman J.W. and Gulbransen E.A., Trans. Amer. Inst. min. (metall.) Engrs. 171 (1947) 344.
49. Laissus J., Rev. Metall. 23(1926) 155.
50. Heindlhofer K. and Larsen B.M., Metal Progr. 26(1934) Sept., p.34.
51. Driscoll T.J. and Needham Jr. P.B., Oxidation of Metals, vol. 13, No.3 (1979) 283.
52. Leygraf C. and Hultquist H., Surface Science, vol. 66 (1976) 69.
53. Cabrera N. and Mott N.F., Rep. Prog. Phys., vol. 12(1949) 12.
54. Ritchie Z.M. and Hunt G.L., Surface Science, vol. 15(1969) 524.
55. D.K. Footner, D.R. Holmes and D. Mortimer, Nature, 216 (1967) 54.
56. D. Mortimer and M.L. Post, Corrosion Science, vol. 8 (1968) 449.
57. D. Mortimer and W.B.A. Sharp, British Corrosion Journal, vol. 3 (1961) p. 61.
58. G.C. Wood and D.P. Whittle, J. of electrochem. Soc. 115 (1968) 133.
59. J. Croll, Ph.D. Thesis, University of Newsouth Wales, Australia, 1971.

60. Gertsricken S. and Dekhtyar I. YA., J. Tech. Phys., Moscow 20(1950) 1005.
61. Brenner S.S., J. electrochem. Soc. 102 (1955) 16.
62. L.A. Morris in 'Source Book on Materials for Elevated Temperature Applications', Elihu F. Bradley, Ed. ASM, 1979, p.198.
63. J.K. van Westenbrugge et al., 'Material Selection and Optimization for Post-SNR 300 Steam Generators', Nuclear Technology 55 (2), 250-258 (November 1981).
64. C. Willby and J. Walser, 'Material Choices for Commercial fast reactor steam generators', pp 40-49 in Int. Conf. Ferritic Steels for Fast Reactor Steam Generators, 30 May - 2 June 1977, British Nuclear Energy Society, London.
65. G. Cunningham, P. Patriarca, and E.E. Hoffman, 'Ferritic Steels as Alternate Structural Materials for High-Temperature Applications', pp 3-6, at the ASM Int. Conf. on Production, Fabrication, Properties and Application of Ferritic Steels for High Temperature Applications, Warren, Pennsylvania, Oct. 6-8, 1981.
66. Rolls R. and Arnold F.V., Corr. Sci., 16 (1976), 613.
67. Pritchard A.M., Antill, J.E., Cottell K.R.J., Peakall K.A. and Trustwell A.E., Oxidation of Metals, 9(1975) 749.
68. Pinder L.W., Corr. Sci. 20 (1981) 749.
69. NACE - Basic Corrosion Course, NACE, NY, 1975, pp 13-17.
70. Murase S., Shiraishi T., Kamemura Y., Mimino T. and Kanero T., 'The Properties of Modified 9% Cr-1% Mo Steel, Tempaloy F-9', pp 116-130 at the ASM Int. Conf. on Production, Fabrication, Properties and Application of Ferritic Steels for High Temperature Applications, Warren, Pennsylvania, Oct. 6-8, 1981.

71. G. Gunz, 'Main Characteristics of 9% Chromium - 2% Molybdenum - Niobium-Vanadium Steel Tubes: Influence of Composition and Thermal Treatment', pp 164-170, in Int. Conf. Ferritic Steels for Fast Reactor Steam Generators, 30 May - 2 June 1977, British Nuclear Energy Society, London.
72. R.K. Williams et al., 'The Physical Properties of 9Cr-1Mo Steel from 300 to 1000 K', paper presented at the 17th Int. Thermal Conductivity Conference, Gaithersburg, Md., June 15-19, 1981.
73. Sikka V.K., Ward C.T. and Thomas K.C., 'Modified 9Cr-1Mo Steel- An Improved Alloy for Steam Generator Application', pp 65-84 at the ASM Int. Conf. on Production, Fabrication, Properties and Application of Ferritic Steels for High Temperature Applications, Warren, Pennsylvania, Oct.6-8, 1981.
74. Booker M.K., Sikka V.K. and Booker B.L.P., 'Comparison of the Mechanical Strength Properties of Several High-Chromium Ferritic Steels', pp 257-273 at the ASM Int. Conf. on Production, Fabrication, Properties and Application of Ferritic Steels for High Temperature Applications, Warren, Pennsylvania, Oct. 6-8, 1981.
75. British Steelmakers' Creep Committee, BSCC High Temperature Data, Iron and Steel Institute, London (1973).
76. Booker M.K. and Booker B.L.P., Automated Analysis of Creep and Tensile Data for Type 321H Stainless Steel, report prepared for the Metals Properties Council for use by the ASME Subgroup on Strength (September 1979).
77. Booker M.K. and Booker B.L.P., 'New Methods for Analysis of Materials Strength Data for the ASME Boiler and Pressure Vessel Code', pp 31-64 in Use of Computers in Managing Material Property Data, MPC-14, American Society of Mechanical Engineers, New York, 1980.
78. James L.A., Fatigue-Crack Growth Behaviour in Ferritic Alloys for Potential GCFR Structural Applications, HEDL-TME 80-71, Hanford Engineering Development Laboratory, Richland, Wash., December 1980.

79. Jones W.B., 'Effects of Mechanical Cycling on the Substructure of Modified 9Cr-1Mo Ferritic Steel', pp 221-235 at the ASM Int. Conf. on Production, Fabrication, Properties and Application of Ferritic Steels for High-Temperature Applications, Warren, Pennsylvania, Oct. 6-8, 1981.
80. Wood D.S., Baldwin A.B. and Williamson K., 'The Creep/Fatigue Behaviour of 9% Cr Steel at 525°C', Conf. on Time and Load Dependent Degradation of Pressure Boundary Materials, IAEA, Innsbruck, 1978, IWG-RRPC-79/2.
81. Sanderson S.J., 'Mechanical Properties and Metallurgy of 9% Cr 1% Mo Steel', pp 85-99 at the ASM Int. Conf. on Production, Fabrication, Properties and Application of Ferritic Steels for High-Temperature Applications, Warren, Pennsylvania, Oct. 6-8, 1981.
82. Orr J., Beckitt F.R. and Fawkes G.D., 'The Physical Metallurgy of Chromium-Molybdenum Steels for Fast Reactor Boilers', in Ferritic Steels for Fast Reactor Steam Generators, British Nuclear Energy Society, 1978 p. 91.

CHAPTER 3

EXPERIMENTAL

3.1 MATERIAL

Modified 9Cr-1Mo steel was obtained from Oak Ridge National Laboratory, Tennessee, U.S.A. through the kind courtesy of Mr. Ashok K. Khare, Chief Metallurgist, National Forge Company, Pennsylvania, U.S.A. in the form of 25 mm thick plate. The chemical composition of the alloy is given below :

Element	Cr	Mo	V	Nb	C	Mn	Si
Wt %	8.46	1.02	0.198	0.072	0.083	0.46	0.41
	S	P	N	Ni	Fe		
	0.004	0.010	0.051	0.09	Balance		

3.2 PROCESSING OF THE MATERIAL

From the received bulk material, small chips were cut and cold rolled to approximately 1.6 mm thickness without any intermediate annealing followed by degreasing and heating in vacuum (10^{-3} Torr) at 860°C for one hour and furnace cooling. The

heat treatment set-up is shown in Figure 3.3. Specimens for both oxidation studies and mechanical tests were made from these annealed strips.

3.3 HIGH PRESSURE OXIDATION SYSTEM

A system was fabricated with inconel and stainless steel tubes to withstand high pressure and high temperature. All the oxidation studies were done in this set-up only. The block diagram of the system is shown in Figure 3.1. The high accuracy pressure measurement and the control systems are shown in Figure 3.2.

At elevated pressures the system was made leakproof with the help of ferrules in all the joints. These ferrules were of stainless steel or brass. They deform slightly in the grooves of the joints and prevent any gas leaking out. This high pressure oxidation system was checked for leakproof from time to time. A brief note about the various components in this system are given below.

A high accuracy digital pressure indicator (DP1) was attached to this set-up. Its accuracy is 0.05% of the reading and its resolution is 1 part in 10^5 . This DP1 essentially consists of 3 different units, viz.

1. High accuracy Sensor Head (Transducer)
2. Electronics Unit
3. Digital readout.

This high accuracy Sensor Head consists of a diaphragm type variable capacitance pressure transducer and an electronic preamplifier. This has 2 ports and measures the differential pressure in the system connected.

The electronics unit is a self contained signal conditioner with a built-in regulated power supply, 10 kHz oscillator, a high accuracy AC to DC converter to provide a very stable ± 10 V DC output which is linear with pressure. The Sensor Head and the electronics unit provide the minimum necessary configuration required for a conversion of pressure into a usable stable DC output.

The third unit is the mountable digital readout which accepts the analog output from the electronics unit. This gives all the pressure values in the digital form. There is a provision to select the units in which pressure is to be displayed.

The furnace attached to the oxidation system had kanthal wire winding with a uniform temperature zone controlled within $\pm 2^{\circ}\text{C}$ with a help of a temperature controller and a relay unit as shown in Fig. 3.2. A calibrated Pt - 10% Pt.Rd thermocouple was used to record the temperature of the furnace. The junction of the thermocouple was kept closest to the specimen in order to record its temperature as accurate as possible.

The rate of change of pressure in the system during the oxidation study was recorded by an X-Y recorder. This rate of change of pressure was directly proportional to the increase in weight of the sample. A bourdan gauge was also there in the system which indicated the approximate pressure in the tube system. In all the experiments on high pressure high temperature oxidation, pure dry oxygen obtained from Indian Oxygen Limited, Kanpur was used.

Fig. 3.4 shows the calibration curve for this high pressure system.

3.4 OXIDATION STUDIES

3.4.1 Specimen Preparation

Rectangular specimens of surface area ranging from 1-1.5 sq.cm. with 1.5 mm diameter hole at one edge to enhance free hanging were used for oxidation studies. Both the sides and edges of the specimen were polished to 4/0 emery paper and cloth polished with 1 μ m alumina powder. These specimens were washed with distilled water and acetone and finally dried. The weight of the samples before and after the experiment were noted.

3.4.2 Oxidation in High Pressure Pure Oxygen

All oxidation studies were done in the high pressure oxidation system as given under the Section 3.3. The oxidation

behaviour was studied at different temperatures and pressures.

Only one sample was oxidized at a time. Free suspension of the sample was achieved by hanging it from hooks attached with the platinum wire. The furnace was raised to the required temperature and the system was then flushed with pure dry oxygen three times to remove the impurities and it was filled with the required pressure.

All the samples were oxidized for 5 hours continuously and the X-Y recorder was allowed to run simultaneously. The drop in pressure readings were noted down periodically. At the end of the fifth hour the exit valve was opened to remove the pressure from the system and the sample was then slowly taken out of the system and cooled. Finally, the sample was weighed and the weight increase of the sample was noted. The physical appearance and the nature of the oxide scale were also noted.

3.4.3 Examination of Oxidation Samples

The oxidized samples were sandwiched between two perspex slabs and they were kept intact using adhesives. The samples were polished and the cross-section was examined by optical microscope.

3.5 MECHANICAL PROPERTIES

3.5.1 Specimen Preparation

From the processed and annealed material (Refer Section 3.2

rectangular strips with longitudinal axis parallel to the rolling direction were cut and tensile specimens as shown in Fig. 3.5 were made. These specimens were made for tensile strength, fatigue strength and creep study. The two sides of the samples were polished to 4/0 emery paper and the edges also had the same surface finish. The specimens were then washed with distilled water and acetone before using in the experiment. After this the specimens were weighed using a microbalance having a readability of 0.05 mg.

3.5.2 Oxidation in Pure Oxygen

The oxidation was carried out in the high pressure oxidation system as given in the Section 3.3. Only one sample was oxidized at a time. The free suspension of the sample was achieved by hanging it from the hooks with a platinum wire. The furnace was raised to 800°C and the system was then flushed with pure dry oxygen obtained from the Indian Oxygen Limited, Kanpur three times to remove the impurities and filled with a pressure of 607.92 KPa (6 atm.). The samples were oxidized for 30,40,50 and 60 minutes in order to have the required oxygen concentrations in it.

At the end of each run, the exit valve was opened to remove the pressure and the samples were taken out of the system and cooled. Finally, the samples were weighed and the weight increase and the physical appearance were noted.

3.5.3 Mechanical Testing

3.5.3.1 Tensile Testing

All the tensile testings at room temperature and at elevated temperatures were carried out with Instron 1195 model. A cylindrical furnace with kanthal wire winding was used to get the desired temperatures. The furnace consists of 3 zones and the required temperature profiles were obtained by varying the voltage and current settings. These settings were adjusted by trail and error in such a way that the maximum temperature occurs at the specimen and not on the grips. Fig. 3.7 shows the temperature profile of the furnace.

Tensile tests were carried at four different temperatures: 23°C (room temperature), 265°C, 375°C and 545°C. Samples of different oxygen concentrations in the range of 0.06 wt % to 0.14 wt % and an untreated (no oxidation) sample were tested at each temperature in air. For the tensile tests at elevated temperatures, the sample was mounted in the train assembly with the help of a hot die steel grip and the bead of a chromel-alumel thermocouple was tied at the gauge region in order to get the spot recording of the temperature. The temperature variation during test at the gauge region was $\pm 3^{\circ}\text{C}$. The strain rate and the chart speed were constant throughout the tensile testings and they were 1.66×10^{-3} /sec and 20 mm/min. After the sample failure, it was removed from the train assembly and the

fractography was analysed with Scanning Electron Microscope.

3.5.3.2 Fatigue testing at room temperature and at higher temperature

The stresses due to various phases of operation deform the structure plastically and this combined with the thermal stresses due to frequent shut downs, the material experiences cycling effect and its life is reduced. In order to study the combined effect on the strength of the material, the low cycle fatigue test was carried out with 810 Material Testing System. The samples were repeatedly cycled with minimum and maximum load in the tensile region. The waveform of applied load is saw tooth type as shown in Fig. 3.6 . The maximum and minimum loads were selected from the tensile test results done at room temperature. The ratio of minimum stress to maximum stress and frequency of cycling were kept constant throughout the testing as 0.1 and 30 cycles/sec. respectively. Tests were carried out till the failure of samples and the corresponding number of cycles to failure were recorded.

Fatigue testing at 545°C was carried out with Instron 1195 model. Mounting and testing of the samples were done in the same way as that in tensile testing at 545°C . Here during the load cycling, the ratio of minimum to maximum load and the cross-head speed were kept constant throughout the testing as 0.1 and 10 mm/min. respectively. The maximum and minimum loads were

selected from the tensile test results done at 545°C. Here, too, the tests were carried out till the failure of the samples and the corresponding number of cycles to failure were recorded.

3.5.3.3 Creep

Creep tests at 550°C were carried out with SATEC system. Various trail settings for voltage and current were done for three zones of furnace (Kanthal wiring) in order to get 550°C at the sample gauge region. A thermocouple head was tied to the gauge region of sample so that the spot temperature could be recorded. The temperature variation during the test was -2°C to +1°C.

Sample was mounted in assembly, and the furnace was put on. As the temperature stabilizes at 550°C, the stress was applied carefully and the timer was put on. From the trail runs made at different stress values, the initial applied stress of 42 kg/mm² was selected. Instant elongation was noted using Cathedometer (readability 0.01 mm) which was preset on the specific mark on the assembly. Then intermittent elongation was noted till the rupture takes place. At the instant of rupture, the machine stops automatically and gives the time to rupture.

3.6 X-RAY ANALYSIS

X-ray diffraction runs were done on the specimens oxidized at different temperatures and pressures and as well as on the treated and broken test samples. Copper with filter was used as target material. Continuous recording of 2 θ vs Intensity was made by diffractometer. The various oxides have been identified from the values of the peaks.

3.7 METALLOGRAPHY

The mechanical tested samples were mounted on perspex slabs using araldite. The cross-sections were metallographically polished on a wheel where alumina powder of 1 μ m particle size was used as suspension. The polished edge of the sample was then etched with 1% picrol for about 50 seconds and examined under optical microscope and the microstructures were photographed.

3.8 FRACTOGRAPHY

The fracture surfaces of mechanical tested samples were examined in the Scanning Electron Microscope (SEM). An aluminium sample holder with a shift to accommodate the sample and a screw to hold it intact was made. The whole fracture surface was scanned and the notable features were photographed.

CHAPTER 4

OXIDATION STUDIES

The oxidation behaviour of modified 9Cr-1Mo steel at various temperatures and pressures is studied using the Isothermal Thermogravimetric Analysis (TGA). In this chapter the results of the same are presented and the oxidation products are examined and discussed.

4.1 THERMOGRAVIMETRY

This is one of the dynamic techniques where the weight change of the sample is measured as some function of time or temperature. A single dynamic thermal run or several isothermal runs give enough data to calculate the rate, order and kinetic activation energy, of the process just occurred⁽¹⁾. The TGA record contains the weight change of the sample on Y-axis and temperature or time on X-axis.

4.1.1 General Oxidation Equation

Alloy oxidation is generally a complex process because, the metals in the alloy will have different affinities for oxygen which is reflected by the different free energies of formation of oxides. Hence, the alloys do not always oxidize according to one of the classical kinetic expression for diffusion limited reaction.

The general equation for any oxidation process is

$$(W)^n = kt \quad (4.1)$$

where

W is the weight gain per unit surface area in time ' t ',

k is the rate constant and

n is the power index which tells about the particular rate law.

When,

$n = 1$, oxidation rate is linear

$n = 2$, oxidation rate is parabolic

$n = 3$, oxidation rate is cubic etc.

Equation (4.1) can be rewritten after taking logarithms on both the sides as,

$$n \log W = \log k + \log t \quad (4.2)$$

The above relationship given in (4.2) is a straight line equation and the plot of $\log W$ vs $\log t$ will yield a straight line. The slope and the intercept of the line gives the value of n and k respectively. The value of n is not an integer in actual cases and its near value is considered.

4.2 OXIDATION BEHAVIOUR OF MODIFIED 9Cr-1Mo FERRITIC STEEL

Isothermal thermogravimetric runs were carried out at various pressures (202.65 - 911.91 KPa) and temperatures

(600 - 900°C) to find out the kinetics of oxidation. Runs were carried out in pure dry oxygen. Linear plots of weight gain vs. time are given in Figs. 4.1 to 4.9 and the thermogravimetric data are summarized in Tables 1-5 in Appendix A. Fig. 4.10 compares the final weight gain (after 5 hours of oxidation) at 600°C and 900°C for the different pressures). Double log plots of weight gain vs time are given in Figs. 4.11 to 4.19 and the values of n and k obtained from these figures are given in Tables 4.1 to 4.5. Here the double log plot has been divided into different straight lines. The slope and intercept for these segments are calculated and are listed in the tables 4.1 to 4.5.

It is observed from Figs. 4.1 to 4.10, that, upto 700°C for all pressures the initial rate of oxidation appeared to be cubic or parabolic and later with increase in oxidation time, the rates tend to be linear. Beyond 700°C and with increasing pressures, the oxidation rates increases. Between 750°-900°C, oxidation is found to be rapid and approximately linear throughout.

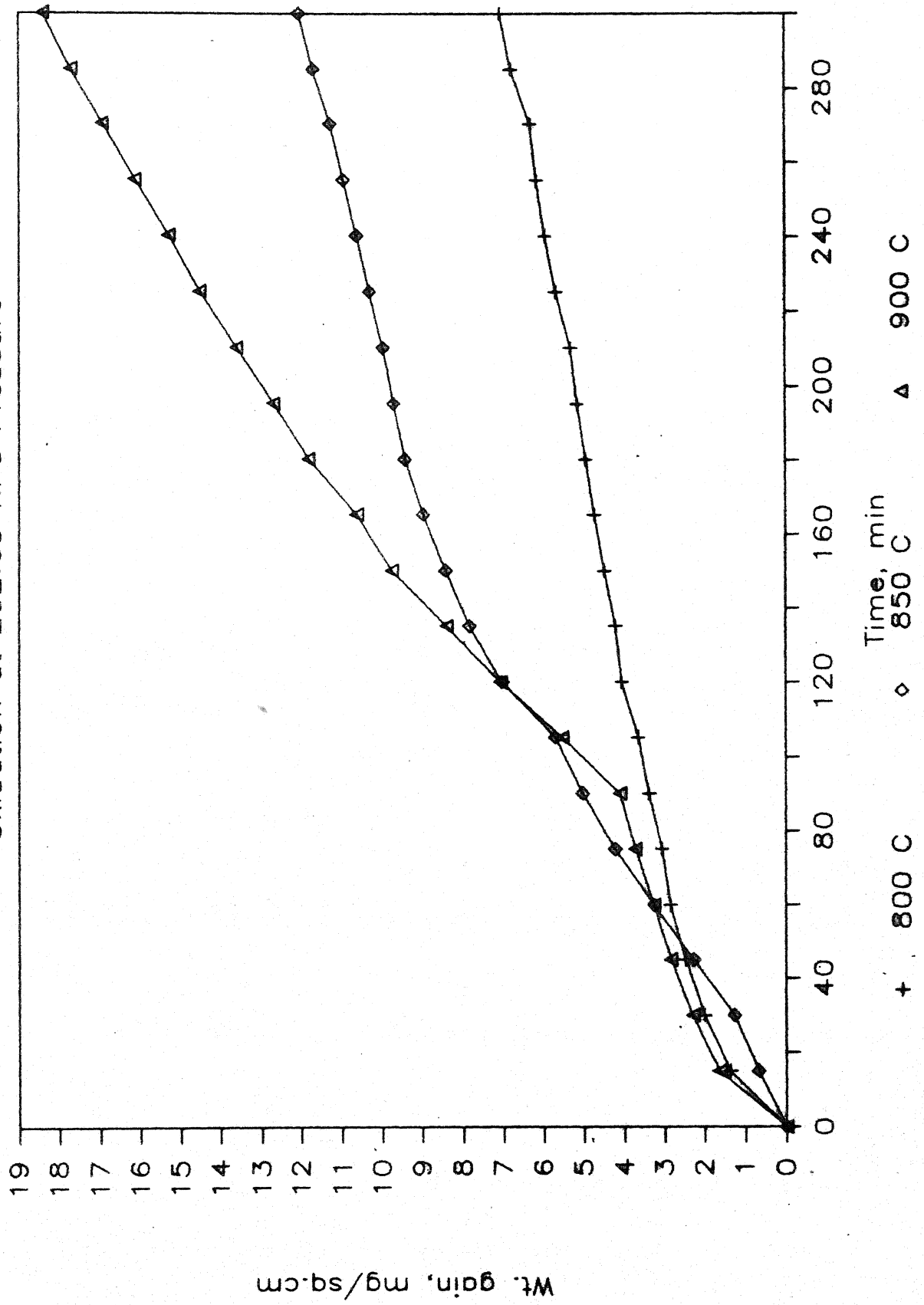
4.2.1 Activation Energy Calculations

As per Arrhenius theory of reaction rates, the rate constant k can be written as,

$$k = A \exp\left(-\frac{E_a}{RT}\right)$$

Fig. 4.2: Plot of wt. gain vs Time

Oxidation at 202.65 kPa Pressure



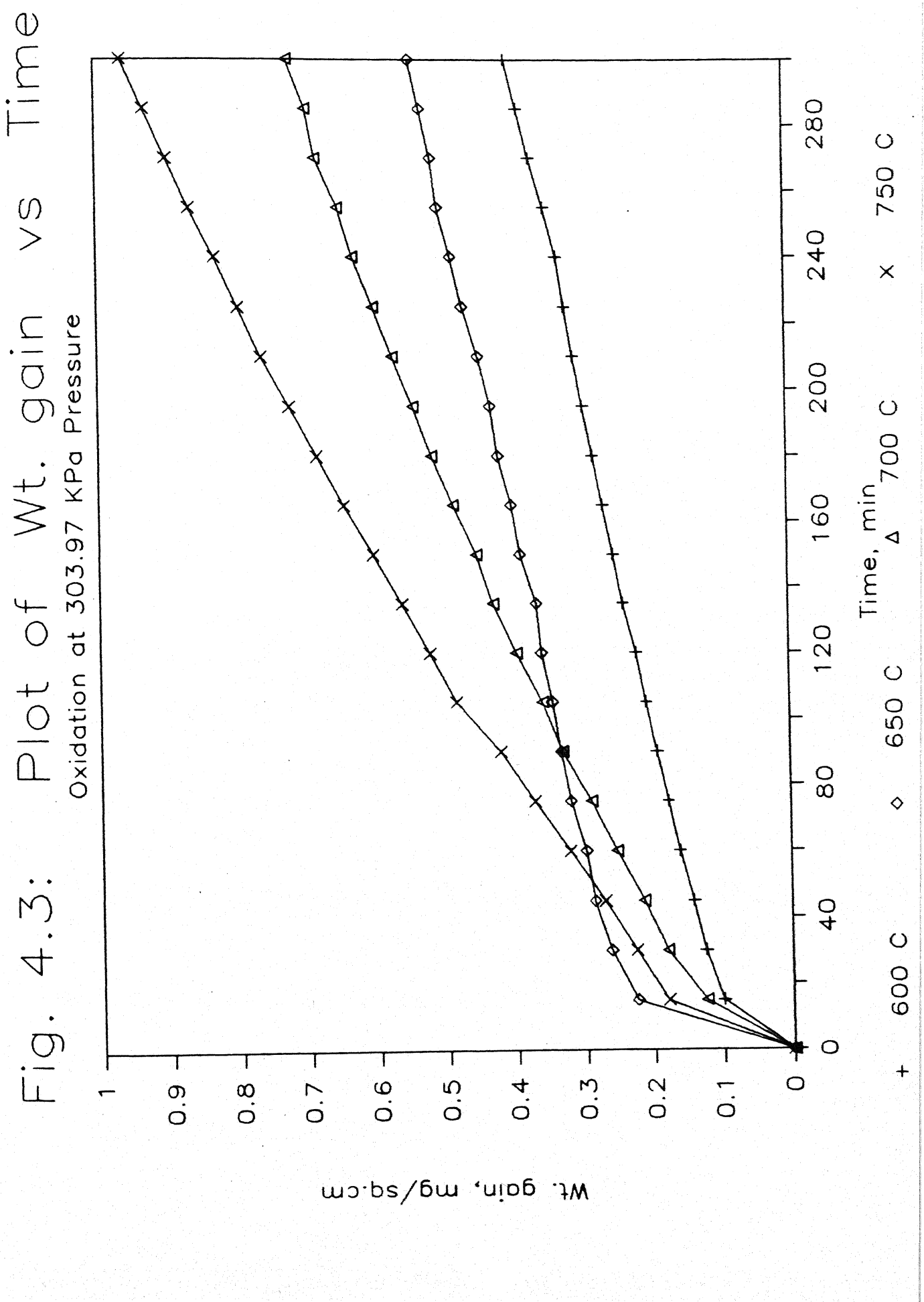
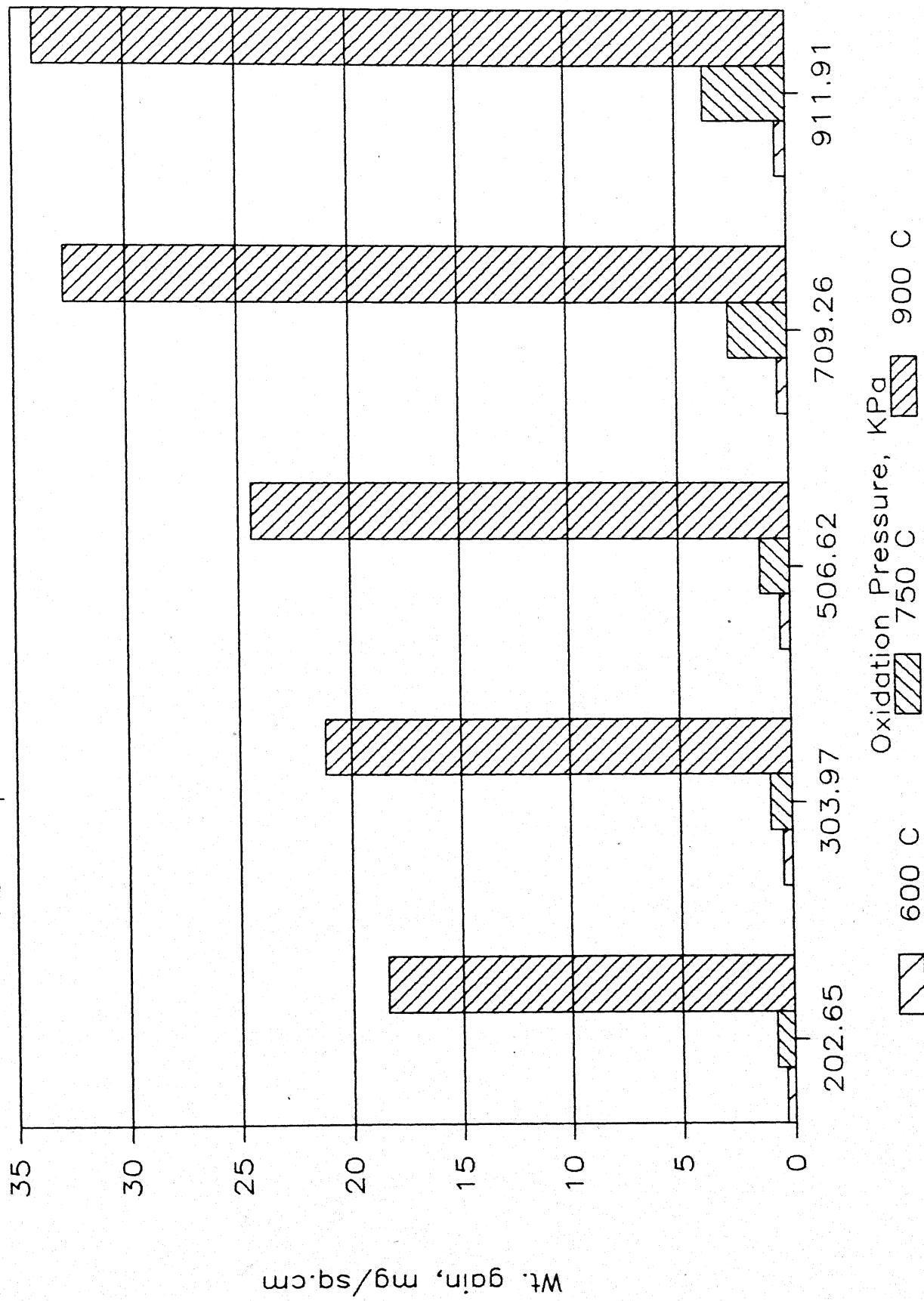


Fig. 4.10 Comparative wt. gains

At Temperatures 600 C, 750 C and 900 C.



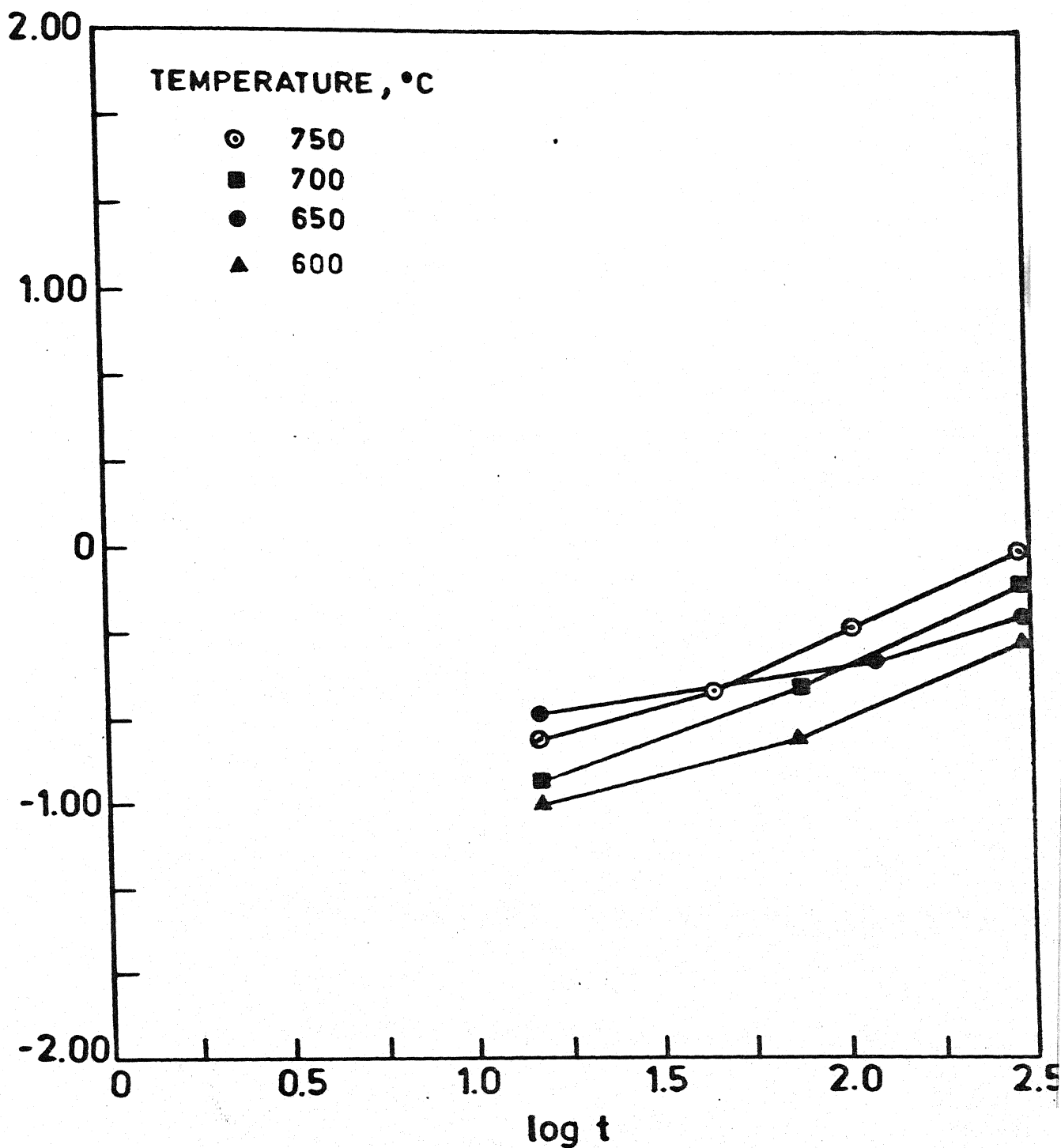


Fig. 4.13 Double log plot of weight gain vs time at 303.97 KPa (3 atm) pressure for various temperatures.

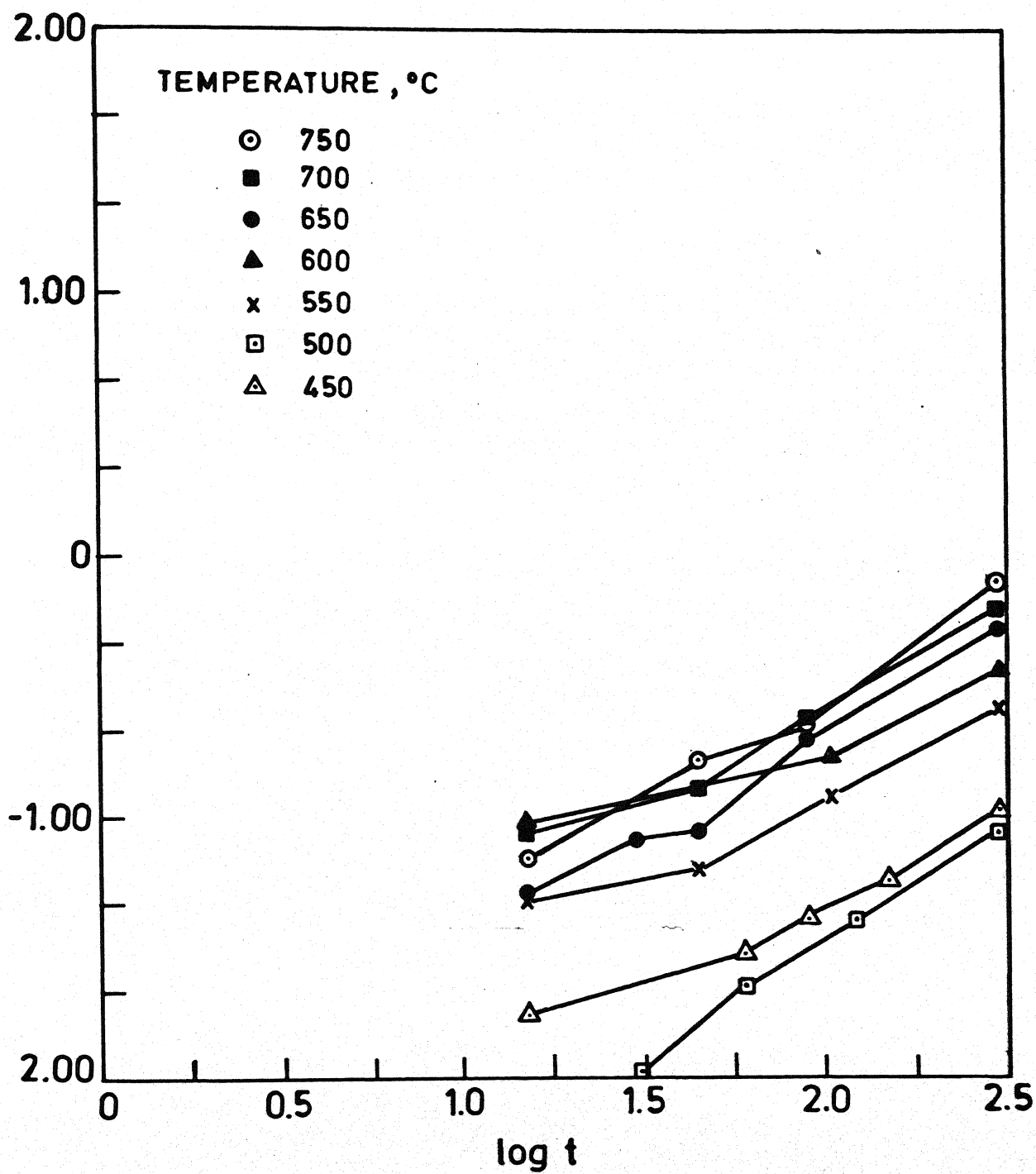


Fig. 3.11 Double log plot of weight gain vs time at 202.65 KPa (2 atm) pressure for various temperatures.

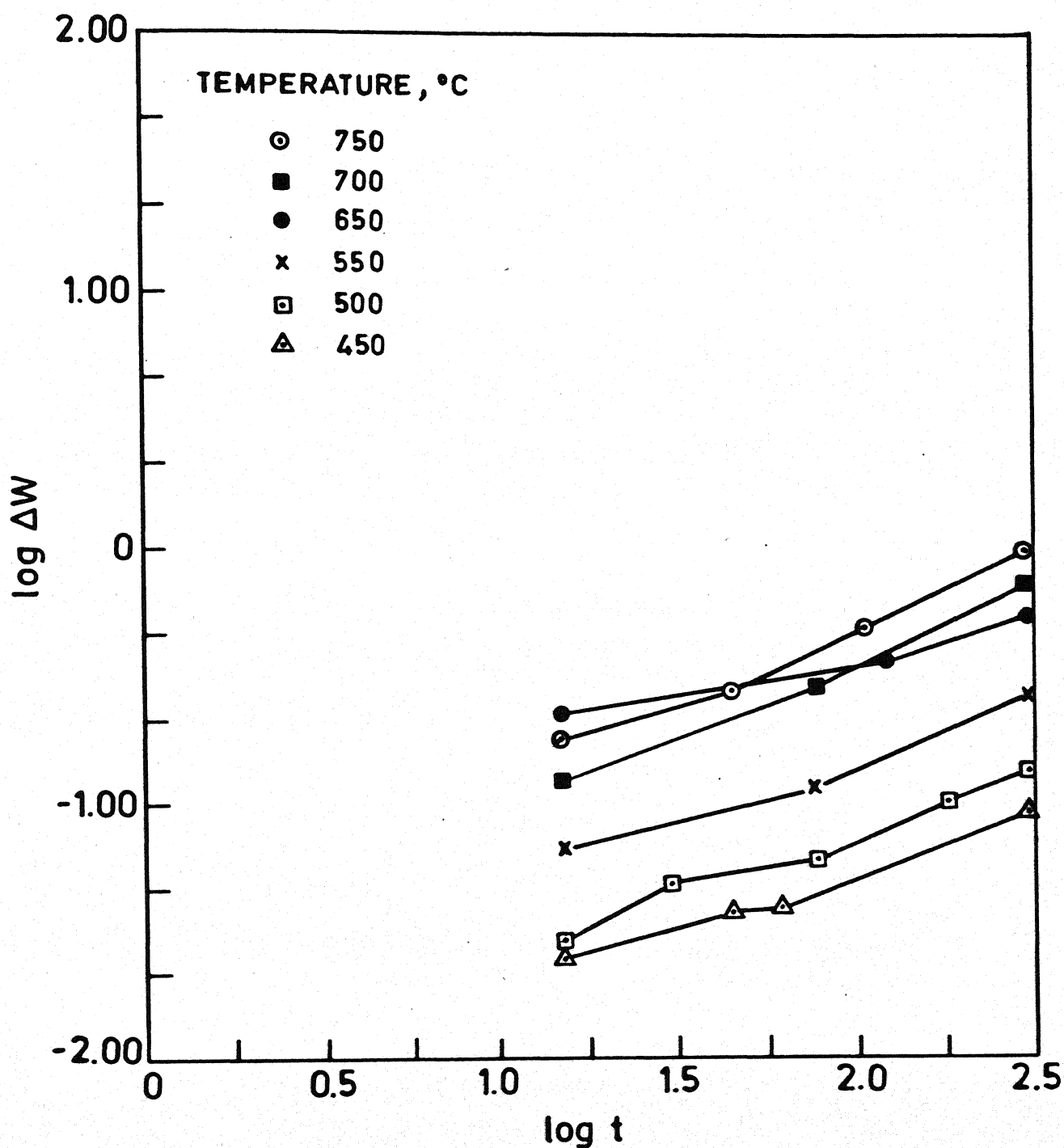


Fig. 3.13 Double log plot of weight gain vs time at 303.97 KPa (3 atm) pressure for various temperatures.

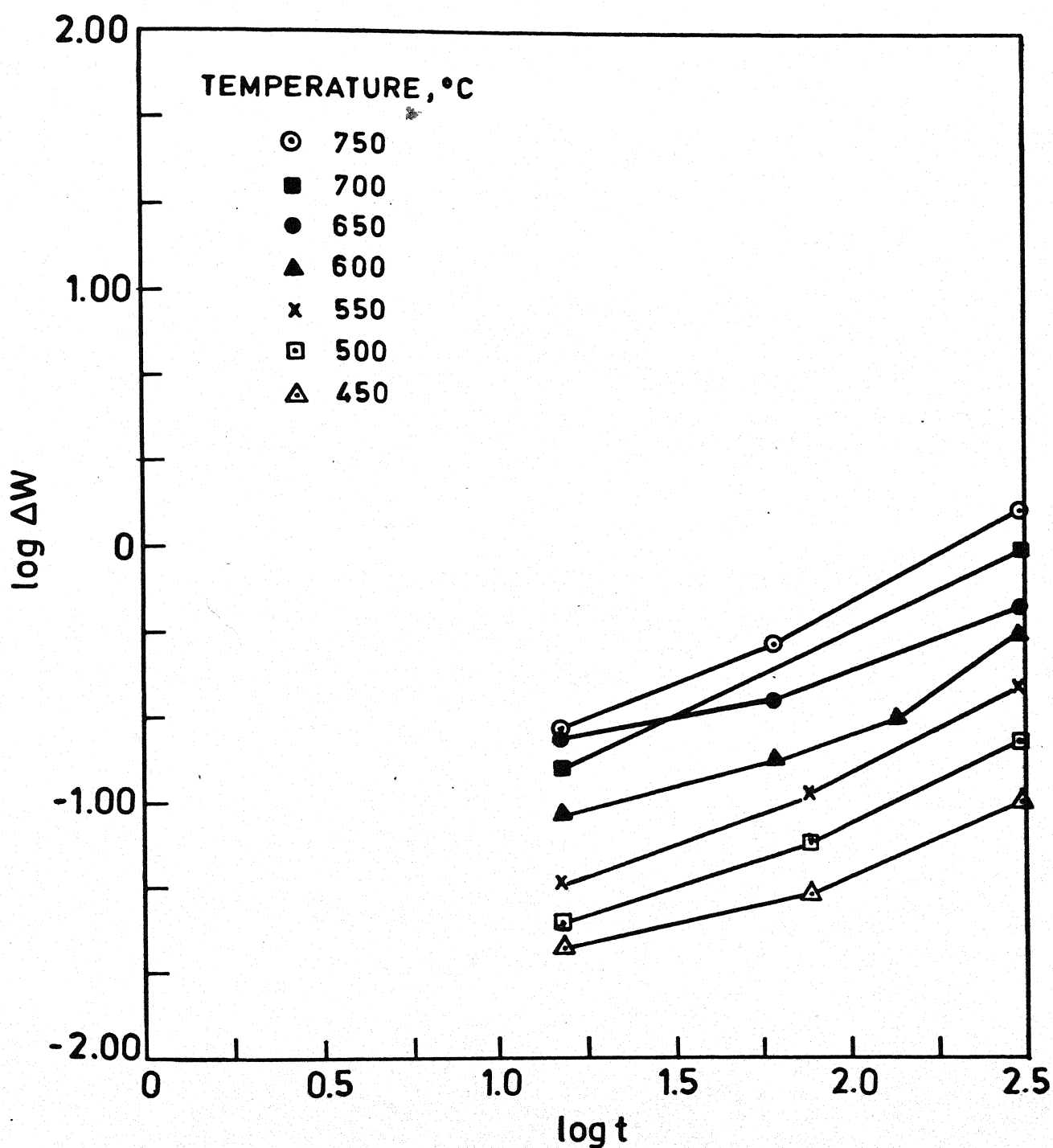


Fig. 3.15 Double log plot of weight gain vs time at 506.62 KPa (5 atm) pressure for various temperatures.

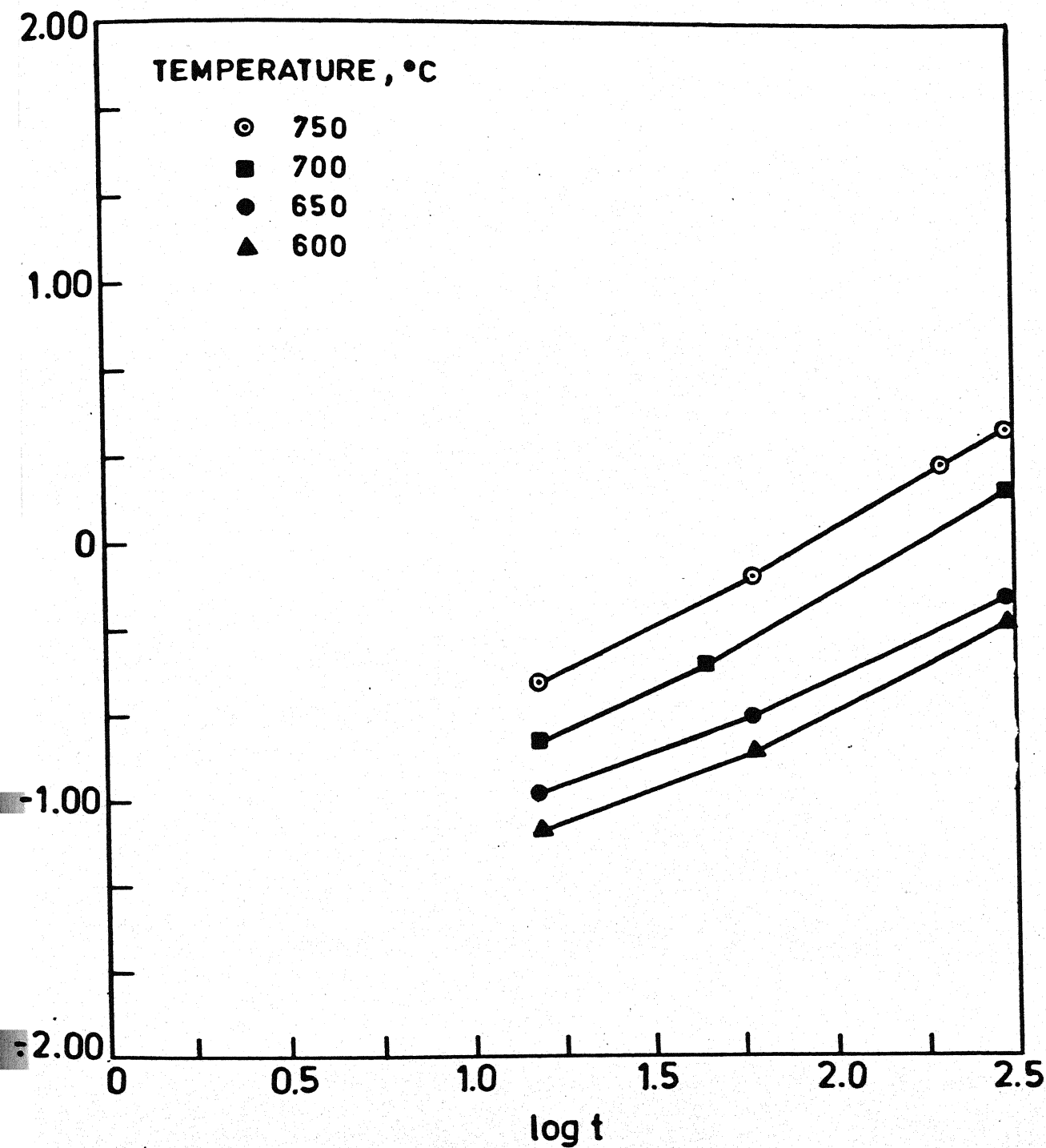


Fig. 3.17 Double log plot of weight gain vs time at 709.26 KPa (7 atm) pressure for various temperature.

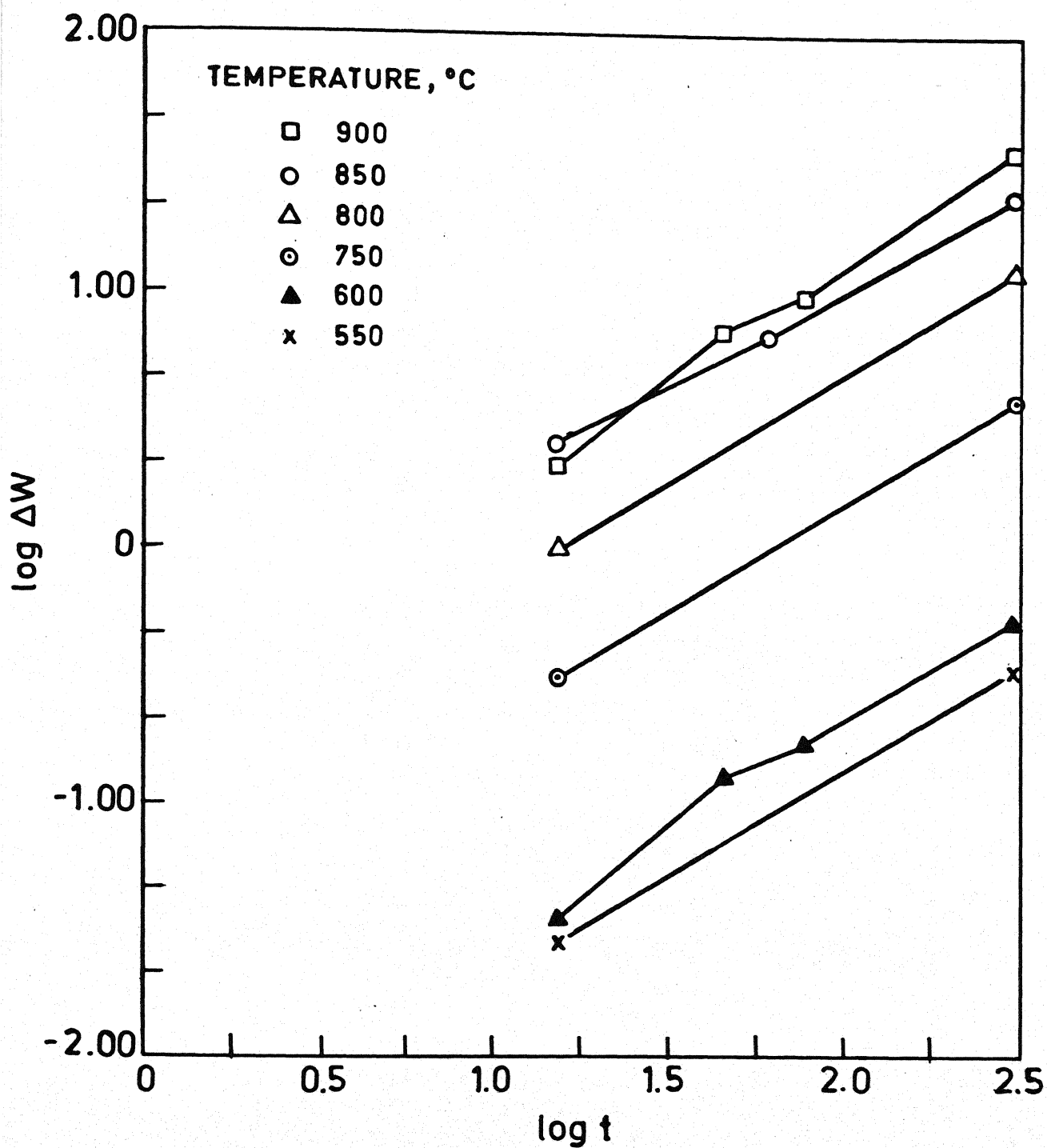


Fig. 3.19 Double log plot of weight gain vs time at 911.91 KPa (9 atm) pressure for various temperatures.

Table 4.1 Variation of n and R according to Equation $(W)^n =$
 Pressure of Oxidation = 202.65 KPa

Temperature $^{\circ}\text{C}$	Time for which ' n ' holds min	Value of n	Value of $k \times 10^{-2}$ $\text{mg cm}^{-2} \text{ min}$
600	0-120	2.91	23.08
	120-300	1.16	12.89
650	0-45	1.50	12.60
	45-300	1.11	8.26
700	0-75	1.27	12.41
	75-135	1.33	1.21
	135-300	1.03	7.48
750	0-45	2.26	19.74
	45-150	1.10	8.99
	150-300	0.96	7.00
800	0-90	1.98	156.00
	90-300	1.67	190.00
850	0-120	0.80	84.04
	120-300	1.87	126.81
900	0-135	1.99	145.67
	135-300	1.01	317.80

Table 4.2 Variation of n and k according to Equation (W) ^{n} = kt .
Pressure of Oxidation = 303.97 KPa

Temperature °C	Time for which 'n' holds, min	Value of n	Value of k $\times 10^{-2}$ mg cm ⁻² min ⁻¹
600	0-75	2.6	25.08
	75-300	1.7	14.89
650	0-300	2.23	25.25
700	0-75	1.39	21.76
	75-300	1.55	17.67
750	0-45	2.68	30.69
	45-105	1.52	19.28
	105-300	1.48	18.96
800	0-30	2.73	75.65
	30-90	1.56	50.71
	90-300	1.51	48.62
850	0-30	2.33	88.34
	30-300	1.54	63.00
900	0-60	1.86	94.41
	60-300	1.57	77.89

Table 4.2 Variation of n and k according to Equation $(W)^n = kt$.
 Pressure of Oxidation = 303.97 KPa

Temperature °C	Time for which 'n' holds, min	Value of n	Value of k $\times 10^{-2}$ mg cm ⁻² min ⁻¹
600	0-75	2.6	25.08
	75-300	1.7	14.89
650	0-300	2.23	25.25
700	0-75	1.39	21.76
	75-300	1.55	17.67
750	0-45	2.68	30.69
	45-105	1.52	19.28
	105-300	1.48	18.96
800	0-30	2.73	75.65
	30-90	1.56	50.71
	90-300	1.51	48.62
850	0-30	2.33	88.34
	30-300	1.54	63.00
900	0-60	1.86	94.41
	60-300	1.57	77.89

Table 4.4 Variation of n and k according to Equation
 $(W)^n = kt$. Pressure of Oxidation = 709.26 KPa

Temperature $^{\circ}\text{C}$	Time for which n holds, min	Value of n	Value of k $\times 10^{-2} \text{ mg cm}^{-2} \text{ min}^{-1}$
600	0-60	1.89	17.44
	60-300	1.40	12.61
650	0-300	1.71	19.20
700	0-45	1.65	22.99
	45-300	2.96	40.98
750	0-60	1.51	27.09
	60-165	1.27	22.11
	165-300	1.19	19.79
800	0-45	1.32	40.18
	45-90	1.44	44.62
	90-300	1.15	32.62
850	0-75	1.13	48.40
	75-150	1.22	54.71
	150-300	1.51	75.35
900	0-300	1.30	68.31

Table 4.5 Variation of n and k according to Equation $(W)^n = kt$.
 Pressure of Oxidation = 911.91 KPa

Temperature °C	Time for which 'n' holds, min	Value of n	Value of k $\times 10^{-2} \text{ mg cm}^{-2} \text{ min}^{-1}$
600	0-45	0.85	5.72
750	0-300	0.82	3.38
800	0-300	1.14	33.62
850	0-60	1.42	64.83
	60-300	1.27	55.32
900	0-50	1.63	44.22
	50-75	1.36	66.89
	75-300	1.10	49.21

where

E_a is the activation energy

A is a constant

R is the universal gas constant, and

T is the temperature

This Arrhenius equation gives the rate of the process where heat energy is the driving force. When logarithm of rate constant is plotted against inverse of temperature, a straight line is obtained and this plot is called the Arrhenius plot. The slope of this line gives the activation energy of the rate controlling process. Such plots are shown in Figs. 4.20 and 4.21 which are for the various pressures of oxidation and between the temperature ranges 600-750°C and 750-900°C respectively. With the activations energies thus calculated from these plots (Figs. 4.21 and 4.22), the rate equations for modified 9Cr-1Mo ferritic steel in the temperature ranges 600-750°C and 750-900°C for the various pressures of oxidation are summarized in Table 4.6. Here the general feature observed is that as the pressure increases, activation energy tends to fall for both the temperature ranges. This clearly indicates the tendency for more oxidation at higher pressures.

4.2.2 Effect of Pressure, Temperature and Time

The oxidation rate increases as the temperature of oxidation is increased, as is seen from Figures 4.1 to 4.10.

Table 4.6 Rate equations for modified 9Cr-1Mo Ferritic Steel in the temperature ranges of 600-750°C, and 750-900°C for various pressures

Temperature range 600-750°C

$$K_p(202.65 \text{ KPa}) = 0.8710 \exp(-122.65 \text{ KJ/RT})$$

$$K_p(303.97 \text{ KPa}) = 0.5012 \exp(-90.99 \text{ KJ/RT})$$

$$K_p(506.62 \text{ KPa}) = 0.0646 \exp(-38.64 \text{ KJ/RT})$$

$$K_p(709.26 \text{ KPa}) = 0.0603 \exp(-31.65 \text{ KJ/RT})$$

Temperature range 750-900°C

$$K_p(202.65 \text{ KPa}) = 1.58 \times 10^2 \exp(-382.17 \text{ KJ/RT})$$

$$K_p(303.97 \text{ KPa}) = 6.3096 \exp(-281.29 \text{ KJ/RT})$$

$$K_p(506.62 \text{ KPa}) = 0.5012 \exp(-91.61 \text{ KJ/RT})$$

$$K_p(709.26 \text{ KPa}) = 0.4169 \exp(-61.49 \text{ KJ/RT})$$

$$K_p(911.91 \text{ KPa}) = 0.1995 \exp(-40.05 \text{ KJ/RT})$$

Upto 750°C the oxidation takes place initially, according to cubic or parabolic law for all the pressures. This is evident from the values of n given in Tables 4.1 to 4.5. In the temperature range below 750°C , after a certain time of oxidation, the rate switches over to near linear law. The samples oxidized above 750°C , at all pressures show rapid increase in weight and the rate law is linear which is evident from the Tables 4.1 to 4.5. In other words at these temperatures 'catastrophic oxidation' takes place. It is found that with increasing temperature, pressure and time, the oxidation seems to be more and the rate law approaches to be linear. This behaviour has been observed by Khanna et al.⁽²⁾

From Table 4.6, we observe that the activation energy falls with increasing pressures which clearly indicates the high diffusion rate of ions through the scale and hence the increased oxidation rates, at elevated pressures. For a particular pressure of oxidation, the activation energy is different in both the temperature ranges. The difference in activation energies show that the rate controlling processes are different at these two temperature ranges.

4.3 EXAMINATION OF OXIDATION PRODUCTS

4.3.1 Metallography

The samples of modified 9Cr-1Mo steel which were oxidised in pure dry oxygen, were examined under a microscope and photographs of the same are given in Figs. 4.22 to 4.40. Details

about the temperature and pressure of oxidation and the magnification are mentioned below each photograph. It can be observed that as the temperature and pressure of oxidation was increased, the oxidation rate also increased. This is in agreement with the thermogravimetric results.

Figs. 4.22 and 4.23 give the oxide-Metal (O/M) interface of the samples oxidised at pressures 303.97 KPa and 506.62 KPa and at a temperature 600°C . It is found that scale thickness is more at 506.62 KPa than at 303.97 KPa. The mechanism of the same is discussed later. Figs. 4.24 to 4.26 show the O/M interface of the samples oxidised at 650°C and pressures, 303.97, 506.62 and 709.26 KPa. It is seen that the oxide scale tends to increase as the temperature and pressure are increased. Figs. 4.27 and 4.28 show the oxidation at 750°C and pressures 506.62 and 709.26 KPa. Here at 506.62 KPa, the scale thickness is less, but the internal oxidation is slightly more. Fig. 4.29 shows the distorted edge of the sample.

Oxidation at 850°C for two different pressures 303.97 KPa and 506.62 KPa are compared in Fig. 4.30 and Fig. 4.31. The oxide scale at 303.97 KPa is thick and adherent, whereas the oxide scale at 506.62 KPa shows visible cracks which is the reason for the high oxidation rate. Fig. 4.32 shows the duplex oxide structure on the metal matrix. Figs. 4.33 to 4.35 show the magnified photograph of the oxide scale formed at a temperature

of 900°C and at pressures 202.65, 303.97 and 506.62 KPa. The duplex oxide structure is very much enlarged. The oxide near the metal is made of iron-chrome spinels and the outer one is iron oxide. At lower pressures, the spinels do not show any voids, but as the pressure is increased, the spinels tend to crack out. With increase in pressure, the iron oxide structure also tends to show a larger cracking of the scale. Fig. 4.36 shows the oxidation at a temperature of 900°C and at 709.26 KPa pressure. The internal stressed oxide structure is very much visible. Due to the internal stresses at such points, the oxide scale tends to crack during the growth process. It is only due to these cracks on the oxide scales and at these temperatures, that 'catastrophic oxidation' takes place. The oxides formed at 911.91 KPa pressure and elevated temperatures were so porous and non-adherent that it spalled and chipped itself while cooling. It is quite evident from all these figures that with the increase in temperature and pressure the oxidation rate is increased and so the weight gain is also high.

Figs. 4.37 to 4.40 show the same duplex oxide structure formed on the metal at a lower magnification. It is quite evident from all these photographs that with increase in temperature and pressure of oxidation, the rate is increased and so oxidation is also high which is in concordance with the thermogravimetric results.



Fig.4.22 Oxide-Metal (O/M) interface of the sample oxidised at 600°C and 303.97 KPa. X800



Fig.4.23 O/M interface of the sample oxidised at 600°C and 506.62 KPa. X800

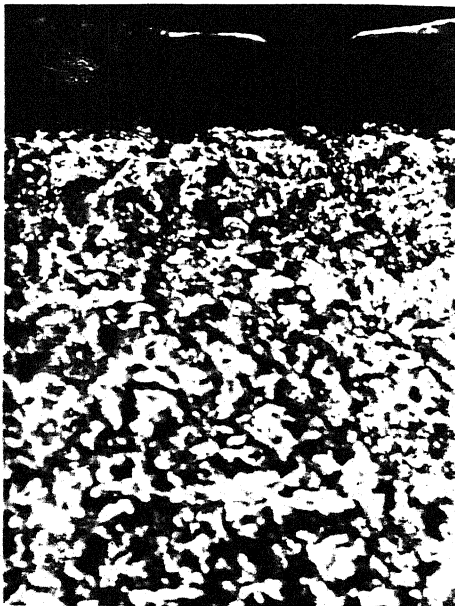


Fig.4.24 O/M interface of the sample oxidised at 650°C and 303.97 KPa. X800

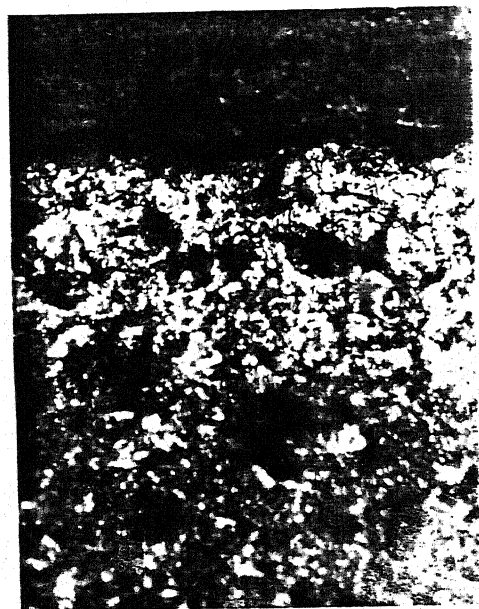


Fig.4.25 O/M interface of the sample oxidised at 650°C and 506.62 KPa. X800

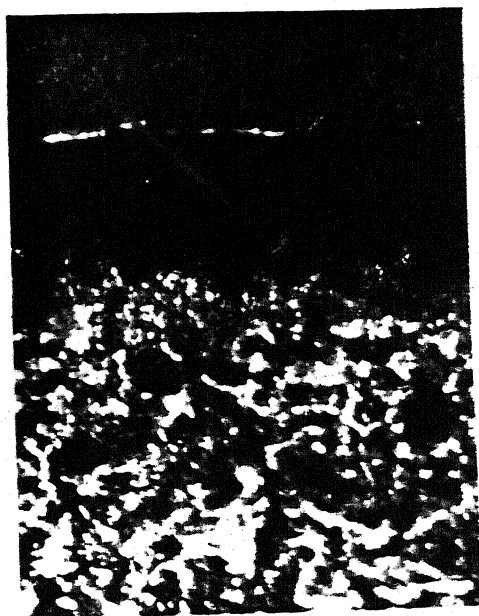


Fig.4.26 O/M interface of the sample oxidised at 650°C and 709.26 KPa. X800

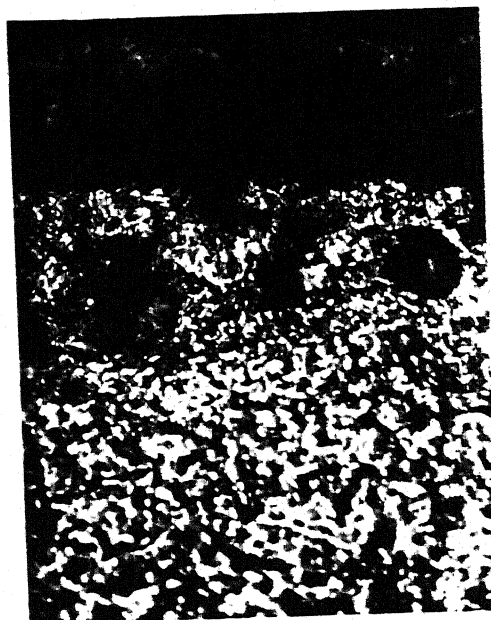


Fig.4.27 O/M interface of the sample oxidised at 750°C and 506.62 KPa. X800

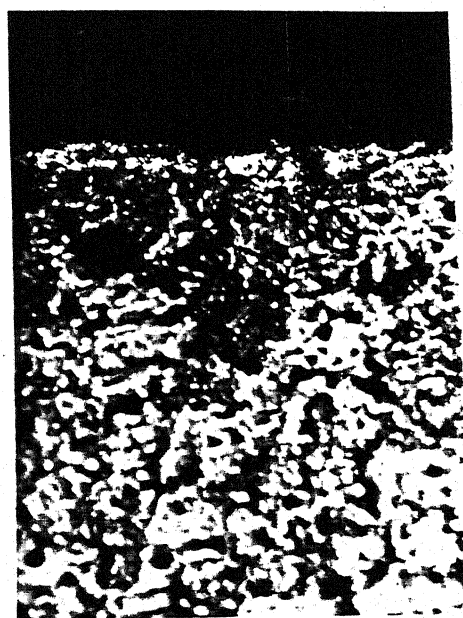


Fig.4.28 O/M interface of the sample oxidised at 750°C and 709.26 KPa. X800

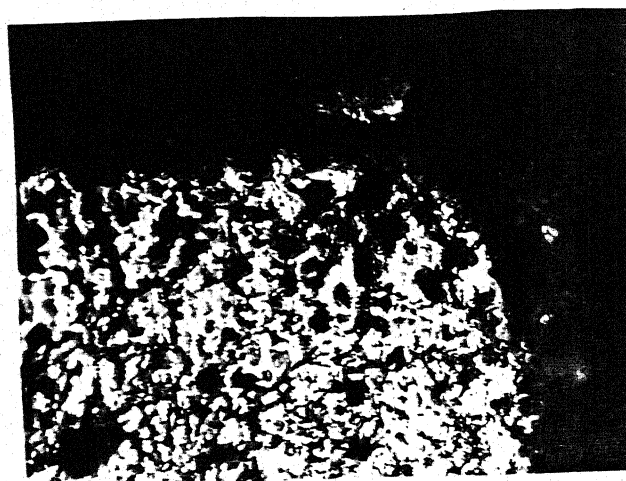


Fig.4.29 Corner of the sample oxidised at 750°C and 709.26 KPa. X800

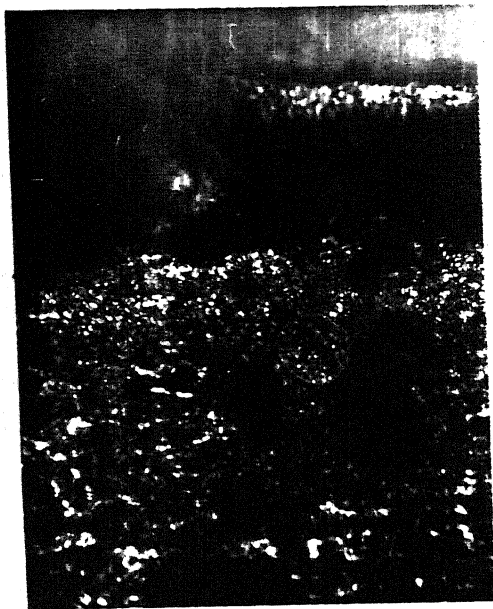


Fig.4.30 O/M of the sample oxidised at 850°C and 303.97 KPa. X800

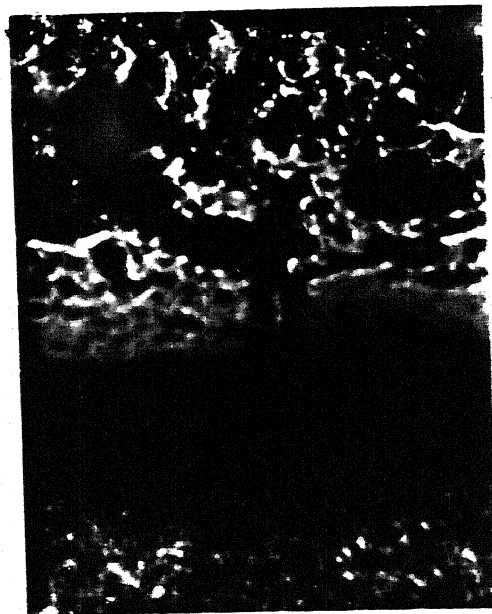


Fig.4.31 Duplex oxide scale of the sample oxidised at 850°C and 506.62 KPa showing cracks in the scale. X800



Fig.4.32 Duplex oxide scale of the sample oxidised at 850°C and 709.26 KPa. X420

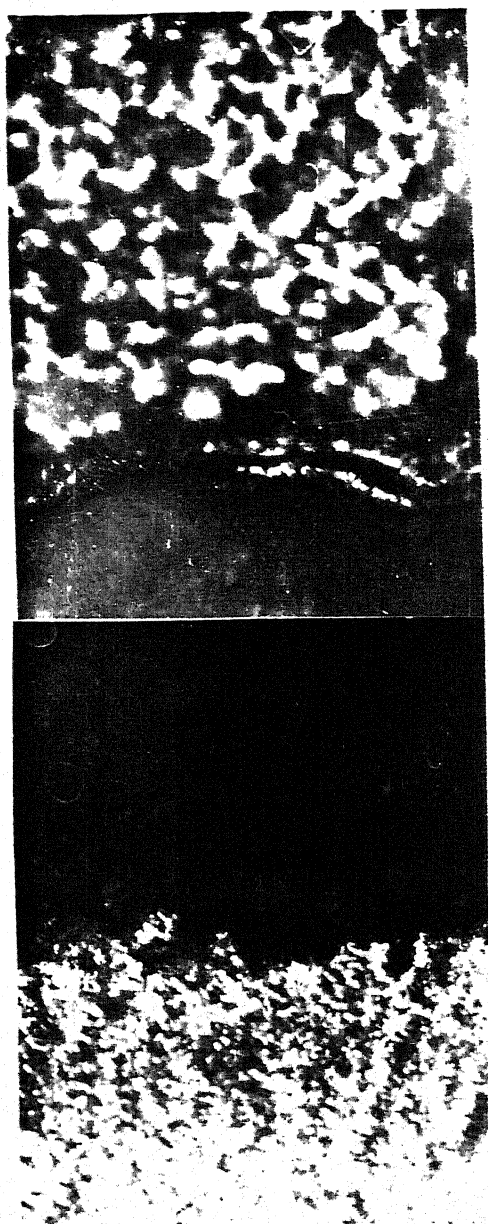


Fig.4.33 Magnified O/M of the sample oxidised at 900°C and 202.65 KPa. X1600

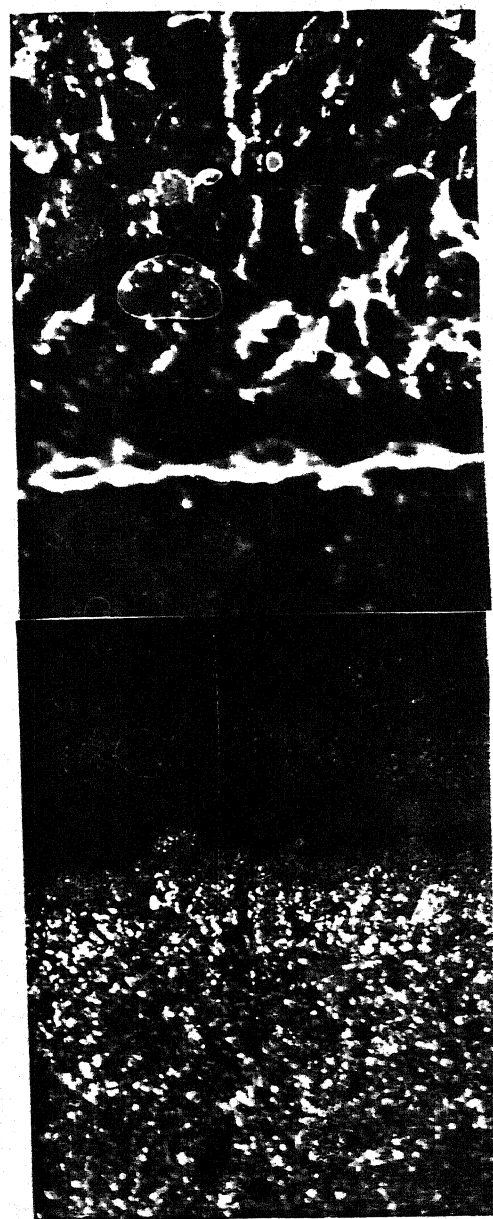


Fig.4.34 Magnified O/M of the sample oxidised at 900°C and 303.97 KPa. X1600

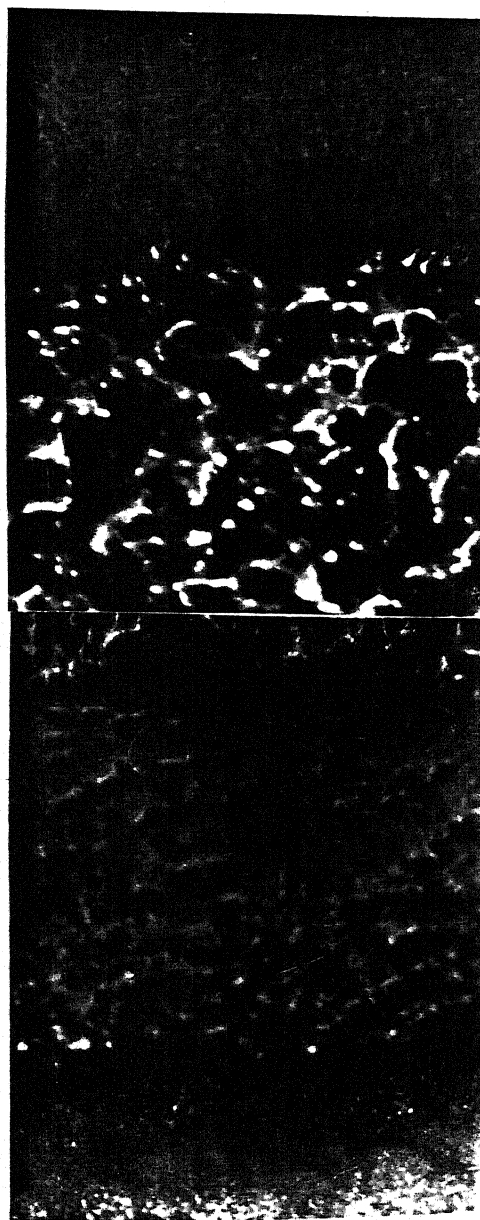


Fig.4.35 Magnified O/M of the sample oxidised at 900°C and 506.62 KPa. X1600

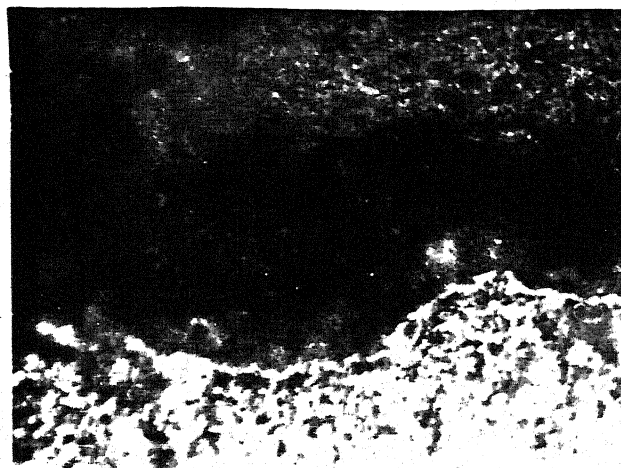


Fig.4.36 O/M of the sample oxidised at 900°C and 709.26 KPa showing the high stress on the oxide scale



Fig.4.37 Duplex oxide scale formed on the sample oxidised at 800°C and 202.65 KPa. X420

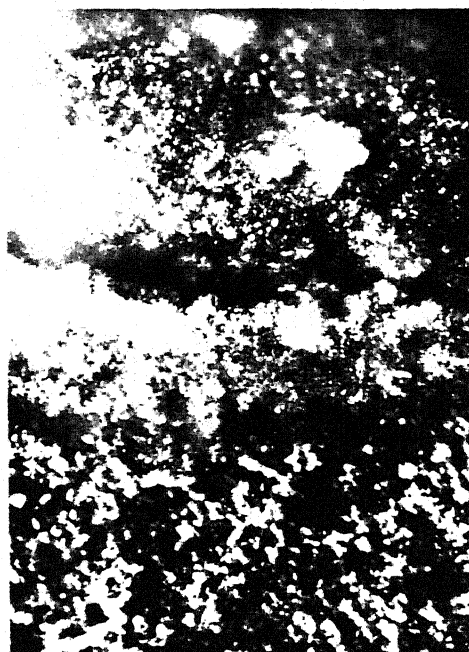


Fig.4.38 Duplex oxide scale formed on the sample oxidised at 800°C and 506.62 KPa. X420



Fig.4.39 Duplex oxide scale formed on the sample oxidised at 800°C and 709.26 KPa showing a high stress on the oxide scale



Fig.4.40 Corner of the sample oxidised at 900°C and 202.65 KPa showing voids. X420

4.3.2 X-ray Analysis

Results of X-ray analysis carried out on the oxidised samples are shown in Appendix B. Here referring to the X-ray diffraction data files, the compounds $\alpha\text{Fe}_2\text{O}_3$, FeCr_2O_4 , $(\text{Fe,Cr})_2\text{O}_3$ etc. were identified in the oxidised samples in addition to those present in the unoxidised samples. Appendix C lists the X-ray diffraction data for some important compounds.

4.4 DISCUSSION

The initial oxidation rate of this modified steel tested at different pressures in the temperature range $600\text{--}750^\circ\text{C}$ is according to the cubic or parabolic rate law and later with increasing time, the rate switches over to linear law. As soon as the initial surface oxidation is over, a protective layer is formed, the rate becomes diffusion controlled and hence the oxidation rate is cubic or parabolic. During this period, at the scale-gas interface the transport of the ions across the scale becomes the rate controlling step and with increasing time, this rate increases and tends to be linear. In the temperature range of $750\text{--}900^\circ\text{C}$, the oxidation is very rapid and is found to be linear throughout. The mechanism postulated for this oxidation is the formation of MoO_2 at the scale-alloy interface which is oxidised to liquid MoO_3 followed by cracking of the scale⁽³⁾. (MoO_3 melts at 801°C but forms low melting eutectics with most oxides). This molten oxide may result in

the dissolution and disruption of the protective scale at high temperatures.

The oxide layer has been found to be made of duplex scale as is seen in Figs. 4.10, 4.14, 4.15 etc. The inner layer consists of iron-chrome spinel and the outer layer is pure iron oxide as reported by other workers on oxidation of iron-chromium alloys⁽⁴⁻¹⁰⁾. In this temperature range of 600-900°C, the outer layer is made of Fe_2O_3 ⁽⁸⁾. The growth of this multilayer will occur by oxidant ingress through the scale cracks as shown in Fig. 4.10. Oxidation takes place by the inward diffusion of oxygen to form an iron-chrome layer at the scale-metal interface and the outward diffusion of iron to form an iron oxide at the scale-gas interface (Refer Figs. 4.10, 4.14, 4.15, etc.)

The observed linear oxidation rate at high temperatures can also be explained by Cabrera-Mott⁽¹¹⁾ theory, according to which of an n type semiconductor formed then this linear rate may be due to the ion transfer in electric field. As explained by Kofstad,⁽¹²⁾ the increasing, rates of oxidation, at high temperatures is due to some phase boundary reactions after rupture of the scale. The linear oxidation rate at high temperatures and pressures can also be explained by the Pilling-Bedworth ratio. At high temperatures, iron oxide is formed at the surface and oxygen diffuses inside to form the oxide

near the metal surface. This new oxide when formed (the Pilling-Bedworth ratio may not be optimum for a protective oxide) expands and causes severe biaxial stresses which eventually causes thermal strain leading to mismatch of the oxide and the metal. Hence the oxide layer cracks. The oxidant ingress will be high at elevated pressures. Also the cracking of the scale exposes the metal to the environment and further oxidation is catastrophic.

References

1. Kubaschewski O. and Hopkins, B.E., 'Oxidation of Metals and Alloys', Butterworths, 1962.
2. Khanna A.S., M.Tech. Thesis, Oxidation Kinetics of 2.5Cr-1Mo Steel in air, oxygen and oxygen-water vapour mixture, IIT Kanpur, May 1980.
3. Brenner S.S., J. electrochemical Soc., 102 (1955) 16.
4. Fujii G.T. and Meussmer R.A., J. electrochemical Soc., 111 (1964) 1215.
5. Webber J., Corr. Sci., 16 (1976) 499.
6. Driscoll T.J. and Needham P.B., Oxidation of Metals, vol. 13, No.3 (1979), 283.
7. Lloyd G.O., British Corr. J., vol.15, No.2 (1980), pp 77.
8. Forrest J.E. and Bell, P.C., Procd. of the European Symposium, 'Corrosion and Mechanical Stress at High Temperature' ed. V. Guttman and M. Martz, May 1980, pp 339-358.
9. Gordovi M.A. et al., Behaviour of Super Heater Alloys at High Temperature in High Pressure Steam, ed. G.E. Lien, ASME, New York (1968), pp 8.

10. Clark C.L. et al., J. Engineering and Power Transactions, Series A, vol.82 (1960), pp 35.
11. Cabrera N. and Mott N.F., Rep. Progr. Phys., vol. 12 (1948-49) pp 163.
12. Kofstad P., Oxidation of Metals at High Temperatures, pp 233.

Figures 5.4 and 5.5 show respectively the variations of uniform and total elongations with oxygen concentration. It shows an increase in elongations with increase in oxygen content in the samples at each test temperature.

The variation observed in reduction of the cross-sectional area with the oxygen concentration is shown in Fig. 5.6. The reduction in area increases considerably with increase in oxygen content and test temperature.

Figures 5.7 to 5.8 show the strengths (ultimate tensile and yield strengths) and ductility measurements (% total elongation and % area of reduction) of the untreated and oxygen treated samples (from 0.06 - 0.14 wt %) at each test temperature. It is evident from these plots that the strength tends to decrease and ductility tends to increase with increasing testing temperatures and oxygen levels in the samples.

The flow curves plotted from yield point to ultimate tensile strength of both the untreated and oxidized samples for the four different test temperatures: 23°C, 265°C, 375°C and 545°C are shown in Figs. 5.9, 5.10, 5.11 and 5.12 respectively. The data were obtained from the same 'load vs elongation' plot. A general feature observed is that the flow curves of both the treated and untreated samples follow the same pattern. In general, the flow curve of an untreated sample is always high and lies above all the treated samples. Also it is noticed that the ductility

CHAPTER 5

RESULTS AND DISCUSSION ON MECHANICAL PROPERTIES

The results of the various tests on the mechanical properties carried out with untreated and oxygen treated samples of modified 9Cr-1Mo steel are summarized and discussed in this chapter.

5.1 TENSILE TEST

The data on mechanical behaviour obtained from the load vs elongation plot have been summarized in Tables 5.1 to 5.4. The variation in ultimate tensile strength with oxygen concentration at various temperatures is shown in Fig. 5.1. A general feature observed is that the tensile strength of the alloy decreases with temperature. When the test temperature is raised from 375 °C to 545 °C, the tensile strength drops to a great extent. This is in agreement with the results obtained by Sikka et al.⁽¹⁾. Also with increase in oxygen concentration in the samples at the test temperatures, the ultimate tensile strength drops considerably.

The variations of the yield strength and engineering fracture strength with oxygen concentration is given in Figures 5.2 and 5.3 respectively. It can be observed that both the properties show the same trend as that of the ultimate tensile strength and decreases continuously with oxygen content and temperature of the test.

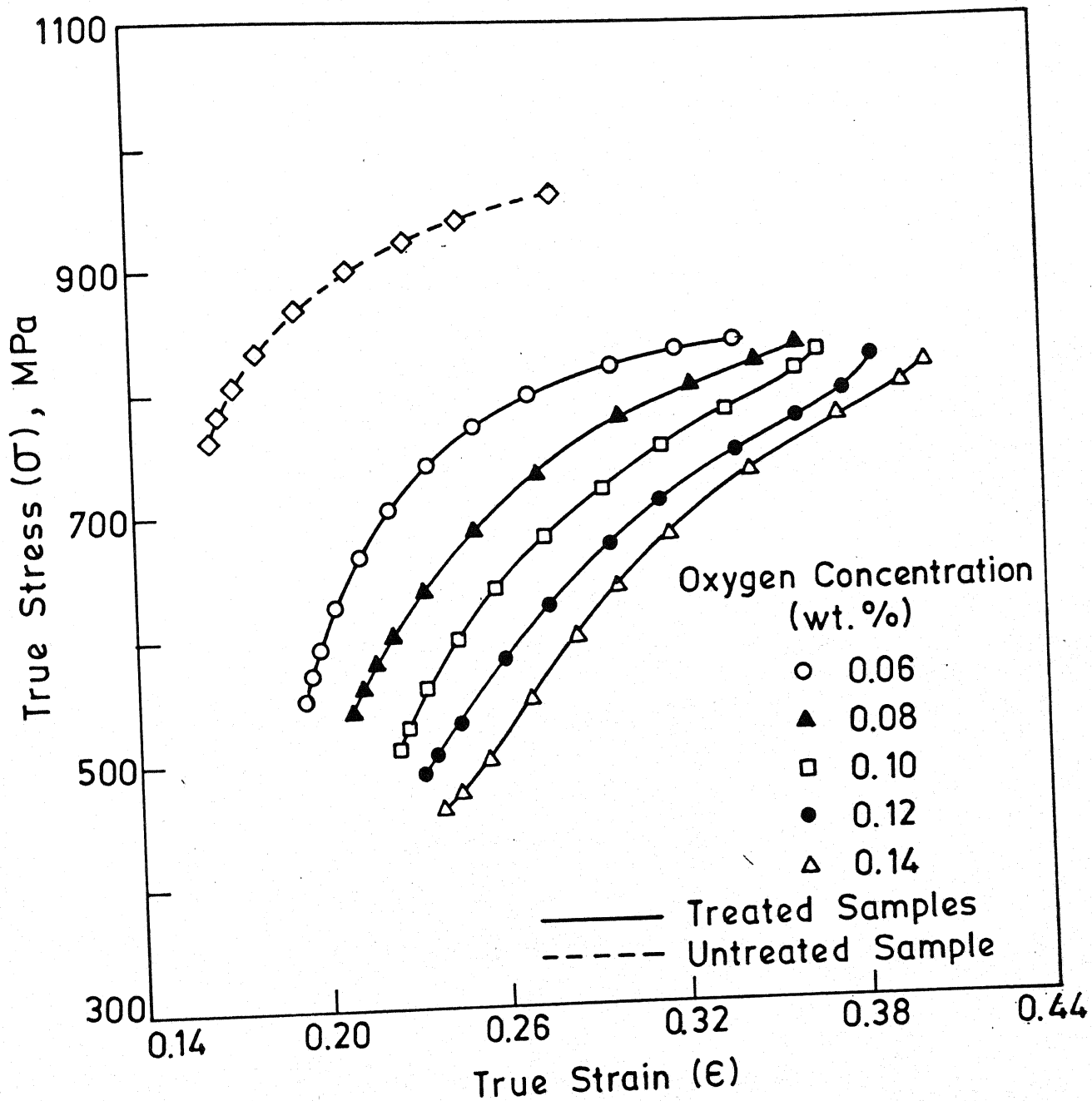
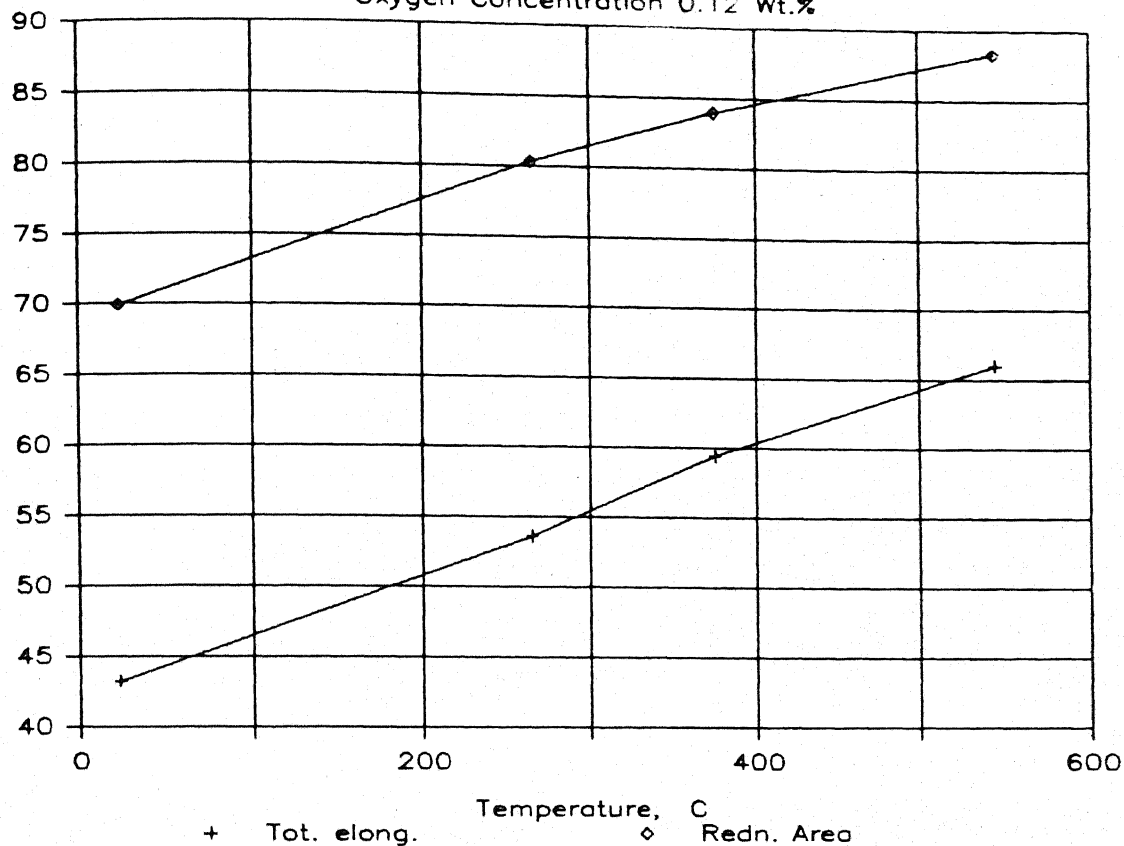


Fig. 5.12 Flow curves of modified 9Cr-1Mo steel tested at 545°C.

Ductilities of Oxidised Samples

Oxygen Concentration 0.12 Wt.%



Ductilities of Oxidised Samples

Oxygen Concentration 0.14 Wt.%

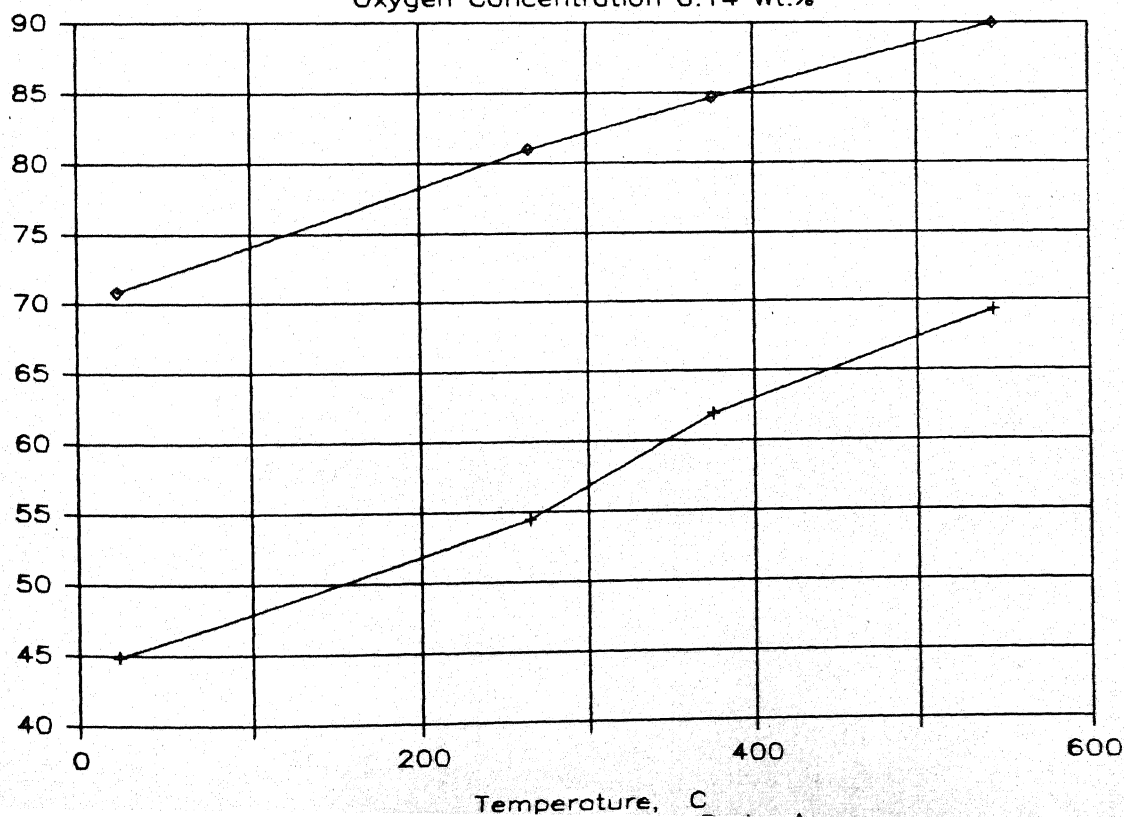


Table 5.1 The Results of Tensile Tests at Room Remperature (23°C)

Oxygen Content wt %	Ultimate Tensile Strength MPa	0.2% Offset Yield Strength MPa	Engineering Fracture Strength MPa
0.00	1125.80	1023.51	824.24
0.06	1007.33	726.08	734.02
0.08	985.76	709.02	720.29
0.10	965.17	693.03	706.37
0.12	943.49	675.87	693.33
0.14	920.64	659.10	679.60

Oxygen Content wt %	<u>Percentage Elongation</u>		Reduction of area %
	Uniform	Total	
0.00	21.5	35.4	59.11
0.06	31.1	40.6	66.47
0.08	32.3	41.7	67.16
0.10	32.5	42.0	68.31
0.12	33.8	43.2	69.92
0.14	34.6	44.9	70.84

Table 5.2 The Results of Tensile Tests at 265°C

Oxygen Content wt %	Ultimate Tensile Strength MPa	0.2% Offset Yield Strength MPa	Engineering Fracture Strength MPa
0.00	996.55	805.51	736.97
0.06	893.77	613.01	612.91
0.08	876.81	604.28	600.65
0.10	861.41	595.75	588.40
0.12	845.92	586.43	576.14
0.14	829.83	577.12	563.88

Oxygen content	Percentage Elongation		Reduction of area %
	Uniform	Total	
0.00	27.4	36.5	61.64
0.06	38.9	52.3	79.12
0.08	40.4	52.6	79.58
0.10	42.6	53.3	79.93
0.12	44.2	53.6	80.27
0.14	46.3	54.4	80.96

Table 5.3 The Results of Tensile Tests at 375°C

Oxygen Content wt %	Ultimate Tensile Strength MPa	0.2% Offset Yield Strength MPa	Engineering Fracture Strength MPa
0.00	969.19	787.57	693.33
0.06	816.01	571.14	557.51
0.08	803.95	566.33	551.62
0.10	792.57	560.15	544.56
0.12	780.31	554.96	537.89
0.14	770.11	549.56	532.01

Oxygen Content wt %	Percentage Elongation		Reduction of area %
	Uniform	Total	
0.00	29.0	40.4	66.47
0.06	39.4	53.0	79.58
0.08	41.1	55.5	80.73
0.10	43.0	56.4	82.57
0.12	45.4	59.4	83.95
0.14	47.1	61.9	84.64

Table 5.4 The Results of Tensile Tests at 545°C

Oxygen Content wt %	Ultimate Tensile Strength MPa	0.2% Offset Yield Strength MPa	Engineering Fracture Strength MPa
0.00	727.06	645.47	399.62
0.06	594.48	442.47	331.46
0.08	579.08	429.04	321.17
0.10	575.75	402.76	309.89
0.12	566.33	383.63	298.61
0.14	556.52	362.35	286.84

Oxygen Content wt %	<u>Percentage Elongation</u>		Reduction of area %
	Uniform	Total	
0.00	32.2	45.0	71.30
0.06	40.3	56.6	80.27
0.08	43.2	60.2	83.03
0.10	44.3	62.6	84.87
0.12	46.9	66.0	88.32
0.14	48.8	69.3	89.93

of the treated samples is more when compared with the ductility of the untreated samples at each test temperature.

5.2 FATIGUE AND CREEP FATIGUE TEST

The results of the low cycle fatigue tests at room temperature (23°C) for both the untreated and oxidized samples are summarized in Table 5.5. The R value (ratio of the minimum stress to maximum stress) was kept at a constant value of 0.1 and the samples were cycled till failure. Fig. 5.13 shows the trend of fatigue strength with the oxygen weight percentage in the samples. It is observed that the fatigue strength drops considerably with increase in oxygen content.

The results of the creep-fatigue tests at 545°C are given in Table 5.6. Here too, the R value was kept at a constant value of 0.1 and the samples were cycled to failure. Fig. 5.14 depicts the variation of fatigue strength with the oxygen level in the samples. It reveals that an increase in oxygen concentration decreases the fatigue strength. Also compared with the fatigue strength at room temperature, the number of cycles to failure at 545°C drops to a great extent.

5.3 CREEP TEST

Table 5.7 summarizes the results of the creep tests done at 550°C for both the untreated and treated samples. Fig. 5.15 shows the creep curves for different oxygen concentrations. Here

Table 5.5 The Results of Low Cycle Fatigue Tests at Room Temperature

Oxygen Content wt %	Frequency cycle/sec	$R = \sigma_{\min}/\sigma_{\max}$	Number of cycles to Failure
0.00	30	0.1	15,280
0.06	30	0.1	12,100
0.08	30	0.1	10,700
0.11	30	0.1	10,200
0.14	30	0.1	8,600

Table 5.6 The Results of Creep-Fatigue Tests at 545°C

oxygen content wt %	$R = \frac{\sigma_{\min}}{\sigma_{\max}}$	Cross-head speed mm/min	Frequency cycles/min	Number of cycles to failure	Time to failure min
0.00	0.1	10	32	5803	190
0.06	0.1	10	35	4626	137
0.08	0.1	10	34	4108	128
0.10	0.1	10	36	3742	111
0.12	0.1	10	35	3415	102

it is evident that any increase in the oxygen level results in increase of rupture time, decrease in secondary creep rate, an increase in instantaneous strain on loading and an increase in rupture strain. The increased oxygen content tends to delay the creep failure.

5.4 X-RAY ANALYSIS

Results of the X-ray analysis carried out on the oxidized and mechanical tested samples are shown in Appendix B. With the comparison of 'd' values listed in Appendix B and those listed in the X-ray diffraction data files, the compounds $(\text{Fe, Cr})_2\text{O}_4$, MoO_3 , FeCr_2O_4 , $\alpha\text{Fe}_2\text{O}_3$ etc. were identified in the oxidized samples in addition to those present in the untreated samples. Appendix C lists the X-ray diffraction data for some important compounds.

5.5 DISCUSSION

5.5.1 Tensile Property

In all the mechanical tests, the samples before treatment were heated at 860°C for two hours and were furnace cooled. Then this was followed by heating in an oxygen atmosphere at 800°C and 607.94 KPa pressure (6 atmospheres) for different periods of time in order to have the alloy of different oxygen contents. During this process of heating, two phenomena are expected to take place. One is the structural change that

Table 5.7 The Results of Creep Test at 550°C

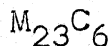
Specimen with 0.00 wt % oxygen		Specimen with 0.08 wt % oxygen		Specimen with 0.13 wt % oxygen	
Time hr	Creep Strain %	Time hr	Creep Strain %	Time hr	Creep Strain %
0	8.6	0	10.0	0	12.3
1.5	28.5	3.8	33.9	4.5	26.5
4.5	38.6	10.5	38.8	16.5	29.0
6.8	43.5	13.8	44.2	25.8	30.1
	Failure		Failure	27.6	59.8
					Failure

leads to tempering and the other is the oxidation of the material, as the environment is rich with oxygen. Here in the experiments, the decrement in mechanical strength of the alloy is attributed to both oxidation as well as to some structural changes during the oxidation process. Various authors⁽²⁻⁷⁾ have observed that the structural changes taking place during heating, is the major cause of mechanical property variation.

The modified 9Cr-1Mo steel is obtained in the normalized and tempered form (normalized at 1038°C for 1h air cooled to R.T.; tempered at 760°C for 1h and finally air cooled to room temperature). The normalizing and tempering heat treatment given to this alloy produces a tempered, fully martensitic structure with a high density of transformation dislocations⁽⁸⁾. According to Baker and Nutting⁽⁹⁾ the sequence of carbide precipitation when tempering a normalized steel at 704°C for one hour is

carbide cementite cementite

+



Fine dispersion of $M_{23}C_6$ and MC precipitates have been found to have the composition of $(Cr, Fe)_{23}C_6$ and $(Nb, V)C$ respectively in modified 9Cr-1Mo steel⁽¹⁰⁾. The carbide precipitation is preferentially along the grain boundaries and gives rise to dispersion hardening. It is this microstructure which gives the strength for this steel as is observed in Figs.5.1 - 5.3 for the untreated samples tested at various temperatures. Comparing with the results of Sikka et al⁽¹⁾, the tensile and yield strength of tested samples are found to be slightly higher which may be due to the higher strain rate used in the present experiments.

Oxidation at 800°C and 607.94 KPa oxygen pressure gives a tempering treatment to the alloy. Also heating the alloy in this atmosphere for a long time would have resulted in the rearrangement of dislocations and also the completion of the sequence of carbide precipitations that occurred during tempering. These precipitates can then coarsen or spheroidize with a resultant loss of both solid solution and dispersion hardening⁽¹¹⁾. It may also be due to rapid diffusion of high pressure, oxygen inside the metal matrix resulting in formation of oxides. So these treatments result in a decrease in the strength of the alloy (tensile, yield and fracture) with increasing oxygen concentrations (i.e., oxidation time). Furthermore, some negligible oxidation of the samples occur even while conducting the test at elevated temperatures.

Mechanical properties are strongly dependent on the temperature at which the test is conducted. In general, strength decreases and ductility increases as the temperature is increased. Thermally activated processes assist deformation and reduce strength at elevated temperatures^(12,13). Furthermore, high temperatures impart a greater mobility of dislocations by the 'climbing process' subsequently leading to an increase of equilibrium concentration of vacancies. In some metals the slip system changes or additional slip systems are introduced with increase of temperature⁽¹⁴⁾. Prolonged exposure at elevated temperatures affects metallurgical stability by grain coarsening, overaging etc. Deformation at grain boundaries becomes an added possibility in high temperature deformation of metals. The path of fracture of metals at elevated temperature is intergranular (or inter crystalline) in contrast to transgranular (or intra crystalline) mode of fracture commonly observed at ordinary temperatures.

In all tensile tests, the strength (ultimate tensile, yield and fracture) decreases with an increase in temperature because of an ease in dislocation movement. At fairly low temperatures, dislocations remain unpinned because the time of testing is too short to permit carbon atoms to collect around dislocations introduced by plastic flow, whereas at high temperatures the carbon atoms are so mobile that they cannot act to pin the dislocations⁽¹⁵⁾.

Fig. 5.17 depicts the transgranular fracture of a specimen tested at room temperature, while Fig. 5.29 shows the mixed mode of fracture (trans and inter granular) at 545°C . The variation of both total elongation and reduction in area, in other words ductility, can be explained in a similar way. Figs. 5.7 and 5.8 show that the total elongation and reduction in ^{have a} area ~~one~~ to one correspondence with the ultimate tensile strength. From Fig. 5.7 it is observed that with increasing temperature and oxygen concentration the strength decreases. When ultimate tensile strength is high, ductility is low and this increases as the ultimate tensile strength drops.

Figs. 5.17 to 5.33 show the fractography studies made on the fractured surface of the samples. All samples have failed with a characteristic ductile fracture⁽¹⁶⁾. Here also, it is to be noted that the metal matrix has shown a ductile fracture whereas, the oxide layer is of a brittle nature which is evident from Figs. 5.24, 5.26, 5.33 etc. In all ductile fractures the dimple size depends upon the number of void nucleating points present in the material. Since the dimple size in the treated sample is small compared to that of the untreated sample, it can be concluded that there are more nucleating sites for the voids in the treated sample and this is observed in Figs. 5.17, 5.30, 5.32 etc. The additional nucleating sites in the treated samples are due to precipitation of carbides.

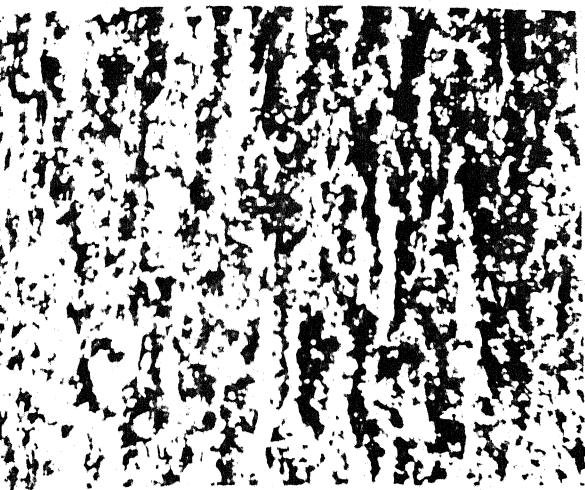


Fig.5.16 Microstructure of the treated normalized and tempered sample. X800

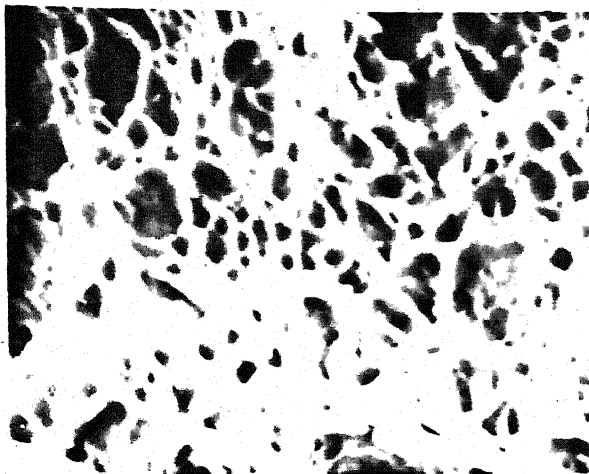


Fig.5.17 Fractured surface of the untreated sample, tensile tested at 23°C. 2000X

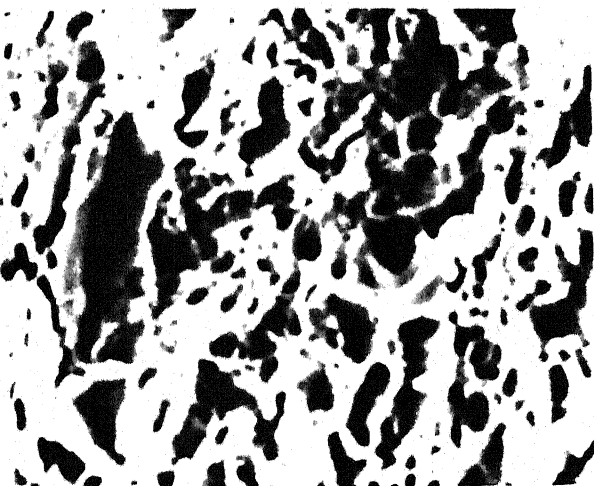


Fig.5.18 Metal matrix of the treated sample, tensile tested at 23°C. X2000

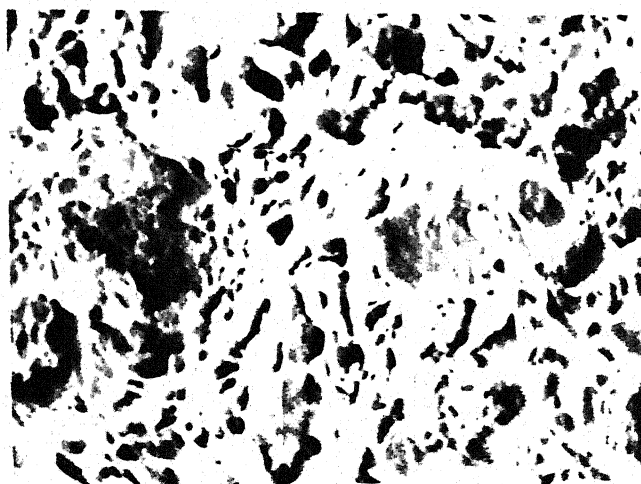


Fig.5.19 Oxide matrix of the sample, tensile tested at 23°C. X2000

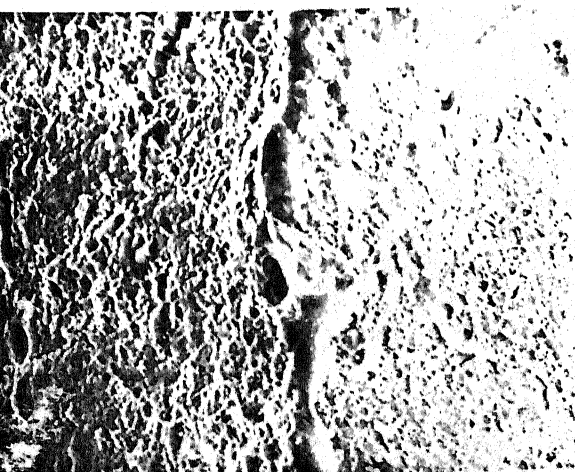


Fig.5.20 O/M interface of the sample, tensile tested at 265°C. X1000

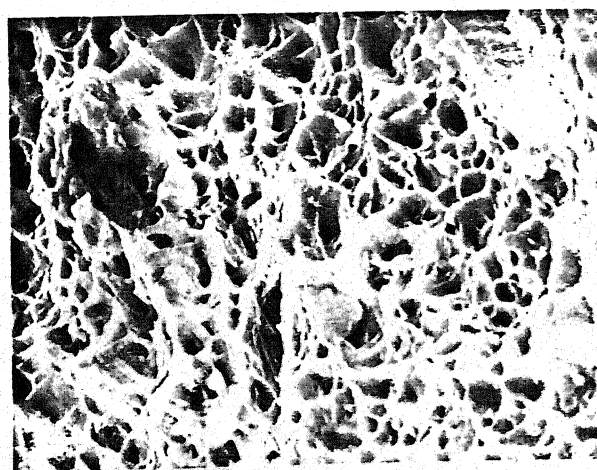


Fig.5.21 Fracture surface of the treated sample, tensile tested at 265°C. X2000

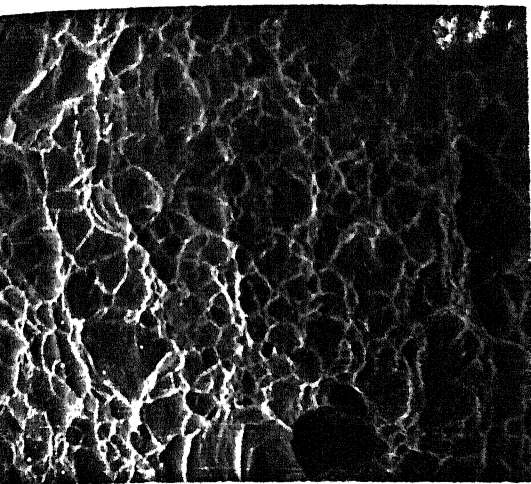


Fig.5.22 Metal matrix of the treated sample, tensile tested at 265°C. X2000

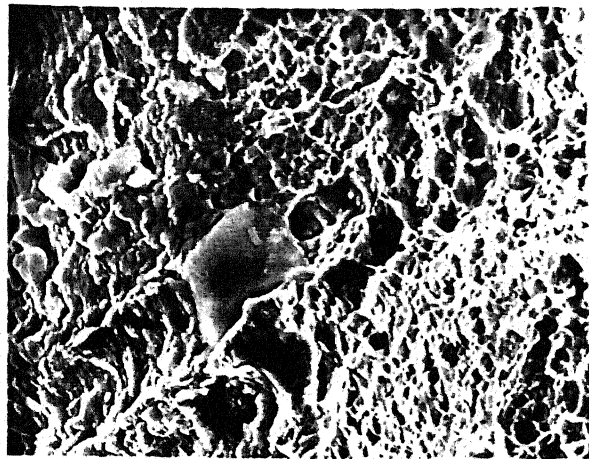


Fig.5.23 O/M interface of the sample, tensile tested at 265°C. X1000

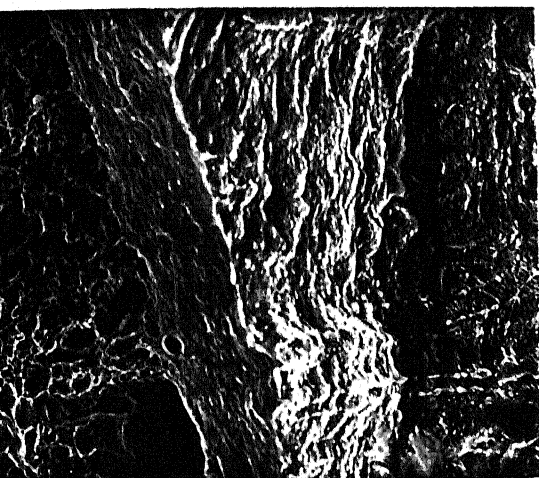


Fig.5.24 O/M interface of the sample, tensile tested at 265°C. X600

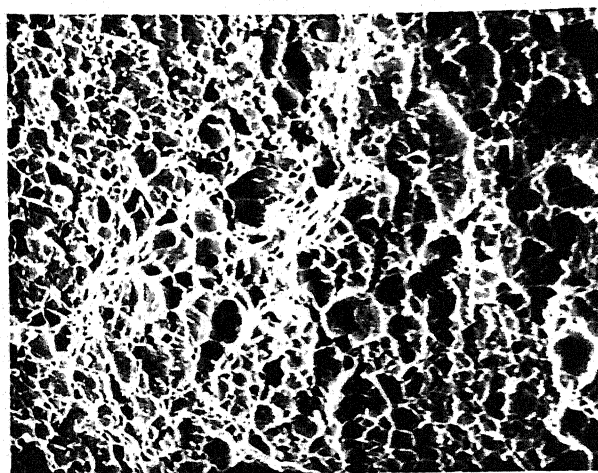


Fig.5.25 Fractured surface of the treated sample, tensile tested at 375°C. X2000

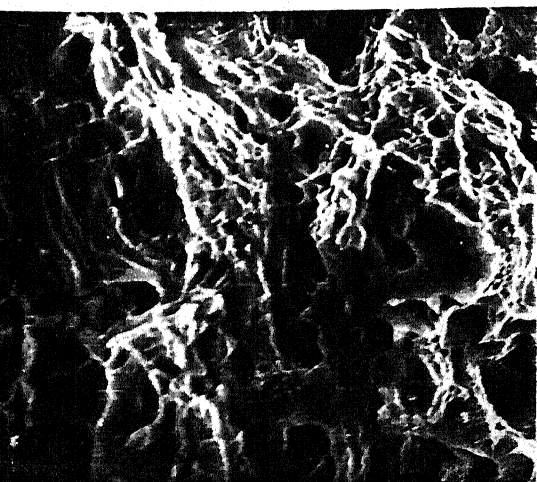


Fig.5.26 Oxide matrix of the sample, tensile tested at 375°C. X2000

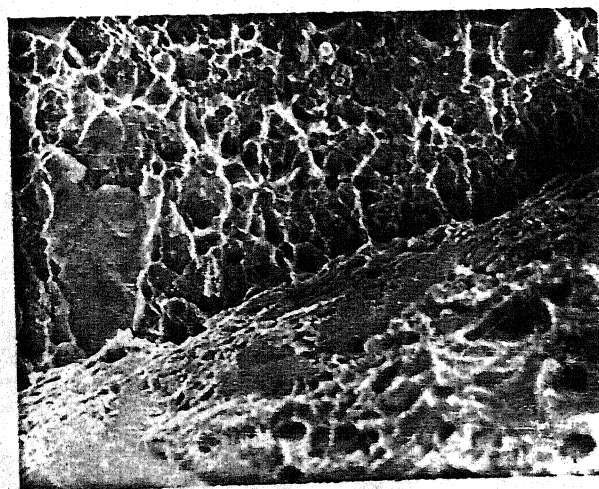


Fig.5.27 O/M interface of the sample, tensile tested at 375°C. X1000

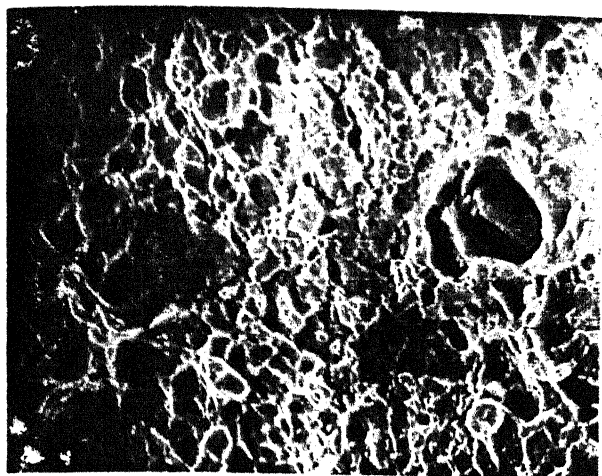


Fig.5.28 Metal matrix of the treated sample, tensile tested at 375°C. X2000

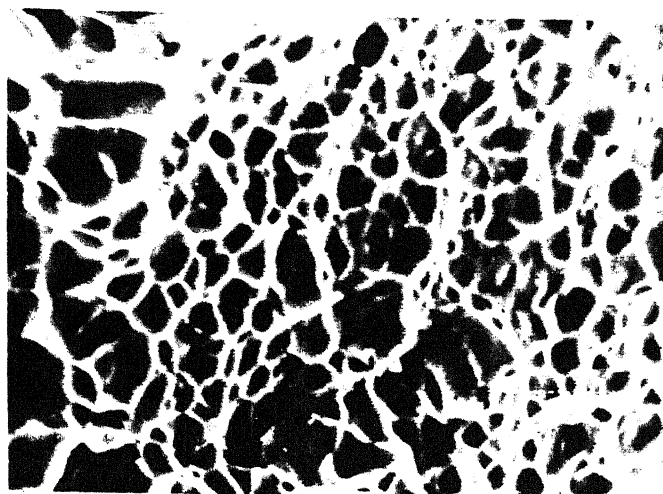


Fig.5.29 Fractured surface of the untreated sample, tensile tested at 545°C. X2000

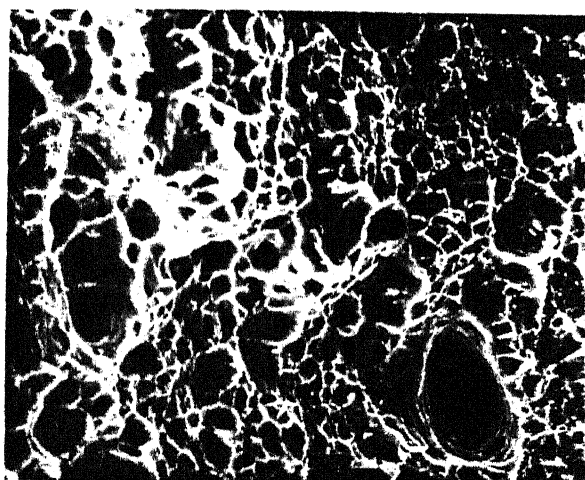


Fig.5.30 Fractured surface of the treated sample, tensile tested at 545°C. X1000

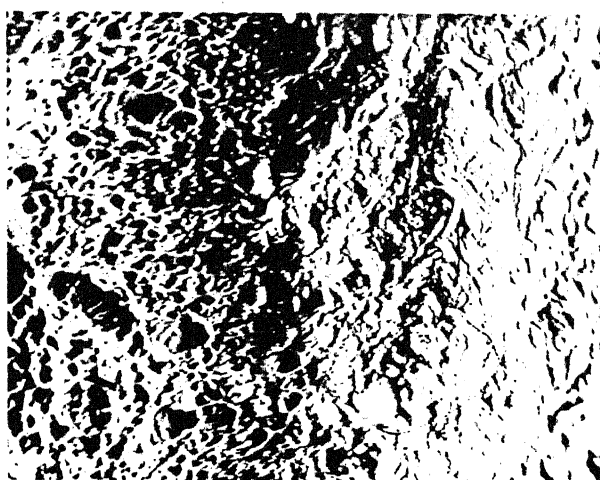


Fig.5.31 O/M interface of the sample, tensile tested at 545°C. X500

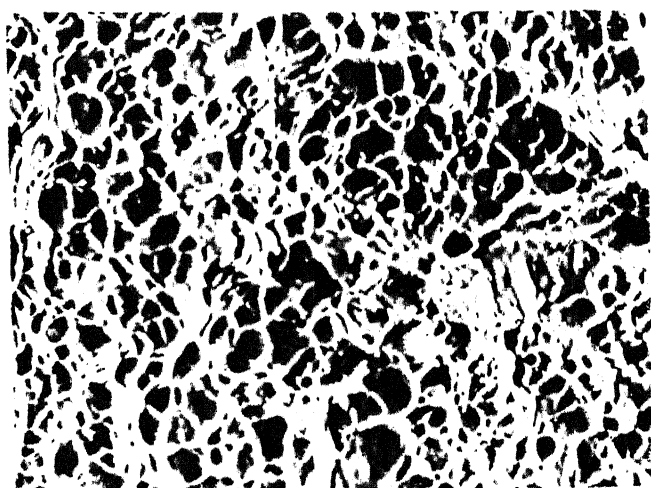


Fig.5.32 Metal matrix of the treated sample, tensile tested at 545°C. X1000

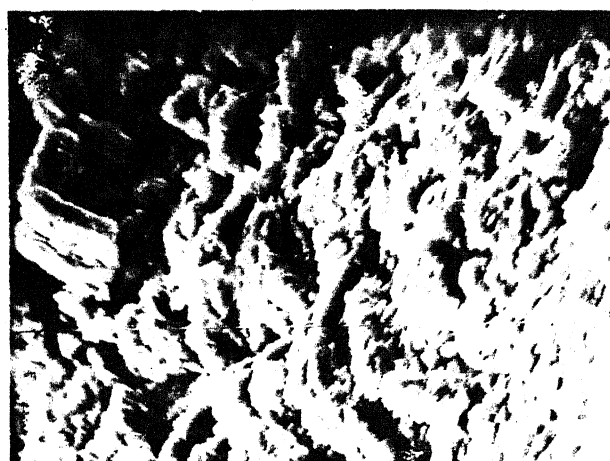


Fig.5.33 Oxide matrix of the sample, tensile tested at 545°C. X1200

5.5.2 Low Cycle Fatigue Property at 23°C and 545°C

The fatigue strength or the number of cycles to failure at room temperature is found to be always more for an untreated sample as when compared to the fatigue strength of the treated samples. It is observed from Fig. 5.13, that with increasing oxygen concentrations, the fatigue strength drops considerably. This is due to a lowering of strength with oxidation time as shown in the tensile properties. Also this is due to the wedging action of the oxide scale on the oxidized samples⁽¹¹⁾ as shown in Figs. 5.35, and 5.36. Fig. 5.37 shows no beach marks on the fracture surface because of rubbing action of two faces.

The fatigue strength at 545°C is still lower compared to the fatigue strength observed at room temperature. The reason for the lowering of strength could be attributed to the influence of 'thermally activated processes' which come into effect at elevated temperatures as has already been dealt elaborately in the tensile property discussions earlier. It is evident from Fig. 5.14, that the increased oxidation time, the increased temperature and the wedging action of oxide scale, all act synergistically and reduce the fatigue strength at 545°C. Figs. 5.38 to 5.40 show the fractography of creep fatigue tested samples. It is observed that ductility is high and so we can conclude that the strength has to be low.

5.5.3 Creep Property

It is evident from Fig. 5.15 , that the creep property is improved by the addition of oxygen in the alloy. May be the cause of the improved characteristics is the microstructural changes that take place in specimens subjected to prolonged exposure at high temperatures. The microstructure transforms towards a more stable bainitic structure. Fine carbides of molybdenum, vanadium and niobium precipitate and stabilize the structure morphology. The change in structure can be observed in Fig. 5.45 . Many authors^(8,17) while reviewing the physical metallurgy of Cr-Mo ferritic steels focussed on microstructural influence on creep behaviour, and have concluded that tempered bainite is the optimum structure and that a fine carbide distribution is the best precipitate morphology. The best carbides are those of molybdenum, vanadium and niobium because they are fine and stable.

Observing the fractography of the creep tested samples (Figs. 5.41to 5.44), it is evident that the void density is more in these samples, and this is due to the extraprecipitation of the carbides under long exposure at high temperatures. They also show a mixed mode of fracture.

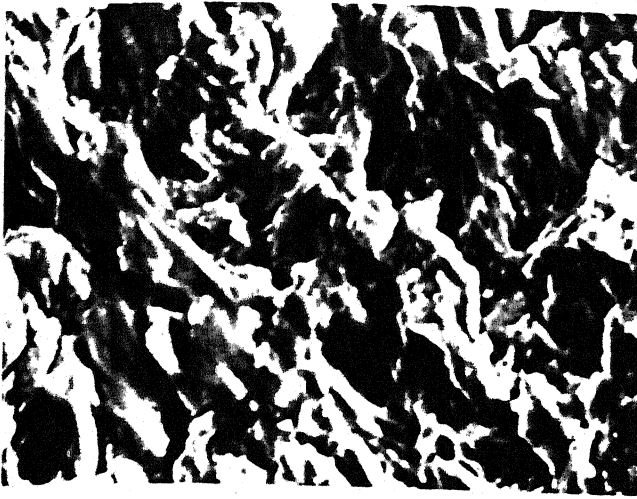


Fig.5.34 Fractured surface of the treated sample, fatigue tested at room temperature. X1000

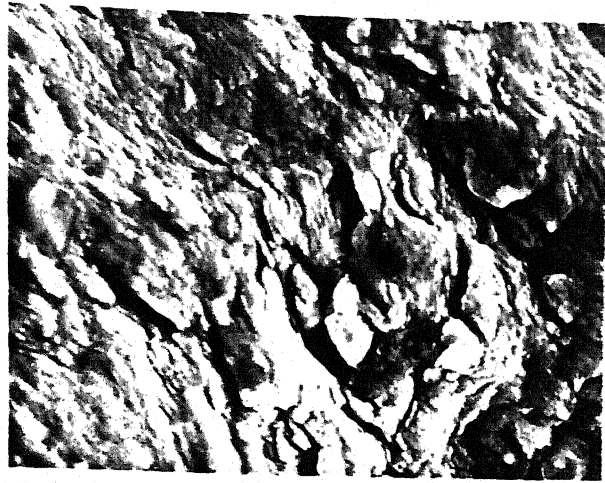


Fig.5.35 Oxide scale on the sample, fatigue tested at room temperature. X2000

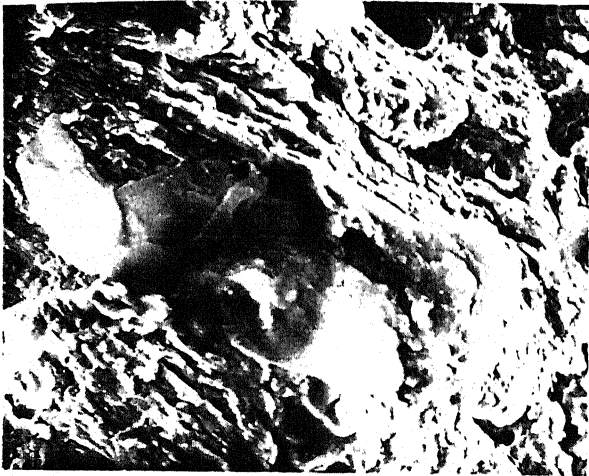


Fig.5.36 O/M on the sample, fatigue tested at room temperature. X1000

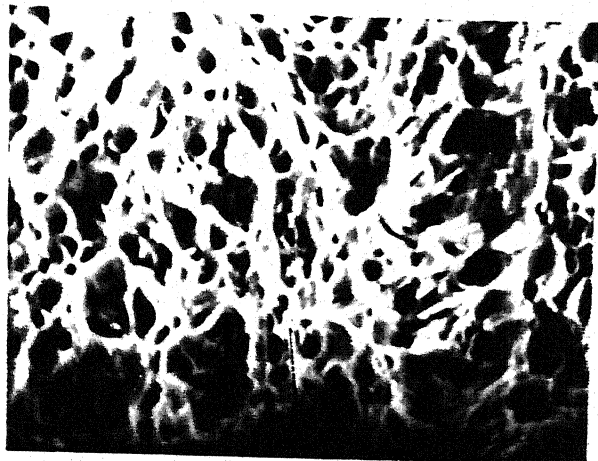


Fig.5.37 Metal matrix of the sample, fatigue tested at room temperature. X2000

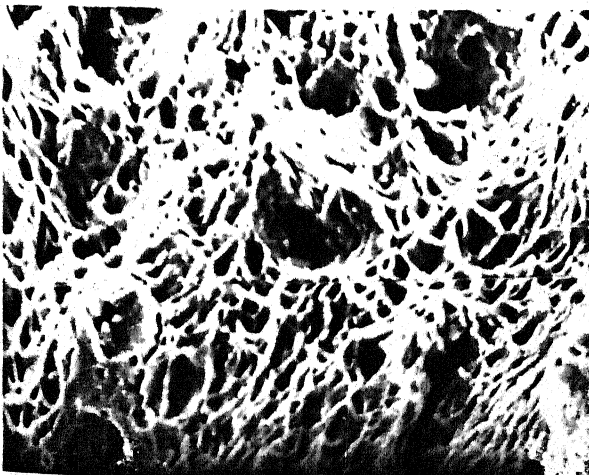


Fig.5.38 Fractured surface of the treated sample, fatigue tested at 545°C. X1000

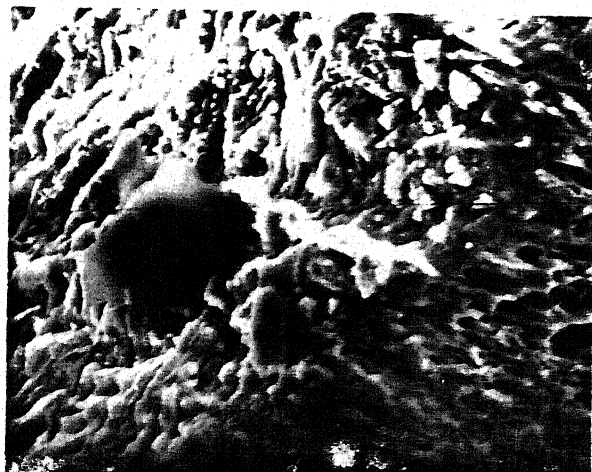


Fig.5.39 O/M interface of the sample fatigue tested at 545°C. X1000

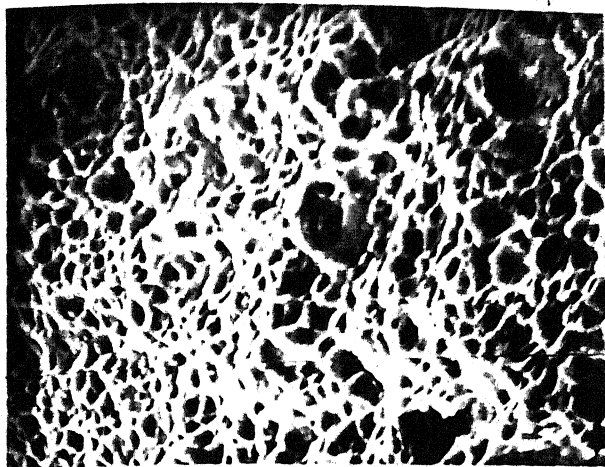


Fig.5.40 Metal matrix of the treated sample, fatigue tested at 545°C. X1000

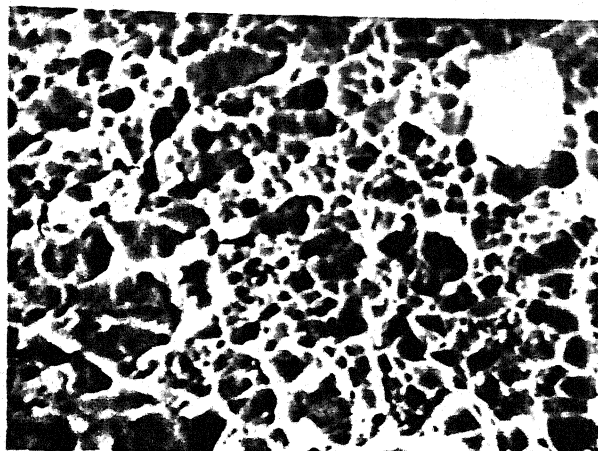


Fig.5.41 Fractured surface of the treated sample, creep tested at 550°C. X2020

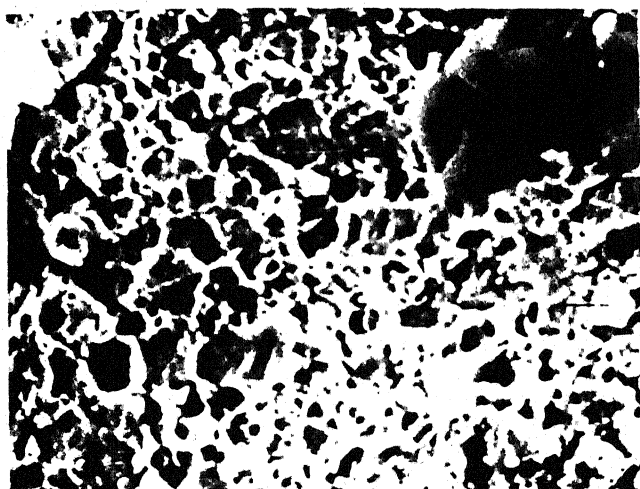


Fig.5.42 Fractograph of the treated sample, creep tested at 550°C. X2000

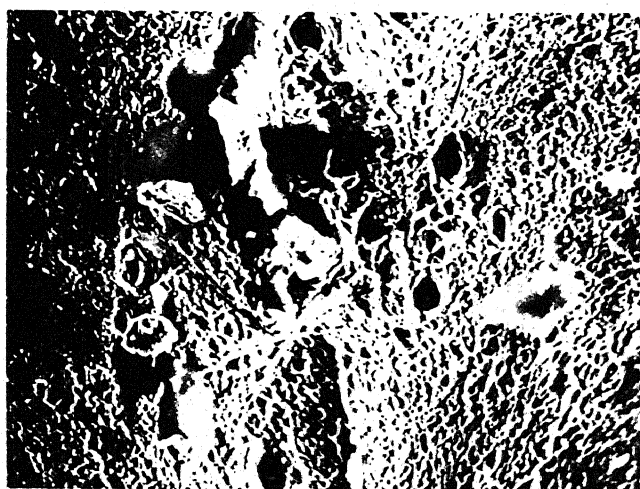


Fig.5.43 O/M of the sample, creep tested at 550°C. X500

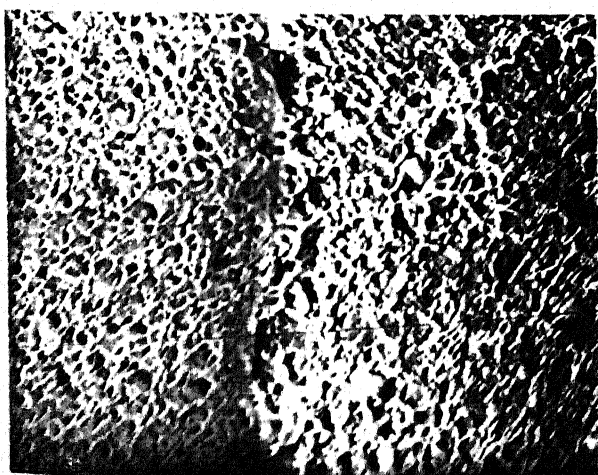


Fig.5.44 O/M of the sample, creep tested at 550°C. X600

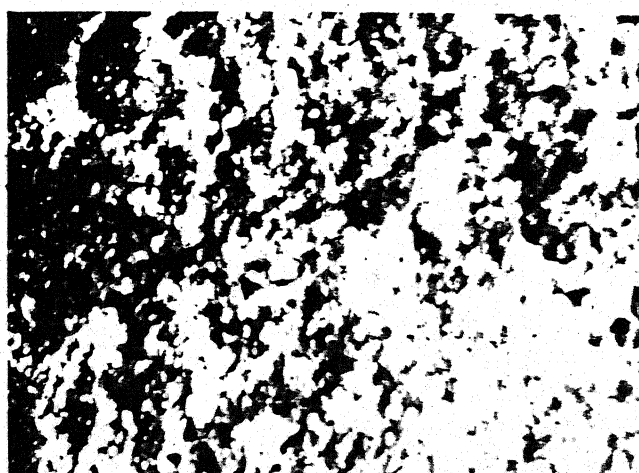


Fig.5.45 Microstructure of the treated sample after creep test at 550°C. X800

References

1. V.K. Sikka, C.T. Ward and K.C. Thomas, 'Modified 9Cr-1Mo Steel - An Improved Alloy for Steam Generator Application', pp 65-84, in ASM Int. Conf. on Production, Fabrication, Properties and Application of Ferritic Steels for High-Temperature Applications, Warren, Pennsylvania, Oct.6-8, 1981.
2. Baird J.D. and Jamieson A., J. Iron and Steel Institute, vol. 204 (1976), pp 793.
3. Klueh R.L., J. Nuclear Materials, vol. 68 (1977), pp 294.
4. Natesan K. et al., Nuclear Technology, vol.28, (1976) pp 441.
5. Klueh R.L., Materials Science and Engineering, vol.35 (1978) p. 239.
6. Brinkman C.R. et al., Nuclear Technology, vol. 28, (1976) pp 490.
7. Pizzo P.P. et al., J. Engineering Materials and Technology, vol. 103 (1981) pp 62.
8. J. Orr, F.R. Beckitt and G.D. Fawkes, 'The Physical Metallurgy of Chromium-Molybdenum Steels for Fast Reactor Boilers', in Ferritic Steels for Fast Reactor Steam Generators, British Nuclear Energy Society, 1978, p. 91.
9. R.G. Baker and J. Nutting, Journal of Iron and Steel Institute, London, vol. 192 (1957), p.257.

10. Wendell B. Jones, 'Effects of Mechanical Cycling on the Substructure of Modified 9Cr-1Mo Ferritic Steel', pp 221-235 in ASM Int. Conf. on Production, Fabrication, Properties and Application of Ferritic Steels for High-Temperature Applications, Warren, Pennsylvania, Oct. 6-8, 1981.
11. C.R. Brinkman et al., Journal of Nuclear Materials, vol. 62 (1976) pp.
12. George E. Dieter, Mechanical Metallurgy, Second Edition, McGraw-Hill International Book Company.
13. M.L. Bernstein and V.A. Zaimovsky, 'Mechanical Properties of Metals', Mir Publishers, Moscow.
14. Dorn et al., 'Materials at High Temperature,
15. F.R. Shanley et al., 'Mechanical Behaviour of Materials at elevated Temperatures', pp.
16. Fractography at Atlas of fractographs, Metals Handbook, ASTM, vol. 9.
17. Chackravarty et al., Heat treatment of creep-resistant steel, Tool and Alloy Steels, April 1978, vol.12, No.1, pp 111.

CHAPTER 6

CONCLUSION

The conclusions on the study of oxidation and mechanical behaviour of modified 9Cr-1Mo ferritic steels are summarized below.

Initially the oxidation rate for all the pressures in the temperature range 600-700°C is either cubic or parabolic and later, with increasing time, the oxidation rate tends to be linear. In the temperature range of 700-900°C, the oxidation behaviour is nearly linear throughout.

The oxide matrix is made of a duplex scale in which the inner layer consists of iron-chrome spinels while the outer layer consists of iron oxide.

The observed multi-layer growth of the oxide scale takes place either by oxidant ingress through the cracks in the scale forming a new duplex layer near the metal, or by oxidation due to volume created by the condensation of vacancies in the metal.

The reduction of the activation energy with increasing pressures, as observed from the rate equations, confirms the rapid formation of oxidation products at high temperatures.

5. Metallographic observation reveals that the oxide scale formed at elevated temperatures has cracks and is porous in nature, and thus the oxidation is catastrophic at high temperatures.
6. The mechanical strength of this modified steel (normalized and tempered) decreases with increase in test temperature. The decrease of strength (tensile, yield and engineering fracture) at the test temperature with increase of oxidation time (i.e., oxygen concentration) is attributed to the microstructural changes.
7. The ductility of this modified steel increases with increase of both temperature and oxygen concentration.
8. The fatigue strength decreases with increase of both temperature and oxygen content. This is attributed to the wedging action of the oxide scale and also due to the microstructure of this steel.
9. The creep strength of this alloy improved with increase of oxygen level in the samples. The creep failure is delayed with the increase of oxygen concentration which is due to the precipitation of carbides which stabilized the structure which is probably of bainitic nature.
10. The fractography study reveals the presence of a higher density of dimples in the treated samples compared to the untreated samples and is due to the precipitation of carbides in the matrix.

CHAPTER 7

SUGGESTIONS FOR FUTURE WORK

The following are the suggestions put forward for future work :

1. The modified 9Cr-1Mo is used at high temperatures due to the formation of a protective scale on the surface. But the protective nature of this scale is lost when the scale cracks due to various phases of operation. The morphology study of the oxide scale is essential to understand its deformation behaviour under stress and extend the protective nature of the scale and hence the life of the plant.
2. The study of oxidation behaviour of this alloy at even more elevated pressures (above atmospheres) in O_2 and CO_2 would be worthwhile.
3. The study of the effect of oxidation on mechanical behaviour with still higher oxygen concentrations is necessary.
4. In this study of mechanical behaviour, the decrease in strength with increase in oxygen concentrations is attributed to the precipitation of carbides. A detailed and systematic study is needed to understand the precipitation behaviour using TEM.

5. The oxidation behaviour and mechanical behaviour are studied individually in the present study. The study of mechanical behaviour under such simulated conditions will be worthwhile.

APPENDIX A

Table 1 Thermogravimetric data of samples oxidised at 202.65 KPa pressure and at different temperatures

Temperature 600°C

Time min	Weight gain mg/cm ²	Time min	Weight gain mg/cm ²
0	0	165	0.2216
15	0.0876	180	0.2326
30	0.1095	195	0.2435
45	0.1259	210	0.2627
60	0.1368	225	0.2791
75	0.1472	240	0.2928
90	0.1557	255	0.3119
105	0.1669	270	0.3256
120	0.1806	285	0.3420
135	0.1943	300	0.3612
150	0.2080		

Temperature 650°C

0	0	165	0.3305
15	0.0516	180	0.3563
30	0.0826	195	0.3769
45	0.0878	210	0.3976
60	0.1291	225	0.4182
75	0.1601	240	0.4437
90	0.1910	255	0.4544
105	0.2272	270	0.4750
120	0.2478	285	0.5008
135	0.2737	300	0.5215
150	0.2995		

Temperature 700°C

Time min	Weight gain ₂ mg/cm ²	Time min	Weight gain ₂ mg/cm ²
0	0	165	0.3516
15	0.0693	180	0.3729
30	0.1119	195	0.3943
45	0.1652	210	0.4209
60	0.1758	225	0.4475
75	0.1918	240	0.4955
90	0.2291	255	0.5434
105	0.2557	270	0.5701
120	0.2824	285	0.5914
135	0.2984	300	0.6127
150	0.3197		

Temperature 750°C

0	0	165	0.4274
15	0.0935	180	0.4742
30	0.1135	195	0.5209
45	0.1269	210	0.5610
60	0.1603	225	0.6078
75	0.1937	240	0.6478
90	0.2204	255	0.6812
105	0.2671	270	0.7079
120	0.2939	285	0.7480
135	0.3390	300	0.7814
150	0.3740		

Temperature 800°C

Time min	Weight gain ₂ mg/cm ²	Time min	Weight gain ₂ mg/cm ²
0	0	165	4.7432
15	1.3703	180	4.9540
30	2.0027	195	5.1648
45	2.4770	210	5.3229
60	2.8459	225	5.6918
75	3.0567	240	5.9554
90	3.3729	255	6.1662
105	3.6365	270	6.3243
120	4.0581	285	6.7986
135	4.2162	300	7.0621
150	4.4797		

Temperature 850°C

0	0	165	8.9884
15	0.6800	180	9.4319
30	1.2714	195	9.7276
45	2.2767	210	9.9937
60	3.2524	225	10.3189
75	5.2281	240	10.6442
90	5.0264	255	10.9694
105	5.7065	270	11.2947
120	7.0370	285	11.7086
135	7.8353	300	12.0634
150	8.4266		

Temperature 900°C

Time min	Weight gain mg/cm ²	Time min	Weight gain mg/cm ²
0	0	165	10.6427
15	1.6454	180	11.8330
30	2.3106	195	12.7082
45	2.8357	210	13.6184
60	3.2558	225	14.5286
75	3.7109	240	15.2988
90	4.0960	255	16.1390
105	5.5314	270	16.9442
120	7.0718	285	17.7144
135	8.4021	300	18.4146
150	9.7674		

Table 2 Thermogravimetric data of samples oxidised at 303.97 KPa pressure and at different temperatures

Temperature 600°C

Time min	Weight gain ₂ mg/cm ²	Time min	Weight gain ₂ mg/cm ²
0	0	165	0.2685
15	0.0992	180	0.2830
30	0.1250	195	0.2959
45	0.1411	210	0.3096
60	0.1604	225	0.3209
75	0.1766	240	0.3322
90	0.1919	255	0.3499
105	0.2080	270	0.3700
120	0.2217	285	0.3869
135	0.2402	300	0.4031
150	0.2540		

Temperature 650°C

0	0	165	0.4024
15	0.2247	180	0.4208
30	0.2632	195	0.4309
45	0.2867	210	0.4476
60	0.2984	225	0.4694
75	0.3202	240	0.4862
90	0.3336	255	0.5046
105	0.3454	270	0.5130
120	0.3605	285	0.5281
135	0.3672	300	0.5432
150	0.3906		

Temperature 700°C

Time min	Weight gain mg/cm ²	Time min	Weight gain mg/cm ²
0	0	165	0.4866
15	0.1242	180	0.5169
30	0.1800	195	0.5432
45	0.2142	210	0.5727
60	0.2533	225	0.5997
75	0.2907	240	0.6284
90	0.3313	255	0.6499
105	0.3608	270	0.6818
120	0.3974	285	0.6953
135	0.4301	300	0.7216
150	0.4532		

Temperature 750°C

0	0	165	0.6455
15	0.1792	180	0.6843
30	0.2258	195	0.7231
45	0.2716	210	0.7642
60	0.3220	225	0.7968
75	0.3732	240	0.8310
90	0.4213	255	0.8674
105	0.4849	270	0.8993
120	0.5222	285	0.9311
135	0.5625	300	0.9621
150	0.6036		

Temperature 800°C

Time min	Weight gain ₂ mg/cm ²	Time min	Weight gain ₂ mg/cm ²
0	0	165	0.7629
15	1.4269	180	6.0273
30	1.8322	195	6.3869
45	2.4143	210	6.6837
60	2.8595	225	7.0604
75	3.2705	240	7.2430
90	3.7728	255	7.5456
105	4.0924	270	7.7567
120	4.5833	285	8.0878
135	4.9999	300	8.3218
150	5.2853		

Temperature 850°C

0	0	165	9.4556
15	2.4133	180	10.1190
30	3.2319	195	10.6411
45	4.0786	210	11.3327
60	4.9254	225	11.7419
75	5.6169	240	12.1936
90	6.3508	255	12.7581
105	6.9718	270	13.1956
120	7.5927	285	13.6613
135	8.1855	300	14.2117
150	8.8206		

Temperature 900°C

Time min	Weight gain mg/cm ²	Time min	Weight gain mg/cm ²
0	0	165	15.0470
15	3.8563	180	15.7728
30	5.4139	195	16.6046
45	6.6691	210	17.2246
60	8.1511	225	18.0412
75	8.7862	240	18.7671
90	9.7541	255	19.4325
105	10.8429	270	20.1433
120	11.1605	285	20.6726
135	12.5971	300	21.1716
150	13.5196		

Table 3 Thermogravimetric data of samples oxidised at 506.62 KPa pressure and at different temperatures

Temperature 600°C

Time min	Weight gain mg/cm ²	Time min	Weight gain mg/cm ²
0	0	165	0.2579
15	0.0908	180	0.2771
30	0.1129	195	0.2969
45	0.1350	210	0.3137
60	0.1461	225	0.3562
75	0.1636	240	0.3772
90	0.1810	255	0.3999
105	0.1898	270	0.4191
120	0.1979	285	0.4337
135	0.2154	300	0.3451
150	0.2363		

Temperature 650°C

0	0	165	0.4040
15	0.1828	180	0.4270
30	0.2109	195	0.4477
45	0.2405	210	0.4654
60	0.2501	225	0.4824
75	0.2804	240	0.5032
90	0.3071	255	0.5187
105	0.3263	270	0.5439
120	0.3507	285	0.5668
135	0.3655	300	0.5816
150	0.3826		

Temperature 700°C

Time min	Weight gain mg/cm ²	Time min	Weight gain mg/cm ²
0	0	165	0.6672
15	0.1382	180	0.7239
30	0.2204	195	0.7365
45	0.2727	210	0.7854
60	0.3407	225	0.8039
75	0.3933	240	0.8337
90	0.4441	255	0.8627
105	0.4974	270	0.8897
120	0.5414	285	0.9270
135	0.5832	300	0.9547
150	0.6242		

Temperature 750°C

0	0	165	0.8547
15	0.1919	180	0.9217
30	0.2777	195	0.9629
45	0.3544	210	1.0284
60	0.4144	225	1.1010
75	0.4856	240	1.1450
90	0.5582	255	1.2029
105	0.6168	270	1.2517
120	0.6803	285	1.3103
135	0.7424	300	1.3452
150	0.7989		

Temperature 800°C

Time min	Weight gain mg/cm ²	Time min	Weight gain mg/cm ²
0	0	165	5.8175
15	0.7343	180	6.2317
30	1.2614	195	6.7871
45	1.7886	210	7.2107
60	2.2781	225	7.6437
75	2.7864	240	8.0673
90	3.2759	255	8.4156
105	3.7654	270	8.8957
120	4.2737	285	9.2911
135	4.7915	300	9.7147
150	5.2339		

Temperature 850°C

0	0	165	13.1069
15	2.7212	180	13.7372
31	4.4548	195	14.4727
45	5.3951	210	15.0295
66	6.9868	225	15.5969
75	7.6067	240	16.0854
90	8.6416	255	16.6738
105	9.6660	270	17.2096
120	10.5643	285	17.6404
135	11.2525	300	18.1237
150	12.2663		

Temperature 900°C

Time min	Weight gain mg/cm ²	Time min	Weight gain mg/cm ²
0	0	165	16.4146
15	3.6200	180	17.3976
30	5.1803	195	18.1778
45	6.8576	210	19.4807
60	8.4180	225	21.0020
75	9.8066	240	21.7665
90	11.0549	255	22.5467
105	12.1939	270	23.1162
120	13.2940	285	23.7872
135	14.9791	300	24.4035
150	15.4706		

Table 4 Thermogravimetric data of samples oxidised at 709.26 KPa pressure and at different temperatures

Temperature 600°C

Time min	Weight gain ₂ mg/cm ²	Time min	Weight gain ₂ mg/cm ²
0	0	165	0.3142
15	0.0754	180	0.3357
30	0.1036	195	0.3557
45	0.1289	210	0.3748
60	0.1552	225	0.3825
75	0.1777	240	0.4062
90	0.2042	255	0.4318
105	0.2250	270	0.4485
120	0.2484	285	0.4646
135	0.2729	300	0.4814
150	0.2925		

Temperature 650°C

0	0	165	0.4080
15	0.1088	180	0.4323
30	0.1501	195	0.4557
45	0.1853	210	0.4794
60	0.2139	225	0.5031
75	0.2446	240	0.5257
90	0.2760	255	0.5477
105	0.3016	270	0.5703
120	0.3312	285	0.5927
135	0.3555	300	0.6127
150	0.3809		

Temperature 700°C

Time min	Weight gain ₂ mg/cm ²	Time min	Weight gain ₂ mg/cm ²
0	0	165	0.9654
15	0.1714	180	1.0362
30	0.2551	195	1.1159
45	0.3378	210	1.1727
60	0.4394	225	1.2424
75	0.4972	240	1.3102
90	0.5828	255	1.3769
105	0.6705	270	1.4457
120	0.7462	285	1.5084
135	0.8299	300	1.5722
150	0.8997		

Temperature 750°C

0	0	165	1.6632
15	0.2899	180	1.7688
30	0.4630	195	1.9578
45	0.5941	210	2.1095
60	0.7307	225	2.2414
75	0.8840	240	2.3430
90	1.0111	255	2.4479
105	1.1636	270	2.5297
120	1.3034	285	2.6178
135	1.4146	300	2.6782
150	1.5543		

Temperature 800°C

Time min	Weight gain mg/cm ²	Time min	Weight gain mg/cm ²
0	0	165	6.3625
15	0.9561	180	6.6048
30	1.5553	195	7.1771
45	2.2083	210	7.6484
60	2.6056	225	7.9514
75	3.1038	240	8.4765
90	3.6020	255	9.1027
105	4.1878	270	9.3720
120	4.7129	285	9.7490
135	5.1775	300	10.2136
150	5.6892		

Temperature 850°C

0	0	165	15.2512
15	2.0994	180	16.1774
30	3.5967	195	16.2237
45	5.1866	210	18.0606
60	6.7766	225	18.7553
75	8.0733	240	19.6600
90	10.1109	255	20.5768
105	11.7934	270	21.2097
120	13.3525	285	21.6573
135	14.3868	300	22.1976
150	14.4331		

Temperature 900°C

Time min	Weight gain mg/cm ²	Time min	Weight gain mg/cm ²
0	0	165	21.2743
15	3.2867	180	22.5961
30	5.5910	195	23.9001
45	7.9131	210	25.3827
60	9.7351	225	26.5259
75	11.4856	240	27.7763
90	13.6470	255	29.1160
105	14.8974	270	30.3485
120	16.5765	285	31.6525
135	18.0411	300	32.7778
150	19.5952		

Table 5 Thermogravimetric data of samples oxidised at 911.91 KPa pressure and at different temperatures

Temperature 600°C

Time min	Weight gain mg/cm ²	Time min	Weight gain mg/cm ²
0	0	165	0.3347
15	0.0344	180	0.3516
30	0.0759	195	0.3738
45	0.1262	210	0.3942
60	0.1529	225	0.4168
75	0.1699	240	0.4394
90	0.1992	255	0.4574
105	0.2305	270	0.4763
120	0.2551	285	0.4950
135	0.2807	300	0.5132
150	0.3007		

Temperature 750°C

0	0	165	2.2327
15	0.3148	180	2.3935
30	0.5332	195	2.5848
45	0.7059	210	2.7591
60	0.9107	225	2.9267
75	1.1257	240	3.1044
90	1.3034	255	3.2585
105	1.4862	270	3.4311
120	1.6622	285	3.5598
135	1.8603	300	3.7155
150	2.1057		

Temperature 800°C

Time min	Weight gain mg/cm ²	Time min	Weight gain mg/cm ²
0	0	165	6.9533
15	0.9805	180	7.4541
30	1.6606	195	8.0498
45	2.1983	210	8.5928
60	2.8362	225	9.1147
75	3.5057	240	9.6682
90	4.0592	255	10.1480
105	4.6285	270	10.6857
120	5.1768	285	11.0863
135	5.7936	300	11.5713
150	6.5579		

Temperature 850°C

0	0	165	14.4725
15	2.5103	180	15.5091
30	4.0043	195	16.5255
45	5.2951	210	17.7044
60	6.6874	225	18.3955
75	7.6438	240	19.7472
90	8.7506	255	20.3469
105	10.0007	270	21.3632
120	11.2202	285	22.2880
135	12.2772	300	23.1316
150	13.3850		

Temperature 900°C

Time min	Weight gain mg/cm ²	Time min	Weight gain mg/cm ²
0	0	165	20.0678
15	2.1197	180	21.6164
30	4.2268	195	23.2284
50	6.9431	210	24.9420
60	8.1997	225	26.4651
75	9.3929	240	28.0391
90	11.6903	255	29.7399
105	13.5435	270	31.1997
120	15.0286	285	32.7228
135	16.7168	300	34.0556
150	18.4050		

APPENDIX B

Results of X-ray Analysis of Modified 9Cr-1Mo Ferritic Steel

$$\lambda_{Cu} = 1.54 \text{ \AA}$$

Specification of specimen	2θ ($^{\circ}$)	d (\AA)	Intensity I	I with respect to I_{\max} (100)
Oxidized at 750 $^{\circ}$ C and 303.97 KPa	33.4	2.6795	49.0	57.64
	35.6	2.5188	47.0	55.29
	44.6	2.0292	68.0	80.00
	65.1	1.4311	75.5	88.82
	82.2	1.1713	85.0	100.00
	82.3	1.1701	83.5	98.23
	116.3	0.9064	82.0	96.47
	116.5	0.9055	73.0	85.88
	116.8	0.9040	78.5	92.35
Oxidized at 800 $^{\circ}$ C and 506.62 KPa	34.2	2.6186	46.0	61.33
	36.7	2.4458	51.5	68.66
	50.5	1.8051	49.0	65.33
	55.1	1.6647	54.0	72.00
	58.6	1.5734	51.0	68.00
	63.5	1.4632	60.0	80.00
	65.0	1.4330	61.0	81.33
	123.4	0.8745	75.0	100.00

Specification	2θ ($^{\circ}$)	d (\AA)	Intensity I	I with respect to I_{\max} (100)
Oxidized at 900 $^{\circ}$ C and 911.91 KPa	33.2	2.6952	45.0	48.38
	39.3	2.2898	63.0	67.74
	57.6	1.5983	60.0	64.51
	71.9	1.3115	83.5	89.78
	72.0	1.3100	83.0	89.24
	84.4	1.1463	78.0	83.87
	107.2	0.9566	93.0	100.00
	107.4	0.9554	92.0	98.92
	132.0	0.8428	90.0	96.77
	132.3	0.8419	90.0	96.77
	133.8	0.8371	88.5	95.16
	139.6	0.8278	89.0	95.69
Oxygen concentra- tion 0.06 wt %, creep fatigue tested at 545 $^{\circ}$ C	33.5	2.6718	41.0	59.85
	44.6	2.0292	68.0	99.27
	44.7	2.0249	68.5	100.00
	65.0	1.4331	52.0	75.91
	65.1	1.4311	52.3	76.35
	82.3	1.1702	57.2	83.50
	82.4	1.1690	56.8	82.92
	82.6	1.1667	55.6	81.17
	116.3	0.9065	50.0	72.99

Specification	2θ ($^{\circ}$)	d (\AA)	Intensity I	I with respect to $I_{\max}(100)$
---------------	-----------------------------	-------------------------	------------------	---

Oxygen concentration	33.3	2.69	35.5	67.62
0.13 wt %, creep	35.8	2.51	37.0	70.48
tested at 550 $^{\circ}$ C	44.6	2.03	51.0	97.14
	54.3	1.69	43.5	82.86
	65.0	1.43	47.5	90.48
	82.2	1.17	52.5	100.00
	99.1	1.01	45.0	85.71
	116.2	0.91	43.7	83.24

Oxygen concentration	24.3	3.66	37.0	61.67
0.08 wt %, fatigue	33.2	2.70	33.5	55.83
tested at room	35.7	2.51	34.5	57.50
temperature	35.8	2.51	34.5	57.50
	44.6	2.03	49.0	81.67
	44.7	2.02	50.3	83.83
	49.8	1.83	38.0	63.33
	54.5	1.68	43.0	71.67
	72.9	1.30	51.0	85.00
	82.2	1.17	60.0	100.00
	116.6	0.91	50.5	84.17

APPENDIX C

X-ray Diffraction Data for some important compounds

Compound	'd' values			I/I ₁			Card No.
$\alpha\text{Fe}_2\text{O}_3$	2.69	1.69	2.51	100	60	50	13-534
$\alpha\text{Fe}_2\text{O}_3$	2.52	2.95	1.61	101	101	101	15-615
Fe_3O_4	2.53	1.61	1.48	100	85	85	11-614
FeO	2.15	2.49	1.52	100	80	60	6-615
$-\text{Fe}_2\text{O}_3 \cdot \text{H}_2\text{O}$	4.21	2.69	2.44	100	80	70	38-97
FeCr_2O_4	2.51	1.91	1.61	100	75	75	4-759
FeMoO_4	2.88	1.68	3.56	100	70	40	16-326
MoO_2	3.41	2.42	1.70	100	85	80	5-0452
MoO_3	3.26	3.81	3.46	100	82	61	5-508
$(\text{Cr}, \text{Fe})_2\text{O}_3$	1.68	3.68	2.69	100	80	80	2-1357
Cr_2N	2.10	2.38	2.22	100	25	25	1-1232
CrN	2.07	2.39	1.46	100	80	80	11-65
Cr_2O_3	2.67	2.48	1.67	100	96	90	6-504
CrO_2	3.11	1.63	2.42	100	75	60	9-332
CrO_3	4.16	3.42	3.36	100	100	100	9-47